Universität Regensburg
Mathematik

Numerical approximation of gradient flows for closed curves in $\mathbb{R}^d$

John W. Barrett, Harald Garcke and Robert Nürnberg

Preprint Nr. 13/2008

Numerical Approximation of Gradient Flows for Closed Curves in $\mathbb{R}^d$

John W. Barrett[†] Harald Garcke[‡] Robert Nürnberg[†]

Abstract

We present parametric finite element approximations of curvature flows for curves in $\mathbb{R}^d$, $d \geq 2$, as well as for curves on two-dimensional manifolds in $\mathbb{R}^3$. Here we consider the curve shortening flow, curve diffusion and the elastic flow. It is demonstrated that the curve shortening and the elastic flows on manifolds can be used to compute nontrivial geodesics, and that the corresponding geodesic curve diffusion flow leads to solutions of partitioning problems on two-dimensional manifolds in $\mathbb{R}^3$. In addition, we extend these schemes to anisotropic surface energy densities. The presented schemes have very good properties with respect to stability and the distribution of mesh points, and hence no remeshing is needed in practice.

Key words. curve shortening flow, geodesic curvature flows, curve diffusion, surface diffusion, elastic flow, Willmore flow, geodesics, parametric finite elements, anisotropy, tangential movement

AMS subject classifications. 65M60, 65M12, 35K55, 53C44, 53C22

1 Introduction

In this paper we introduce numerical methods for the approximation of evolving curves in $\mathbb{R}^d$, $d \geq 2$. The evolution laws considered all aim to reduce an energy, where the energy will be either the length functional, the curvature (Willmore-) functional, or possibly anisotropic versions of these. All the flows will be gradient flows, which hence have a variational structure, and this will be heavily used when we derive the numerical approximations. The L^2-gradient flow for the length of a curve in $\mathbb{R}^d$ leads to curvature flow, also called curve shortening flow. If instead an appropriate H^{-1}-gradient flow is considered, one obtains a fourth order flow called curve or surface diffusion. If we restrict the curves considered to lie on a two-dimensional manifold in $\mathbb{R}^d$, we obtain, as an L^2-gradient flow, the geodesic curvature flow and, as an H^{-1}-gradient flow, geodesic surface diffusion. We will propose a parametric finite element approximation for these flows.

[†]Department of Mathematics, Imperial College London, London, SW7 2AZ, UK
[‡]NWF I – Mathematik, Universität Regensburg, 93040 Regensburg, Germany

Willmore flow of curves, also called elastic flow of curves, in higher codimension is obtained as the L^2-gradient flow of the curvature integral

$$\mathcal{W}(\Gamma) = \tfrac{1}{2} \int_\Gamma |\vec{\varkappa}|^2 \, \mathrm{d}s \,, \tag{1.1}$$

where $\vec{\varkappa}$ is the curvature vector of a curve Γ in $\mathbb{R}^d$. This leads to a flow, which is nonlinear in the curvature. We will extend our parametric approximation to this flow as well. On restricting Γ to lie on a two-dimensional manifold and on replacing $\vec{\varkappa}$ in (1.1) with the geodesic curvature vector, we obtain geodesic Willmore flow of curves. In addition, we will also consider gradient flows for weighted, or anisotropic, length, as well as anisotropic versions of (1.1) and the corresponding geodesic energy.

The present authors in recent work, Barrett, Garcke, and Nürnberg (2007b), Barrett, Garcke, and Nürnberg (2007a) and Barrett, Garcke, and Nürnberg (2008b), have introduced a new numerical approach for the approximation of geometric evolution equations. An important feature of this approach is that the resulting new numerical schemes have very good properties with respect to the equidistribution of mesh points. This is an important issue, as many discretizations can lead to coalescence of mesh points during the evolution or lead to very irregular meshes; which, in turn, lead to ill-conditioned discrete problems. The equidistribution property in these methods is formulated intrinsically in a natural variational discretization of curvature, and no remeshing is needed in practice. So far, the method introduced in Barrett, Garcke, and Nürnberg (2007b) has been restricted to evolving curves and surfaces of codimension one. In this paper, we demonstrate that it is possible to introduce an extension of this approach, which also allows it to approximate curvature flows in higher codimension. We will discuss all the flows mentioned above. Since our approach makes substantial use of the variational structure, we will first derive these evolution laws as gradient flows, see Section 2.

Fundamental to many approaches, which numerically approximate evolving curves in a parametric way, is the identity

$$\vec{x}_{ss} = \vec{\varkappa} \,, \tag{1.2}$$

where $\vec{x}$ is the position vector, $\vec{\varkappa}$ is the curvature vector and s is arclength of the curve. In Dziuk (1991), for the first time, a weak formulation of (1.2) was used, in order to approximate problems involving curvature. In particular, a weak formulation of the equation

$$\vec{x}_t = \vec{x}_{ss} \tag{1.3}$$

can be used to approximate curvature flow numerically. It turns out, see Section 2, that the equation (1.3) leads to parameterizations, $\vec{x}$, of an evolving curve in which the motion is in the curve's normal direction. As it is possible to reparameterize a given curve, it is not necessary to use such a parameterization. We will instead discretize the identity

$$\vec{P}\,\vec{x}_t = \vec{x}_{ss} \,, \tag{1.4}$$

where $\vec{P}$ is the projection onto the part normal to the curve. Solutions to (1.4) parameterize the same evolving curve as (1.3), if the initial data parameterize the same curve, as

the tangential part of $\vec{x}_t$ is not prescribed. As all parameterizations of a curve evolving under the curve shortening flow are solutions to (1.4), one can hence consider (1.4) as the proper geometric formulation of curvature flow.

Let us briefly discuss existing parametric approximations of the flows discussed in this paper. Parametric finite element approximations of curves in $\mathbb{R}^d$, $d \geq 2$, have been considered for curve shortening flow in Dziuk (1994), for curve diffusion and Willmore flow in Dziuk, Kuwert, and Schätzle (2002), and for Willmore flow also in Deckelnick and Dziuk (2007). In addition, the approach in Dziuk (1994) for isotropic curve shortening flow for $d \geq 2$, on using ideas from Dziuk (1999) for the anisotropic case for $d = 2$, was recently extended to anisotropic surface energies in Pozzi (2007).

To our knowledge, so far no parametric approximations for geodesic evolution equations exist in the literature. Numerical approximations of geodesic curvature flow based on level set techniques are presented in Chopp and Sethian (1993), Cheng, Burchard, Merriman, and Osher (2002) and Spira and Kimmel (2007). The computation of minimizers to the geodesic equivalent of the energy (1.1) has been considered in Brunnett and Crouch (1994) for a sphere, and in Linnér and Renka (2005) for general manifolds. For readers not familiar with numerical methods for geometric evolution equations, we refer to Deckelnick, Dziuk, and Elliott (2005) for a recent overview.

The outline of the paper is as follows. In Section 2 we derive the evolution equations, emphasizing their variational structure, and discuss how to extend these isotropic flows to their anisotropic counterparts. Finite element approximations of these evolution laws are introduced in Section 3, where we prove also well-posedness, stability and mesh properties of theses schemes. In Section 4 we discuss possible solution methods for the arising discrete systems. Finally in Section 5, we present several computations illustrating properties of the considered geometric evolution equations, and of our numerical approximations.

2 Geometric evolution equations for curves

In this section we derive the geometric evolution equations studied in this paper.

Curve shortening flow

For a closed smooth curve Γ in $\mathbb{R}^d$ parameterized by $\vec{x} : I \to \mathbb{R}^d$, $I := \mathbb{R}/\mathbb{Z}$, we have that the length of Γ is given by

$$|\Gamma| := \int_I |\vec{x}_\rho| \, \mathrm{d}\rho \,. \tag{2.1}$$

For all $\vec{\eta} : I \to \mathbb{R}^d$, we obtain that the first variation of $|\Gamma|$ in the direction $\vec{\eta}$ is as follows. Choose $\vec{y} : I \times (-\varepsilon_0, \varepsilon_0) \to \mathbb{R}^d$ with $\vec{y}(\rho, 0) = \vec{x}(\rho)$, $\vec{y}_\varepsilon(\rho, 0) = \vec{\eta}(\rho)$ and compute

$$[\delta|\Gamma|](\vec{\eta}) := \frac{\mathrm{d}}{\mathrm{d}\varepsilon} \int_I |\vec{y}_\rho| \, \mathrm{d}\rho \,|_{\varepsilon=0} = \int_I \frac{\vec{x}_\rho}{|\vec{x}_\rho|} \,.\, \vec{\eta}_\rho \, \mathrm{d}\rho = \int_\Gamma \vec{x}_s \,.\, \vec{\eta}_s \, \mathrm{d}s = - \int_\Gamma \vec{\varkappa} \,.\, \vec{\eta} \, \mathrm{d}s \,, \tag{2.2}$$

where $\vec{\eta}_s := \vec{\eta}_\rho / |\vec{x}_\rho|$ is the differentiation of $\vec{\eta}$ with respect to arclength and $\vec{\varkappa} := \vec{x}_{ss}$ is the curvature vector. In order to define a gradient flow for the length $|\Gamma|$, we need to

introduce an inner product for functions $\vec{\eta} : I \to \mathbb{R}^d$. In this paper an inner product will be a positive semi-definite, symmetric bilinear form. It should be noted that variations of a curve Γ parameterized by $\vec{x}$ in a direction $\vec{\eta}$ have a tangential part, which correspond to leading order to reparameterizations of the curve Γ; and a normal part, which actually leads to proper variations of the curve. We therefore introduce the following inner product for functions $\vec{\eta}, \vec{\chi} : I \to \mathbb{R}^d$

$$(\vec{\eta}, \vec{\chi})_{2,nor} := \int_\Gamma \vec{P}\,\vec{\eta}\,.\,\vec{P}\,\vec{\chi}\,\mathrm{d}s\,, \tag{2.3}$$

where $\vec{P} := \vec{Id} - \vec{x}_s \otimes \vec{x}_s$ is the projection onto the part normal to Γ. Here $\vec{Id}$ is the identity operator on $\mathbb{R}^d$. The corresponding semi-norm is denoted by $\|\cdot\|_{2,nor}$. The inner product $(\cdot,\cdot)_{2,nor}$ is the L^2-inner product of the normal part of vector valued functions on the curve Γ. Now a time dependent function $\vec{x}$ is a solution to the gradient flow equation for $|\Gamma|$ with respect to $(\cdot,\cdot)_{2,nor}$, if

$$(\vec{x}_t, \vec{\eta})_{2,nor} = -\int_\Gamma \vec{x}_s\,.\,\vec{\eta}_s\,\mathrm{d}s$$

for all $\vec{\eta} : I \to \mathbb{R}^d$. Using the facts that $\vec{P}^T = \vec{P}$ and $\vec{P}^2 = \vec{P}$, we hence obtain the following system

$$\vec{P}\,\vec{x}_t = \vec{x}_{ss}\,, \tag{2.4}$$

i.e. the normal part of the velocity vector is given by the curvature vector $\vec{\varkappa} = \vec{x}_{ss}$. This gradient flow has the property that the length $|\Gamma|$ decreases fastest, when compared to all other velocities of the curve having the same $\|.\|_{2,nor}$-norm. This is in accordance with Taylor and Cahn (1994) and Luckhaus and Sturzenhecker (1995), who considered geometric evolution equations as gradient flows. The formulation (2.4) has many solutions in $\vec{x}$, but they all parameterize the same evolving curve. For $d = 2$ we obtain, choosing a unit normal $\vec{\nu}$ to the curve and setting

$$\mathcal{V} := \vec{x}_t\,.\,\vec{\nu}\,, \qquad \vec{x}_{ss} = \varkappa\,\vec{\nu}, \tag{2.5}$$

the familiar law

$$\mathcal{V} = \varkappa\,.$$

As stated already in the introduction, the formulation (2.4) has the advantage that if a parameterization of an evolving curve fulfills (2.4), then also all reparameterizations fulfill (2.4).

We now introduce a suitable weak formulation of (2.4), which will form the basis of our fully discrete parametric finite element approximation. Since $\vec{\varkappa}$ is normal to the curve, we can rewrite (2.4) as

$$\vec{P}\,\vec{x}_t = \vec{P}\,\vec{\varkappa}\,, \qquad \vec{\varkappa} = \vec{x}_{ss}\,. \tag{2.6}$$

On defining the test function space

$$\underline{V}_{\vec{x}} := \{\vec{\eta} : I \to \mathbb{R}^d : \vec{\eta} \text{ is smooth and } \vec{\eta}\,.\,\vec{x}_s = 0\}\,, \tag{2.7}$$

we obtain the following weak formulation of (2.6):

$$\int_\Gamma (\vec{x}_t - \vec{\varkappa}) \,.\, \vec{\eta} \,\mathrm{d}s = 0 \quad \forall\, \vec{\eta} \in \underline{V}_{\vec{\tau}}\,, \qquad \int_\Gamma \vec{\varkappa} \,.\, \vec{\eta} \,\mathrm{d}s + \int_\Gamma \vec{x}_s \,.\, \vec{\eta}_s \,\mathrm{d}s = 0 \quad \forall\, \vec{\eta}\,, \tag{2.8}$$

where we note again that $\vec{\varkappa} \in \underline{V}_{\vec{\tau}}$.

Curve diffusion

For curves in $\mathbb{R}^2$ surface diffusion (also called curve diffusion) is given as

$$\mathcal{V} = \vec{x}_t \,.\, \vec{\nu} = -\varkappa_{ss}\,, \qquad \varkappa\, \vec{\nu} = \vec{x}_{ss}. \tag{2.9}$$

This evolution law can be interpreted as the H^{-1}-gradient flow of the length functional (2.1), see Taylor and Cahn (1994). In Dziuk, Kuwert, and Schätzle (2002) the curve diffusion flow was generalized to higher codimensions as

$$\vec{x}_t = -\vec{\nabla}_s^{\,2}\, \vec{\varkappa}\,, \qquad \vec{\varkappa} = \vec{x}_{ss}\,, \tag{2.10}$$

where $\vec{\nabla}_s\, \vec{\eta} := \vec{P}\, \vec{\eta}_s$ is the normal component of $\vec{\eta}_s$, and $\vec{\nabla}_s^{\,2}\, \cdot := \vec{\nabla}_s\, (\vec{\nabla}_s\, \cdot)$. We now demonstrate that (2.10) can in fact also be viewed as an H^{-1}-gradient flow of length, i.e. we generalize the observation of Taylor and Cahn (1994) to higher codimensions.

As in the case of the L^2-gradient flow and as in the case of codimension 1, see Taylor and Cahn (1994), we only want to account for the normal part of a possible variation of a curve. In order to define the H^{-1}-inner product, we need to invert the operator $-\vec{\nabla}_s^{\,2}$ on a suitable subspace, see again Taylor and Cahn (1994) for the case of codimension 1. Therefore, we first of all identify the kernel of $-\vec{\nabla}_s^{\,2}$, where we only want to consider $-\vec{\nabla}_s^{\,2}$ applied to functions for which the tangential part disappears. For such functions, an integration by parts formula holds for $\vec{\nabla}_s$, see Dziuk, Kuwert, and Schätzle (2002); and hence we obtain that

$$\int_\Gamma -\vec{\nabla}_s^{\,2}\, \vec{\eta}_1 \,.\, \vec{\eta}_2 \,\mathrm{d}s = \int_\Gamma \vec{\nabla}_s\, \vec{\eta}_1 \,.\, \vec{\nabla}_s\, \vec{\eta}_2 \,\mathrm{d}s \qquad \forall\, \vec{\eta}_1, \vec{\eta}_2 \in \underline{V}_{\vec{\tau}}\,, \tag{2.11}$$

where we recall (2.7). This implies that in order to find the kernel of $-\vec{\nabla}_s^{\,2}$, we need to find functions $\vec{\eta} \in \underline{V}_{\vec{\tau}}$ with $\vec{\nabla}_s\, \vec{\eta} = 0$. Choosing an orthonormal basis $\{\vec{\nu}_i(\rho)\}_{i=1}^{d-1}$ of $\{\vec{x}_s\}^\perp$, we can express $\vec{\eta}$ as $\vec{\eta}(\rho) = \sum_{i=1}^{d-1} \alpha_i(\rho)\, \vec{\nu}_i(\rho)$, $\rho \in I$. It follows that

$$\vec{0} = \vec{\nabla}_s\, \vec{\eta} = \sum_{i=1}^{d-1} (\alpha_i\, \vec{\nabla}_s\, \vec{\nu}_i + \alpha_{i,s}\, \vec{\nu}_i)\,, \tag{2.12}$$

and hence $\{\alpha_i\}_{i=1}^{d-1}$ satisfy the system of ODEs

$$\alpha_{j,s} = -\sum_{i=1}^{d-1} \alpha_i\, \vec{\nabla}_s\, \vec{\nu}_i \,.\, \vec{\nu}_j\,, \quad j = 1 \to d-1\,.$$

In addition, the functions α_i have to be periodic. As at most $(d-1)$ linearly independent solutions $\vec{\alpha} = (\alpha_1, \ldots, \alpha_{d-1})^T$ of (2.12) exist, we obtain that the kernel

$$\ker(-\vec{\nabla}_s^{\,2}) := \{\vec{\eta} \in \underline{V}_{\vec{\tau}} : \vec{\nabla}_s\, \vec{\eta} = \vec{0}\} \tag{2.13}$$

is at most $(d-1)$-dimensional. We observe that this kernel is $(d-1)$-dimensional if Γ lies in a two-dimensional affine hyperplane $\vec{z}_0 + \mathcal{H}$ in $\mathbb{R}^d$, where $\mathcal{H} = \text{span}\{\vec{z}_1, \vec{z}_2\} \subset \mathbb{R}^d$ and $\vec{z}_i$, $i = 0 \to 2$, are fixed. To see this, assume w.l.o.g. that $\vec{\nu}_1(\rho) \in \mathcal{H}$, $\rho \in I$, and that $\vec{\nu}_i(\rho) = \vec{\nu}_i(0)$ for all $\rho \in I$, $i = 2 \to d-1$. Then it follows that the functions $\vec{\eta} = \vec{\nu}_i$, $i = 1 \to d-1$, form a basis of $\ker(-\vec{\nabla}_s^2)$.

We set $\mathcal{R} := \{\vec{\eta} \in \underline{V}_{\vec{\varGamma}} : \int_\Gamma \vec{\eta} \,.\, \vec{v} \,\mathrm{d}s = 0 \text{ for all } \vec{v} \in \ker(-\vec{\nabla}_s^2)\}$, and define for all $\vec{v} \in \mathcal{R}$ a function $\vec{u}_{\vec{v}} \in \mathcal{R}$ as the solution of

$$\int_\Gamma \vec{\nabla}_s \, \vec{u}_{\vec{v}} \,.\, \vec{\nabla}_s \, \vec{\eta} \,\mathrm{d}s = \int_\Gamma \vec{v} \,.\, \vec{\eta} \,\mathrm{d}s \qquad \forall \; \vec{\eta} \in \underline{V}_{\vec{\varGamma}} \,.$$

Existence of $\vec{u}_{\vec{v}}$ follows from the Fredholm alternative, but for sake of brevity we do not present the details here. However, this can be made rigorous. Setting $(-\vec{\nabla}_s^2)^{-1} \, \vec{v} := \vec{u}_{\vec{v}}$, we define the H^{-1}-inner product for $\vec{v}, \vec{w} : \Gamma \to \mathbb{R}^d$ with $\vec{P} \, \vec{v}, \vec{P} \, \vec{w} \in \mathcal{R}$ as

$$(\vec{v}, \vec{w})_{-1} := \int_\Gamma \vec{\nabla}_s \, [(-\vec{\nabla}_s^2)^{-1} \, \vec{P} \, \vec{v}] \,.\, \vec{\nabla}_s \, [(-\vec{\nabla}_s^2)^{-1} \, \vec{P} \, \vec{w}] \,\mathrm{d}s = \int_\Gamma \vec{v} \,.\, (-\vec{\nabla}_s^2)^{-1} \, \vec{P} \, \vec{w} \,\mathrm{d}s \,.$$

Now the gradient flow of $|\Gamma|$ with respect to the H^{-1}-inner product is defined via

$$(\vec{x}_t, \vec{\eta})_{-1} = -\int_\Gamma \vec{x}_s \,.\, \vec{\eta}_s \,\mathrm{d}s \,, \tag{2.14}$$

which has to hold for all $\vec{\eta}$ with $\vec{P} \, \vec{\eta} \in \mathcal{R}$. The identity (2.14) is equivalent to

$$\int_\Gamma [(-\vec{\nabla}_s^2)^{-1} \, \vec{P} \, \vec{x}_t] \,.\, \vec{\eta} \,\mathrm{d}s = \int_\Gamma \vec{\varkappa} \,.\, \vec{\eta} \,\mathrm{d}s,$$

and hence we obtain that

$$\vec{P} \, \vec{x}_t = -\vec{\nabla}_s^2 \, \vec{\varkappa} \tag{2.15}$$

as the H^{-1}-gradient flow of length. In the special case $d = 2$ we obtain, on recalling the definitions in (2.5) and on noting that $-\vec{\nabla}_s^2 \, (\varkappa \, \vec{\nu}) \equiv -\varkappa_{ss} \, \vec{\nu}$, the flow (2.9), i.e. the surface diffusion flow in the plane. We note that a parametric finite element approximation for (2.9) was considered by the authors in Barrett, Garcke, and Nürnberg (2007b).

Similarly to (2.8), and on recalling (2.11), we obtain the following weak formulation of (2.15):

$$\int_\Gamma \vec{x}_t \,.\, \vec{\eta} \,\mathrm{d}s - \int_\Gamma \vec{\nabla}_s \, \vec{\varkappa} \,.\, \vec{\nabla}_s \, \vec{\eta} \,\mathrm{d}s = 0 \quad \forall \; \vec{\eta} \in \underline{V}_{\vec{\varGamma}} \,, \qquad \int_\Gamma \vec{\varkappa} \,.\, \vec{\eta} \,\mathrm{d}s + \int_\Gamma \vec{x}_s \,.\, \vec{\eta}_s \,\mathrm{d}s = 0 \quad \forall \; \vec{\eta} \,, \tag{2.16}$$

where we recall that $\vec{\varkappa} \in \underline{V}_{\vec{\varGamma}}$. This formulation will form the basis of our variational approximation of curve diffusion.

Let us now identify the stationary solutions of (2.15).

LEMMA. 2.1. *For a closed C^2-curve $\Gamma \subset \mathbb{R}^d$, $d \geq 2$, it holds that $\vec{\nabla}_s^2 \, \vec{\varkappa} = \vec{0}$ if and only if Γ is a (possibly multiply covered) circle.*

Proof. Arguing as above, we first obtain via an energy argument that stationary solutions fulfill $\vec{\nabla}_s \vec{\varkappa} = 0$. As Γ is closed, we find a point on Γ such that $|\vec{x}_{ss}| \neq 0$ and we define $\vec{\nu} := \vec{x}_{ss}/|\vec{x}_{ss}|$ and $\varkappa := |\vec{x}_{ss}|$ in a suitable neighbourhood of this point. Since $\vec{\nu}_s \,.\, \vec{\nu} = \frac{1}{2}\,\partial_s |\vec{\nu}|^2 = 0$ and $\vec{x}_{ss} \,.\, \vec{x}_s = \frac{1}{2}\,\partial_s\,|\vec{x}_s|^2 = 0$ we obtain that

$$\vec{0} = \vec{\nabla}_s\,(\varkappa\,\vec{\nu}) = \varkappa_s\,\vec{\nu} + \varkappa\,\vec{\nu}_s - \varkappa\,(\vec{\nu}_s \,.\, \vec{x}_s)\,\vec{x}_s\,.$$

This implies that $\varkappa_s = 0$ and hence $|\vec{x}_{ss}|$ is a constant. In addition, we obtain that $\vec{\nu}_s$ and $\vec{x}_s$ are parallel, and hence $\vec{x}_{sss}$ equals $\vec{x}_s$ up to a fixed multiplicative factor. This implies the existence of a $\gamma \in \mathbb{R}$ and a $\vec{c} \in \mathbb{R}^d$ such that

$$\vec{x}_{sss} = \gamma\,\vec{x}_s \quad \text{and} \quad \vec{x}_{ss} = \gamma\,(\vec{x} + \vec{c})\,.$$

We now choose an orthogonal matrix $\vec{Q}$ such that $\vec{w} := \vec{Q}\,(\vec{x}+\vec{c})$ fulfills $\vec{w}(0) \in \operatorname{span}\{\vec{e}_1, \vec{e}_2\}$ and $\vec{w}_s(0) \in \operatorname{span}\{\vec{e}_1, \vec{e}_2\}$, where $\{\vec{e}_i\}_{i=1}^d$ are the standard orthonormal vectors in $\mathbb{R}^d$. Since $\vec{w}$ solves $\vec{w}_{ss} = \gamma\,\vec{w}$, we conclude from the unique solvability of the initial value problem for $\vec{w}_{ss} = \gamma\,\vec{w}$ that $\vec{w}(\rho) \in \operatorname{span}\{\vec{e}_1, \vec{e}_2\}$ for all $\rho \in I$. Moreover, we conclude that $\vec{w}$ parameterizes a circle. This proves the claim. □

Only the single covered circle is stable. Multiply covered circles are unstable already in the plane, $d = 2$, which has been shown in Chou (2003) and which can also be deduced from a linear stability analysis similar to the one in Garcke, Ito, and Kohsaka (2005).

We remark that curve diffusion is driven not only by curvature, but also by the torsion of a curve. In particular, we obtain for $d = 3$, on setting $\varkappa\,\vec{\nu} := \vec{x}_{ss}$ with $|\vec{\nu}| = 1$, that

$$\vec{\nabla}_s^2\,\vec{\varkappa} = (\varkappa_{ss} - \varkappa\,\beta^2)\,\vec{\nu} - (2\,\varkappa_s\,\beta + \varkappa\,\beta_s)\,\vec{b}\,,$$

where $\vec{b} := \vec{x}_s \times \vec{\nu}$ and $\vec{b}_s = \beta\,\vec{\nu}$ with β being the torsion. We remark that $\vec{\nabla}_s^2\,\vec{\varkappa} = \vec{0}$ implies that $\beta \equiv 0$.

Geodesic curvature flow

Moreover, we will consider the evolution of curves on a given two-dimensional manifold $\mathcal{M} \subset \mathbb{R}^3$. We assume that $\mathcal{M}$ is given by a function $F \in C^2(\mathbb{R}^3)$ such that

$$\mathcal{M} = \{\vec{z} \in \mathbb{R}^3 : F(\vec{z}) = 0\} \qquad \text{and} \qquad |F'(\vec{z})| = 1 \quad \forall\ \vec{z} \in \mathcal{M}\,, \tag{2.17}$$

where here and throughout we use $\cdot'$ as a shorthand notation for the gradient ∇, and similarly $\cdot''$ for the matrix of second derivatives D^2. We set $\vec{n}_F(\vec{z}) := F'(\vec{z})$ to be the unit normal to $\mathcal{M}$. Then for a given closed curve Γ on $\mathcal{M}$, parameterized by $\vec{x} : I \to \mathcal{M}$, we define $\vec{\nu}_F(\rho) := \vec{n}_F(\vec{x}(\rho)) = F'(\vec{x}(\rho))$ as the unit normal to $\mathcal{M}$ evaluated at $\vec{x}(\rho)$, $\rho \in I$. We also set $\vec{\nu}_{\mathcal{M}} := \vec{x}_s \times F'(\vec{x}) = \vec{x}_s \times \vec{\nu}_F$ as the unit normal to Γ, which is a vector perpendicular to $\vec{x}_s$ lying in the tangent space to $\mathcal{M}$. We now define the L^2-gradient flow of the length $|\Gamma|$ for a closed curve $\Gamma \subset \mathcal{M}$. Here variations are restricted to lie on $\mathcal{M}$, and we choose $\vec{y} : I \times (-\varepsilon_0, \varepsilon_0) \to \mathcal{M}$ with $\vec{y}(\rho, 0) = \vec{x}(\rho)$ and $\vec{y}_\varepsilon(\cdot, 0) = \vec{\eta} \in \underline{V}_F$, where

$$\underline{V}_F := \{\vec{\eta} : I \to \mathbb{R}^d : \vec{\eta} \text{ is smooth and } \vec{\eta} \,.\, \vec{\nu}_F = 0\}\,. \tag{2.18}$$

The first variation of length now yields that

$$[\delta|\Gamma|](\vec{\eta}) = \int_\Gamma \vec{x}_s \,.\, \vec{\eta}_s \,\mathrm{d}s = -\int_\Gamma \vec{x}_{ss} \,.\, \vec{\eta}\,\mathrm{d}s = -\int_\Gamma \varkappa_{\mathcal{M}}\,\vec{\nu}_{\mathcal{M}} \,.\, \vec{\eta}\,\mathrm{d}s = -\int_\Gamma \vec{\varkappa}_{\mathcal{M}} \,.\, \vec{\eta}\,\mathrm{d}s\,.$$

Here $\varkappa_{\mathcal{M}}$ is the geodesic curvature, and $\vec{\varkappa}_{\mathcal{M}} \equiv \varkappa_{\mathcal{M}}\,\vec{\nu}_{\mathcal{M}}$ is the geodesic curvature vector. Since $\vec{\eta} \in \underline{V}_F$ lies in the tangent space of $\mathcal{M}$ and $\vec{x}_{ss}$ is perpendicular to $\vec{x}_s$, we obtain that the projection of $\vec{x}_{ss}$ onto the tangent space of $\mathcal{M}$ is parallel to $\vec{\nu}_{\mathcal{M}}$. Hence the above representation follows. Of course $\vec{x}_{ss}$, in general, does not lie in the tangent space to $\mathcal{M}$, and we introduce also the normal curvature $\varkappa_F$ and obtain that

$$\vec{x}_{ss} = \varkappa_{\mathcal{M}}\,\vec{\nu}_{\mathcal{M}} + \varkappa_F\,\vec{\nu}_F\,.$$

Now the L^2-gradient flow of length on a manifold $\mathcal{M}$ is given as

$$\vec{P}_{\mathcal{M}}\,\vec{x}_t = \vec{\varkappa}_{\mathcal{M}}\,,$$

where $\vec{P}_{\mathcal{M}}\,\vec{\chi} := (\vec{\chi}\,.\,\vec{\nu}_{\mathcal{M}})\,\vec{\nu}_{\mathcal{M}}$. Obviously, this is equivalent to

$$\mathcal{V}_{\mathcal{M}} := \vec{x}_t \,.\, \vec{\nu}_{\mathcal{M}} = \varkappa_{\mathcal{M}}\,, \tag{2.19}$$

where of course $\vec{x}_t$ is restricted to lie in the tangent space to $\mathcal{M}$, i.e. $\vec{x}_t \in \underline{V}_F$. Since geodesics are stationary solutions to geodesic curvature flow, one can try to use the flow to compute geodesics as long time limits. We will show that this is possible, e.g. in cases where the initial data are not homotopic to a point; see Section 5.

Geodesic surface diffusion

In order to define geodesic surface diffusion, we need to define an H^{-1}-inner product. As the projection $\vec{P}_{\mathcal{M}}$ has a one-dimensional range, it is enough to define an H^{-1}-inner product on scalar functions. For $\chi, \eta : \Gamma \to \mathbb{R}$ with $\int_\Gamma \chi\,\mathrm{d}s = \int_\Gamma \eta\,\mathrm{d}s = 0$, we set

$$(\chi,\eta)_{-1} := \int_\Gamma \partial_s\,[(-\partial_{ss})^{-1}\chi]\,\partial_s\,[(-\partial_{ss})^{-1}\eta]\,\mathrm{d}s = \int_\Gamma \chi\,(-\partial_{ss})^{-1}\eta\,\mathrm{d}s\,,$$

where $(-\partial_{ss})^{-1}\eta$ is a solution of $-u_{ss} = \eta$. The H^{-1}-gradient flow is then given as

$$(-\partial_{ss})^{-1}(\vec{x}_t \,.\, \vec{\nu}_{\mathcal{M}}) = \varkappa_{\mathcal{M}} \quad \Leftrightarrow \quad \vec{x}_t \,.\, \vec{\nu}_{\mathcal{M}} = -(\varkappa_{\mathcal{M}})_{ss}\,, \tag{2.20}$$

where we again require $\vec{x}_t \in \underline{V}_F$, in order to guarantee that $\vec{x}$ remains on $\mathcal{M}$ during the evolution. If we define geodesic surface diffusion with the help of a vector-valued inner product, we obtain the same flow. We leave the details to the reader.

Since geodesic surface diffusion is a gradient flow of length, we obtain that length decreases during the flow. For the planar case, see Elliott and Garcke (1997), the enclosed area, area(Γ), is preserved. The same holds true for geodesic surface diffusion, since

$$\frac{\mathrm{d}}{\mathrm{d}t}\,\mathrm{area}(\Gamma) = \int_\Gamma \vec{x}_t \,.\, \vec{\nu}_{\mathcal{M}}\,\mathrm{d}s = -\int_\Gamma (\varkappa_{\mathcal{M}})_{ss}\,\mathrm{d}s = 0\,, \tag{2.21}$$

where the first identity is shown in e.g. Barbosa, do Carmo, and Eschenburg (1988) or Garcke and Wieland (2006, (2.9)), and the second identity follows by integration since the curve is closed. We remark that the area preserving and length decreasing property leads to a flow which can be used to solve the following isoperimetric problem: Minimize the length of a closed curve amongst all curves enclosing a prescribed area.

Willmore flow of curves

An elastic energy for curves is given as

$$\mathcal{W}_\lambda(\Gamma) := \int_\Gamma (\tfrac{1}{2}\,|\vec{\varkappa}|^2 + \lambda)\,\mathrm{d}s\,, \tag{2.22}$$

where $\lambda \in \mathbb{R}$ is a given constant. We now consider the L^2-gradient flow of $\mathcal{W}_\lambda$, and hence we have to compute the first variation of $\mathcal{W}(\Gamma) := \frac{1}{2}\int_\Gamma |\vec{\varkappa}|^2\,\mathrm{d}s$. Since we want to generalize this idea later on, we firstly review a variant of computing the first variation of $\mathcal{W}(\Gamma)$, which was introduced in Dziuk (2007).

We consider variations $\vec{y} : I \times (-\varepsilon_0, \varepsilon_0) \to \mathbb{R}^d$ with $\vec{y}(\rho, 0) = \vec{x}(\rho)$ and $\vec{y}_\varepsilon(\rho, 0) = \vec{\chi}(\rho)$. Defining $\vec{\varkappa}(\rho, \varepsilon)$, $\varepsilon \in (-\varepsilon_0, \varepsilon_0)$, as the curvature vector of the curve parameterized by $\vec{y}(\rho, \varepsilon)$, we obtain that

$$[\delta\mathcal{W}(\Gamma)](\vec{\chi}) = \frac{\mathrm{d}}{\mathrm{d}\varepsilon}\mathcal{W}(\Gamma)\,|_{\varepsilon=0} = \int_\Gamma \vec{\varkappa}\,.\,\vec{\varkappa}_\varepsilon\,\mathrm{d}s + \tfrac{1}{2}\int_\Gamma |\vec{\varkappa}|^2\,\vec{x}_s\,.\,\vec{\chi}_s\,\mathrm{d}s\,, \tag{2.23}$$

where the last term arises from differentiating the arclength in $\int_\Gamma |\vec{\varkappa}|^2\,\mathrm{d}s \equiv \int_I |\vec{\varkappa}|^2\,|\vec{x}_\rho|\,\mathrm{d}\rho$. Of course, for ease of exposition there is abuse of notation here and below, since $\vec{\varkappa} \equiv \vec{\varkappa}(\cdot, 0)$ and $\vec{\varkappa}_\varepsilon \equiv \vec{\varkappa}_\varepsilon(\cdot, 0)$ in (2.23). Differentiating the identity

$$\int_I \frac{\vec{x}_\rho}{|\vec{x}_\rho|}\,.\,\vec{\eta}_\rho\,\mathrm{d}\rho = \int_\Gamma \vec{x}_s\,.\,\vec{\eta}_s\,\mathrm{d}s = -\int_\Gamma \vec{\varkappa}\,.\,\vec{\eta}\,\mathrm{d}s = -\int_I \vec{\varkappa}\,.\,\vec{\eta}\,|\vec{x}_\rho|\,\mathrm{d}\rho$$

with respect to ε, we obtain, on keeping $\vec{\eta} : \Gamma \to \mathbb{R}^d$ fixed, that

$$\int_\Gamma \vec{P}\,\vec{\chi}_s\,.\,\vec{\eta}_s\,\mathrm{d}s = -\int_\Gamma \vec{\varkappa}_\varepsilon\,.\,\vec{\eta}\,\mathrm{d}s - \int_\Gamma (\vec{\varkappa}\,.\,\vec{\eta})\,(\vec{x}_s\,.\,\vec{\chi}_s)\,\mathrm{d}s\,.$$

On choosing $\vec{\eta} = \vec{\varkappa}$ in the identity above, we derive from (2.23) that

$$\begin{aligned}[\delta\mathcal{W}(\Gamma)](\vec{\chi}) &= -\int_\Gamma \vec{\varkappa}_s\,.\,\vec{P}\,\vec{\chi}_s\,\mathrm{d}s - \tfrac{1}{2}\int_\Gamma |\vec{\varkappa}|^2\,\vec{x}_s\,.\,\vec{\chi}_s\,\mathrm{d}s = \int_\Gamma [(\vec{\nabla}_s\,\vec{\varkappa})_s + \tfrac{1}{2}\,(|\vec{\varkappa}|^2\,\vec{x}_s)_s]\,.\,\vec{\chi}\,\mathrm{d}s \\ &= \int_\Gamma (\vec{\nabla}_s^2\,\vec{\varkappa} + \tfrac{1}{2}\,|\vec{\varkappa}|^2\,\vec{\varkappa})\,.\,\vec{\chi}\,\mathrm{d}s\,, \end{aligned} \tag{2.24}$$

where $\vec{\nabla}_s\,\vec{\chi} = \vec{P}\,\vec{\chi}_s$, recall (2.10). Here the last identity follows since

$$\vec{\nabla}_s^2\,\vec{\varkappa} = (\vec{\nabla}_s\,\vec{\varkappa})_s - [(\vec{\nabla}_s\,\vec{\varkappa})_s\,.\,\vec{x}_s]\,\vec{x}_s = (\vec{\nabla}_s\vec{\varkappa})_s + (\vec{\varkappa}_s\,.\,\vec{\varkappa})\,\vec{x}_s\,,$$

where we have noted that $(\vec{\nabla}_s\,\vec{\varkappa})_s = \vec{\varkappa}_{ss} - (\vec{\varkappa}_s\,.\,\vec{x}_s)_s\,\vec{x}_s - (\vec{\varkappa}_s\,.\,\vec{x}_s)\,\vec{x}_{ss}$. Hence the L^2-gradient flow of $\mathcal{W}_\lambda(\Gamma)$ with respect to the inner product (2.3) is given as

$$\vec{P}\,\vec{x}_t = -(\vec{\nabla}_s\,\vec{\varkappa})_s - \tfrac{1}{2}\,(|\vec{\varkappa}|^2\,\vec{x}_s)_s + \lambda\,\vec{\varkappa} = -\vec{\nabla}_s^2\,\vec{\varkappa} - \tfrac{1}{2}\,|\vec{\varkappa}|^2\,\vec{\varkappa} + \lambda\,\vec{\varkappa}\,, \tag{2.25}$$

where we have noted the first two terms in the last integral in (2.24) are normal. The flow (2.25), in general for $\lambda = 0$, is called elastic flow of curves, or Willmore flow of curves. An alternative formulation replaces $\vec{P}\,\vec{x}_t$ by $\vec{x}_t$, see Dziuk, Kuwert, and Schätzle (2002) and Deckelnick and Dziuk (2007). A weak formulation of (2.25) can be obtained as follows. We find on testing the first equation in (2.25) with a test function $\vec{\eta} \in \underline{V}_{\vec{x}}$, integrating over Γ, using integration by parts for ∂_s, and noting that $\vec{\nabla}_s\,\vec{\varkappa}\,.\,\vec{\eta}_s = \vec{P}\,\vec{\varkappa}_s\,.\,\vec{\eta}_s = \vec{P}\,\vec{\varkappa}_s\,.\,\vec{P}\,\vec{\eta}_s = \vec{\nabla}_s\,\vec{\varkappa}\,.\,\vec{\nabla}_s\,\vec{\eta}$, that

$$\int_\Gamma (\vec{x}_t - \lambda\,\vec{\varkappa})\,.\,\vec{\eta}\,\mathrm{d}s - \int_\Gamma \vec{\nabla}_s\,\vec{\varkappa}\,.\,\vec{\nabla}_s\,\vec{\eta}\,\mathrm{d}s - \tfrac{1}{2}\int_\Gamma |\vec{\varkappa}|^2\,\vec{x}_s\,.\,\vec{\eta}_s\,\mathrm{d}s = 0 \quad \forall\ \vec{\eta} \in \underline{V}_{\vec{x}}\,, \tag{2.26a}$$

$$\int_\Gamma \vec{\varkappa}\,.\,\vec{\eta}\,\mathrm{d}s + \int_\Gamma \vec{x}_s\,.\,\vec{\eta}_s\,\mathrm{d}s = 0 \quad \forall\ \vec{\eta}\,, \tag{2.26b}$$

where $\vec{\varkappa} \in \underline{V}_{\vec{x}}$ as usual. Finally, we note that the energy (2.22) with $\lambda = 0$ can be reduced by scaling, as e.g. an expanding circle continuously reduces the energy $\mathcal{W}_\lambda$, and that a parameter $\lambda > 0$ acts as a penalization term for growth in the curve's length. Hence it is also of interest to study a length preserving gradient flow of $\mathcal{W}$. This can be achieved by choosing a time dependent $\lambda(t)$ in (2.25), such that $\int_\Gamma \vec{x}_t\,.\,\vec{\varkappa}\,\mathrm{d}s = 0$, recall (2.2), which leads to

$$\lambda(t) = -\frac{\frac{1}{2}\int_\Gamma |\vec{\varkappa}|^2\,\vec{x}_s\,.\,\vec{\varkappa}_s\,\mathrm{d}s + \int_\Gamma |\vec{\nabla}_s\,\vec{\varkappa}|^2\,\mathrm{d}s}{\int_\Gamma |\vec{\varkappa}|^2\,\mathrm{d}s}\,. \tag{2.27}$$

Geodesic Willmore flow of curves

We now consider an elastic energy for curves, which are restricted to lie on a two dimensional manifold $\mathcal{M}$ in $\mathbb{R}^3$ as above. We define

$$\mathcal{W}_{\mathcal{M},\lambda}(\Gamma) := \int_\Gamma (\tfrac{1}{2}\,|\vec{\varkappa}_{\mathcal{M}}|^2 + \lambda)\,\mathrm{d}s\,,$$

and $\mathcal{W}_{\mathcal{M}}(\Gamma) := \frac{1}{2}\int_\Gamma |\vec{\varkappa}_{\mathcal{M}}|^2\,\mathrm{d}s$. Here we recall that $|\vec{\varkappa}_{\mathcal{M}}|^2 = (\varkappa_{\mathcal{M}})^2$, where $\varkappa_{\mathcal{M}}$ is the geodesic curvature. In what follows we will need the second fundamental form $\mathrm{I\!I}$ of $\mathcal{M}$, which is given as

$$\mathrm{I\!I}_{\vec{z}}(\vec{\tau}_1, \vec{\tau}_2) := -[\partial_{\vec{\tau}_1}\,\vec{n}_F(\vec{z})]\,.\,\vec{\tau}_2 = -F''(\vec{z})\,\vec{\tau}_1\,.\,\vec{\tau}_2 \quad \forall\ \vec{\tau}_1, \vec{\tau}_2 \in \mathcal{T}_{\vec{z}}\mathcal{M}\,, \quad \vec{z} \in \mathcal{M}\,, \tag{2.28}$$

where $\mathcal{T}_{\vec{z}}\mathcal{M}$ denotes the tangent space of $\mathcal{M}$ at $\vec{z}$. We note that $\mathrm{I\!I}_{\vec{z}}(\cdot,\cdot)$ is a symmetric bilinear form. We will need also the Gauß curvature $\mathcal{K}$ of $\mathcal{M}$, which is given by $\mathcal{K}(\vec{z}) := \det\left(\mathrm{I\!I}_{\vec{z}}(\vec{\tau}_i, \vec{\tau}_j)\right)_{i,j=1}^2$, where $\vec{\tau}_1$, $\vec{\tau}_2 \in \mathcal{T}_{\vec{z}}\mathcal{M}$ are two orthonormal vectors. Hence on Γ we can compute the Gauß curvature of $\mathcal{M}$ as

$$\mathcal{K}(\vec{x}) = \mathrm{I\!I}(\vec{x}_s, \vec{x}_s)\,\mathrm{I\!I}(\vec{\nu}_{\mathcal{M}}, \vec{\nu}_{\mathcal{M}}) - \mathrm{I\!I}(\vec{x}_s, \vec{\nu}_{\mathcal{M}})\,\mathrm{I\!I}(\vec{\nu}_{\mathcal{M}}, \vec{x}_s)\,, \tag{2.29}$$

where, here and throughout, we suppress the subscript $\vec{x}$ of $\mathrm{I\!I}$.

In the following theorem the first variation of $\mathcal{W}_{\mathcal{M}}(\Gamma)$ is computed. We refer to Langer and Singer (1984) for an alternative approach. However, the version presented here has the advantage that we directly obtain a weak formulation.

THEOREM. 2.1. *The first variation of $\mathcal{W}_{\mathcal{M}}(\Gamma)$ in a direction $\vec{\chi} \in \underline{V}_F$, recall (2.18), is given as*

$$[\delta \mathcal{W}_{\mathcal{M}}(\Gamma)](\vec{\chi}) = -\int_\Gamma [(\vec{\varkappa}_{\mathcal{M}})_s \,.\, \vec{P}\,\vec{\chi}_s + \tfrac{1}{2}\,|\vec{\varkappa}_{\mathcal{M}}|^2\,\vec{x}_s \,.\, \vec{\chi}_s - \varkappa_{\mathcal{M}}\,\varkappa_F\,\mathrm{I\!I}(\vec{\chi},\vec{\nu}_{\mathcal{M}})]\,\mathrm{d}s\,, \tag{2.30a}$$

or equivalently

$$[\delta \mathcal{W}_{\mathcal{M}}(\Gamma)](\vec{\chi}) = \int_\Gamma ((\varkappa_{\mathcal{M}})_{ss} + \tfrac{1}{2}\,(\varkappa_{\mathcal{M}})^3 + \mathcal{K}\,\varkappa_{\mathcal{M}})\,(\vec{\chi}\,.\,\vec{\nu}_{\mathcal{M}})\,\mathrm{d}s\,. \tag{2.30b}$$

Proof. Let $\vec{y}(\rho,\varepsilon) \in \mathcal{M}$ be a variation of a curve Γ such that $\vec{y}(\rho,0) = \vec{x}(\rho)$ and $\vec{y}_\varepsilon(\cdot,0) = \vec{\chi} \in \underline{V}_F$. We compute

$$\frac{\mathrm{d}}{\mathrm{d}\varepsilon}\int_\Gamma \tfrac{1}{2}\,|\vec{\varkappa}_{\mathcal{M}}|^2\,\mathrm{d}s\,|_{\varepsilon=0} = \int_\Gamma \vec{\varkappa}_{\mathcal{M}}\,.\,(\vec{\varkappa}_{\mathcal{M}})_\varepsilon\,\mathrm{d}s + \int_\Gamma \tfrac{1}{2}\,|\vec{\varkappa}_{\mathcal{M}}|^2\,\vec{x}_s\,.\,\vec{\chi}_s\,\mathrm{d}s\,,$$

with a similar abuse of notation, here and below, as in (2.23). The geodesic curvature $\varkappa_{\mathcal{M}}$ and the normal curvature $\varkappa_F$ are given via

$$\int_\Gamma (\varkappa_{\mathcal{M}}\,\vec{\nu}_{\mathcal{M}} + \varkappa_F\,\vec{\nu}_F)\,.\,\vec{\eta}\,\mathrm{d}s + \int_\Gamma \vec{x}_s\,.\,\vec{\eta}_s\,\mathrm{d}s = 0$$

which has to hold for all $\vec{\eta} : I \to \mathbb{R}^3$. Writing this identity as an integral over I, we obtain after differentiation with respect to ε that

$$\begin{aligned}\int_\Gamma [\,(\varkappa_{\mathcal{M}})_\varepsilon\,\vec{\nu}_{\mathcal{M}} + \varkappa_{\mathcal{M}}\,(\vec{\nu}_{\mathcal{M}})_\varepsilon + (\varkappa_F)_\varepsilon\,\vec{\nu}_F + \varkappa_F\,(\vec{\nu}_F)_\varepsilon\,]\,.\,\vec{\eta}\,\mathrm{d}s \\ + \int_\Gamma ([\varkappa_{\mathcal{M}}\,\vec{\nu}_{\mathcal{M}} + \varkappa_F\,\vec{\nu}_F]\,.\,\vec{\eta})\,(\vec{x}_s\,.\,\vec{\chi}_s)\,\mathrm{d}s + \int_\Gamma \vec{P}\,\vec{\chi}_s\,.\,\vec{\eta}_s\,\mathrm{d}s = 0\,.\end{aligned}$$

We now choose $\vec{\eta} = \vec{\varkappa}_{\mathcal{M}} \equiv \varkappa_{\mathcal{M}}\,\vec{\nu}_{\mathcal{M}}$ and use the identities $(\vec{\nu}_{\mathcal{M}})_\varepsilon\,.\,\vec{\nu}_{\mathcal{M}} = 0$ and $\vec{\nu}_F\,.\,\vec{\nu}_{\mathcal{M}} = 0$ to obtain that

$$\int_\Gamma (\varkappa_{\mathcal{M}})_\varepsilon\,\varkappa_{\mathcal{M}} + \varkappa_F\,\varkappa_{\mathcal{M}}\,(\vec{\nu}_F)_\varepsilon\,.\,\vec{\nu}_{\mathcal{M}})\,\mathrm{d}s + \int_\Gamma |\vec{\varkappa}_{\mathcal{M}}|^2\,\vec{x}_s\,.\,\vec{\chi}_s\,\mathrm{d}s + \int_\Gamma (\vec{\varkappa}_{\mathcal{M}})_s\,.\,\vec{P}\,\vec{\chi}_s = 0\,.$$

Since $(\vec{\nu}_F)_\varepsilon\,.\,\vec{\nu}_{\mathcal{M}} = -\mathrm{I\!I}(\vec{y}_\varepsilon(\cdot,0),\vec{\nu}_{\mathcal{M}}) = -\mathrm{I\!I}(\vec{\chi},\vec{\nu}_{\mathcal{M}})$ we obtain (2.30a).

Integration by parts yields, as $\vec{\chi} \in \underline{V}_F$, that

$$\begin{aligned}-\int_\Gamma \tfrac{1}{2}\,|\vec{\varkappa}_{\mathcal{M}}|^2\,\vec{x}_s\,.\,\vec{\chi}_s\,\mathrm{d}s &= \int_\Gamma \vec{\varkappa}_{\mathcal{M}}\,.\,(\vec{\varkappa}_{\mathcal{M}})_s\,(\vec{x}_s\,.\,\vec{\chi})\,\mathrm{d}s + \int_\Gamma \tfrac{1}{2}\,|\vec{\varkappa}_{\mathcal{M}}|^2\,\vec{x}_{ss}\,.\,\vec{\chi}\,\mathrm{d}s \\ &= \int_\Gamma \vec{\varkappa}_{\mathcal{M}}\,.\,(\vec{\varkappa}_{\mathcal{M}})_s\,(\vec{x}_s\,.\,\vec{\chi})\,\mathrm{d}s + \int_\Gamma \tfrac{1}{2}\,(\varkappa_{\mathcal{M}})^3\,(\vec{\nu}_{\mathcal{M}}\,.\,\vec{\chi})\,\mathrm{d}s\,,\end{aligned}$$

and that

$$\int_\Gamma (\vec{\varkappa}_{\mathcal{M}})_s\,.\,\vec{P}\,\vec{\chi}_s\,\mathrm{d}s = -\int_\Gamma (\vec{P}\,(\vec{\varkappa}_{\mathcal{M}})_s)_s\,.\,\vec{\chi}\,\mathrm{d}s\,.$$

It follows that

$$(\vec{P}(\vec{\varkappa}_{\mathcal{M}})_s)_s = (\varkappa_{\mathcal{M}})_{ss}\,\vec{\nu}_{\mathcal{M}} + (\varkappa_{\mathcal{M}})_s\,(\vec{\nu}_{\mathcal{M}})_s + (\varkappa_{\mathcal{M}})_s\,\vec{P}\,(\vec{\nu}_{\mathcal{M}})_s + \varkappa_{\mathcal{M}}\,(\vec{P}\,(\vec{\nu}_{\mathcal{M}})_s)_s\,.$$

Since $(\vec{\nu}_{\mathcal{M}})_s\,.\,\vec{\nu}_{\mathcal{M}} = 0$ and since $\vec{\chi}$, $\vec{\nu}_{\mathcal{M}} \in \underline{V}_F$, we obtain that $\vec{P}\,(\vec{\nu}_{\mathcal{M}})_s\,.\,\vec{\chi} = 0$, and hence that

$$\begin{aligned}(\vec{P}\,(\vec{\nu}_{\mathcal{M}})_s)_s\,.\,\vec{\chi} &= ([(\vec{\nu}_{\mathcal{M}})_s\,.\,\vec{\nu}_F]\,\vec{\nu}_F)_s\,.\,\vec{\chi} = ((\vec{\nu}_{\mathcal{M}})_s\,.\,\vec{\nu}_F)\,((\vec{\nu}_F)_s\,.\,\vec{\chi}) = -(\vec{\nu}_{\mathcal{M}}\,.\,(\vec{\nu}_F)_s)\,((\vec{\nu}_F)_s\,.\,\vec{\chi})\\ &= -\mathrm{I\!I}(\vec{\nu}_{\mathcal{M}},\vec{x}_s)\,\mathrm{I\!I}(\vec{\chi},\vec{x}_s)\,.\end{aligned}$$

Similarly, on noting that $\vec{\chi} = (\vec{\chi}\,.\,\vec{x}_s)\,\vec{x}_s + (\vec{\chi}\,.\,\vec{\nu}_{\mathcal{M}})\,\vec{\nu}_{\mathcal{M}}$, we have that

$$\begin{aligned}(\varkappa_{\mathcal{M}})_s\,(\vec{\nu}_{\mathcal{M}})_s\,.\,\vec{\chi} &= (\varkappa_{\mathcal{M}})_s\,((\vec{\nu}_{\mathcal{M}})_s\,.\,\vec{x}_s)\,(\vec{\chi}\,.\,\vec{x}_s) = -(\varkappa_{\mathcal{M}})_s\,(\vec{\nu}_{\mathcal{M}}\,.\,\vec{x}_{ss})\,(\vec{\chi}\,.\,\vec{x}_s)\\ &= -(\varkappa_{\mathcal{M}})_s\,\varkappa_{\mathcal{M}}\,(\vec{\chi}\,.\,\vec{x}_s) = -(\vec{\varkappa}_{\mathcal{M}})_s\,.\,\vec{\varkappa}_{\mathcal{M}}\,(\vec{\chi}\,.\,\vec{x}_s)\,.\end{aligned} \tag{2.31}$$

Combining the above identities yields that

$$\begin{aligned}[\delta\mathcal{W}_{\mathcal{M}}(\Gamma)](\vec{\chi}) = \int_\Gamma ((\varkappa_{\mathcal{M}})_{ss} + \tfrac{1}{2}\,(\varkappa_{\mathcal{M}})^3)\,(\vec{\chi}\cdot\vec{\nu}_{\mathcal{M}})\,\mathrm{d}s\\ + \int_\Gamma \varkappa_{\mathcal{M}}\,[\mathrm{I\!I}(\vec{x}_s,\vec{x}_s)\,\mathrm{I\!I}(\vec{\chi},\vec{\nu}_{\mathcal{M}}) - \mathrm{I\!I}(\vec{\nu}_{\mathcal{M}},\vec{x}_s)\,\mathrm{I\!I}(\vec{\chi},\vec{x}_s)]\;\mathrm{d}s,\end{aligned}$$

where we have noted that $\mathrm{I\!I}(\vec{x}_s,\vec{x}_s) = \vec{\nu}_F\,.\,\vec{x}_{ss} = \varkappa_F$. Finally, noting the decomposition of $\vec{\chi}$ as used in (2.31) above and on recalling (2.29), we have that

$$\begin{aligned}&\mathrm{I\!I}(\vec{x}_s,\vec{x}_s)\,\mathrm{I\!I}(\vec{\chi},\vec{\nu}_{\mathcal{M}}) - \mathrm{I\!I}(\vec{\nu}_{\mathcal{M}},\vec{x}_s)\,\mathrm{I\!I}(\vec{\chi},\vec{x}_s)\\ &\qquad= (\vec{\chi}\,.\,\vec{\nu}_{\mathcal{M}})\,[\mathrm{I\!I}(\vec{x}_s,\vec{x}_s)\,\mathrm{I\!I}(\vec{\nu}_{\mathcal{M}},\vec{\nu}_{\mathcal{M}}) - \mathrm{I\!I}(\vec{x}_s,\vec{\nu}_{\mathcal{M}})\,\mathrm{I\!I}(\vec{\nu}_{\mathcal{M}},\vec{x}_s)]\\ &\qquad\quad+ (\vec{\chi}\,.\,\vec{x}_s)\,[\mathrm{I\!I}(\vec{x}_s,\vec{x}_s)\,\mathrm{I\!I}(\vec{x}_s,\vec{\nu}_{\mathcal{M}}) - \mathrm{I\!I}(\vec{\nu}_{\mathcal{M}},\vec{x}_s)\,\mathrm{I\!I}(\vec{x}_s,\vec{x}_s)] = (\vec{\chi}\,.\,\vec{\nu}_{\mathcal{M}})\,\mathcal{K}\,.\end{aligned}$$

Hence combining the above identities yields the desired result (2.30b). □

The L^2-gradient flow of the elastic energy $\mathcal{W}_{\mathcal{M},\lambda}(\Gamma)$ is hence given as

$$\mathcal{V}_{\mathcal{M}} = \vec{x}_t\,.\,\vec{\nu}_{\mathcal{M}} = -(\varkappa_{\mathcal{M}})_{ss} - \tfrac{1}{2}\,(\varkappa_{\mathcal{M}})^3 + (\lambda - \mathcal{K})\,\varkappa_{\mathcal{M}}\,. \tag{2.32}$$

Obviously Theorem 2.1 can be used to formulate a weak formulation of this gradient flow equation. The flow (2.32) can be applied to compute periodic geodesics, i.e. curves with zero geodesic Willmore energy, $\mathcal{W}_{\mathcal{M}}(\Gamma) = 0$, see e.g. Linnér and Renka (2005). In particular, it is possible to compute closed geodesics also in cases where the initial curve is homotopic to a point. A situation which is of course always the case if the manifold is diffeomorphic to a sphere. In such a case, the geodesic curvature flow cannot be used in general to compute closed geodesics, but the flow (2.32) can be generically used; see Langer and Singer (1984) or Linnér and Renka (2005) for more information. Finally, a length preserving flow of (2.32), similarly to (2.25) with (2.27), can also be considered.

Anisotropic flows

Here we give a short overview on how to extend some of the previously introduced geometric evolution equations to the case of anisotropic surface energy densities. We start with the simplest flow, i.e. curve shorting flow in $\mathbb{R}^d$, $d \geq 2$.

In many applications the energy of a surface in $\mathbb{R}^d$ depends locally on the orientation in space. For the case of curves in $\mathbb{R}^d$, $d \geq 2$, the local orientation is given by the unit tangent $\vec{x}_s$. Hence we introduce an anisotropic surface energy of the form

$$|\Gamma|_\phi := \int_\Gamma \phi(\vec{x}_s)\, \mathrm{d}s\,,$$

where $\Gamma \subset \mathbb{R}^d$ is a closed curve and $\phi \in C^2(\mathbb{R}^d \setminus \{\vec{0}\}, \mathbb{R}_{>0}) \cap C(\mathbb{R}^d, \mathbb{R}_{\geq 0})$ is a given anisotropic energy density, cf. also Pozzi (2007). In this paper, we assume that the function ϕ is absolutely homogeneous of degree one, i.e.

$$\phi(\lambda\, \vec{p}) = |\lambda|\, \phi(\vec{p}) \quad \forall\, \vec{p} \in \mathbb{R}^d\,,\ \forall\, \lambda \in \mathbb{R}\,.$$

The one-homogeneity immediately implies that

$$\phi'(\vec{p})\,.\,\vec{p} = \phi(\vec{p}) \quad \text{and} \quad \phi''(\vec{p})\,\vec{p} = \vec{0} \qquad \forall\, \vec{p} \in \mathbb{R}^d \setminus \{\vec{0}\}\,, \tag{2.33}$$

where we recall that ϕ' denotes the gradient and ϕ'' the matrix of second derivatives of ϕ. In the isotropic case we have that $\phi(\vec{p}) = |\vec{p}|$ and so $\phi(\vec{x}_s) = 1$, which means that $|\Gamma|_\phi$ reduces to $|\Gamma|$, the length of Γ. For an introduction to anisotropic surface energies in general, and to Wulff shapes in particular, we refer to Giga (2006), Deckelnick, Dziuk, and Elliott (2005) and the references therein.

The first variation of $|\Gamma|_\phi$ is derived analogously to the isotropic case, recall (2.2), as

$$[\delta|\Gamma|_\phi](\vec{\eta}) = \int_\Gamma \phi'(\vec{x}_s)\,.\,\vec{\eta}_s\, \mathrm{d}s = -\int_\Gamma [\phi'(\vec{x}_s)]_s\,.\,\vec{\eta}\, \mathrm{d}s\,.$$

The quantity $\vec{\varkappa}_\phi := [\phi'(\vec{x}_s)]_s$ can be viewed as an anisotropic curvature vector, and we obtain that

$$\vec{P}\,\vec{x}_t = [\phi'(\vec{x}_s)]_s = \vec{\varkappa}_\phi \tag{2.34}$$

as the gradient flow of $|\Gamma|_\phi$ with respect to the inner product $(\cdot,\cdot)_{2,nor}$. Here we have noted that $\vec{\varkappa}_\phi = \phi''(\vec{x}_s)\,\vec{\varkappa} \in \underline{V}_{\vec{\tau}}$, on recalling from (2.33) that $\phi''(\vec{x}_s)\,\vec{x}_s = \vec{0}$. The flow (2.34) is called anisotropic curve shortening flow and is the natural anisotropic analogue of (2.4).

Similarly, one can introduce anisotropic curve diffusion

$$\vec{P}\,\vec{x}_t = -\vec{\nabla}_s^{\,2}\,\vec{\varkappa}_\phi \tag{2.35}$$

as the H^{-1}-gradient flow of $|\Gamma|_\phi$. Moreover, it is possible to define the natural anisotropic analogues of the previously introduced geodesic curve shortening and geodesic surface diffusion flow. We leave the details to the interested reader.

In addition, the gradient flow for an anisotropic version of (2.22) is of interest; see e.g. Clarenz (2004) and Diewald (2005), where the corresponding energy for hypersurfaces in $\mathbb{R}^3$ is treated. Similarly to (2.24), the first variation of the anisotropic Willmore energy

$$\mathcal{W}_\phi(\Gamma) := \tfrac{1}{2} \int_\Gamma |\vec{\varkappa}_\phi|^2\, \mathrm{d}s$$

can be computed as

$$[\delta\mathcal{W}_\phi(\Gamma)](\vec{\chi}) = \frac{\mathrm{d}}{\mathrm{d}\varepsilon}\mathcal{W}_\phi(\Gamma)\,|_{\varepsilon=0} = \int_\Gamma \vec{\varkappa}_\phi \,.\, \vec{\varkappa}_{\phi,\varepsilon}\,\mathrm{d}s + \tfrac{1}{2}\int_\Gamma |\vec{\varkappa}_\phi|^2\,\vec{x}_s\,.\,\vec{\chi}_s\,\mathrm{d}s\,,$$

where we have adopted the same notation as in (2.23). Analogously to the isotropic case, we then obtain, on recalling (2.33), that

$$\begin{aligned}[\delta\mathcal{W}_\phi(\Gamma)](\vec{\chi}) &= -\int_\Gamma [\phi''(\vec{x}_s)\,(\vec{\varkappa}_\phi)_s]\,.\,\vec{\chi}_s\,\mathrm{d}s - \tfrac{1}{2}\int_\Gamma |\vec{\varkappa}_\phi|^2\,\vec{x}_s\,.\,\vec{\chi}_s\,\mathrm{d}s\\ &= \int_\Gamma [(\phi''(\vec{x}_s)\,(\vec{\varkappa}_\phi)_s)_s + \tfrac{1}{2}\,(|\vec{\varkappa}_\phi|^2\,\vec{x}_s)_s]\,.\,\vec{\chi}\,\mathrm{d}s\,. \end{aligned} \tag{2.36}$$

On noting that in the isotropic case, $\phi(\vec{p}) = |\vec{p}|$, we have that $\phi''(\vec{x}_s) = \vec{P}$, we see that (2.36) is the natural anisotropic analogue of (2.24). Hence the L^2-gradient flow of

$$\mathcal{W}_{\phi,\lambda}(\Gamma) := \mathcal{W}_\phi(\Gamma) + \lambda\,|\Gamma|_\phi$$

with respect to the inner product (2.3) is given as

$$\vec{P}\,\vec{x}_t = -(\phi''(\vec{x}_s)\,(\vec{\varkappa}_\phi)_s)_s - \tfrac{1}{2}\,(|\vec{\varkappa}_\phi|^2\,\vec{x}_s)_s + \lambda\,\vec{\varkappa}_\phi\,, \tag{2.37}$$

where as in the isotropic case, we use the fact that the term in square brackets in the last integral in (2.36) is normal.

Naturally, an anisotropic version of (2.32) can also be computed. On defining the anisotropic geodesic curvature vector by $\vec{\varkappa}_{\phi,\mathcal{M}} := \varkappa_{\phi,\mathcal{M}}\,\vec{\nu}_{\mathcal{M}}$, where $\varkappa_{\phi,\mathcal{M}} := \vec{\varkappa}_\phi\,.\,\vec{\nu}_{\mathcal{M}}$ and similarly $\varkappa_{\phi,F} := \vec{\varkappa}_\phi\,.\,\vec{\nu}_F$, we obtain the first variation of $\mathcal{W}_{\phi,\mathcal{M}}(\Gamma) := \frac{1}{2}\int_\Gamma |\vec{\varkappa}_{\phi,\mathcal{M}}|^2\,\mathrm{d}s$ in a direction $\vec{\chi} \in \underline{V}_F$, similarly to (2.30a), as

$$[\delta\mathcal{W}_{\phi,\mathcal{M}}(\Gamma)](\vec{\chi}) = -\int_\Gamma \left[[\phi''(\vec{x}_s)\,(\vec{\varkappa}_{\phi,\mathcal{M}})_s]\,.\,\vec{\chi}_s + \tfrac{1}{2}\,|\vec{\varkappa}_{\phi,\mathcal{M}}|^2\,\vec{x}_s\,.\,\vec{\chi}_s - \varkappa_{\phi,\mathcal{M}}\,\varkappa_{\phi,F}\,\mathrm{I\!I}(\vec{\chi},\vec{\nu}_{\mathcal{M}})\right]\,\mathrm{d}s\,. \tag{2.38}$$

A wide class of anisotropies can either be modelled or at least very well approximated by, see Barrett, Garcke, and Nürnberg (2008c),

$$\phi(\vec{p}) = \sum_{\ell=1}^{L}\phi_\ell(\vec{p}) = \sum_{\ell=1}^{L}\sqrt{\vec{p}\,.\,\vec{G}_\ell\,\vec{p}} \quad\Rightarrow\quad \phi'(\vec{p}) = \sum_{\ell=1}^{L}[\phi_\ell(\vec{p})]^{-1}\,\vec{G}_\ell\,\vec{p} \quad \forall\ \vec{p} \in \mathbb{R}^d\setminus\{\vec{0}\}\,, \tag{2.39}$$

where $\vec{G}_\ell \in \mathbb{R}^{d\times d}$, $\ell = 1 \to L$, are symmetric and positive definite; and in this paper we will restrict our analysis to anisotropies of the form (2.39). For later purposes, we note for all $\vec{p} \in \mathbb{R}^d\setminus\{\vec{0}\}$ that

$$\phi''(\vec{p}) = \sum_{\ell=1}^{L}[\phi_\ell(\vec{p})]^{-1}\left[\vec{Id} - [\phi_\ell(\vec{p})]^{-2}\,(\vec{G}_\ell\,\vec{p})\otimes\vec{p}\right]\vec{G}_\ell \tag{2.40}$$

is positive semi-definite. In the recent paper Barrett, Garcke, and Nürnberg (2008a), we introduced parametric finite element approximations for anisotropic geometric evolution equations in the plane, i.e. $d = 2$; and showed that for the class of anisotropy densities that correspond to the choice (2.39), unconditionally stable fully discrete approximations are obtained. In the present paper, this analysis will be extended to the flow of curves in $\mathbb{R}^d$, $d \geq 3$, as well as to the anisotropic geodesic flows mentioned above.

3 Finite Element Approximation

In this section we introduce finite element approximations of the curvature flows discussed in Section 2. We will use the variational structure of the flows and aim to generalize the approach introduced in Barrett, Garcke, and Nürnberg (2007b) in a way that one still has good mesh properties, so that no heuristic remeshing will be required in practice.

We introduce the decomposition $I = \cup_{j=1}^{J} I_j$, $J \geq 3$ of $I = \mathbb{R}/\mathbb{Z}$ into intervals given by the nodes $q_j, I_j = [q_{j-1}, q_j]$. Let $h_j = |I_j|$ and $h = \max_{j=1\to J} h_j$ be the maximal length of a grid element. Then the necessary finite element spaces are defined as follows

$$\underline{V}^h := \{\vec{\chi} \in C(I, \mathbb{R}^d) : \vec{\chi}|_{I_j} \text{ is linear } \forall\ j = 1 \to J\} =: [W^h]^d \subset H^1(I, \mathbb{R}^d),$$

where $W^h \subset H^1(I, \mathbb{R})$ is the space of scalar continuous (periodic) piecewise linear functions, with $\{\chi_j\}_{j=1}^J$ denoting the standard basis of W^h. In addition, let $\vec{\pi}^h : C(I, \mathbb{R}^d) \to \underline{V}^h$ be the standard Lagrange interpolation operator. Throughout this paper, we make use of the periodicity of I, i.e. $q_J \equiv q_0$, $q_{J+1} \equiv q_1$ and so on. In addition, let $0 = t_0 < t_1 < \ldots < t_{M-1} < t_M = T$ be a partitioning of $[0, T]$ into possibly variable time steps $\tau_m := t_{m+1} - t_m$, $m = 0 \to M-1$. We set $\tau := \max_{m=0\to M-1} \tau_m$.

For scalar and vector functions $u, v \in L^2(I, \mathbb{R}^{(d)})$ we introduce the L^2-inner product $\langle \cdot, \cdot \rangle_m$ over the current polygonal curve Γ^m, which is described by the vector function $\vec{X}^m \in \underline{V}^h$, as follows

$$\langle u, v \rangle_m := \int_{\Gamma^m} u \,.\, v \,\mathrm{d}s = \int_I u \,.\, v\, |\vec{X}^m_\rho| \,\mathrm{d}\rho\,.$$

Here and throughout this paper, $\cdot^{(*)}$ denotes an expression with or without the superscript $*$, and similarly for subscripts. In addition, if u, v are piecewise continuous, with possible jumps at the nodes $\{q_j\}_{j=1}^J$, we define the mass lumped inner product $\langle \cdot, \cdot \rangle_m^h$ as

$$\langle u, v \rangle_m^h := \tfrac{1}{2} \sum_{j=1}^{J} |\vec{X}^m(q_j) - \vec{X}^m(q_{j-1})| \left[(u \,.\, v)(q_j^-) + (u \,.\, v)(q_{j-1}^+) \right],$$

where we define $u(q_j^\pm) := \lim_{\varepsilon \searrow 0} u(q_j \pm \varepsilon)$. Furthermore, we note that on Γ^m we have almost everywhere that

$$u_s \,.\, v_s = \frac{u_\rho \,.\, v_\rho}{|\vec{X}^m_\rho|^2} \qquad \text{and} \qquad \vec{\nabla}_s \,\vec{u} \,.\, \vec{\nabla}_s \,\vec{v} = \frac{\vec{P}^m \,\vec{u}_\rho \,.\, \vec{P}^m \,\vec{v}_\rho}{|\vec{X}^m_\rho|^2} = \frac{\vec{P}^m \,\vec{u}_\rho \,.\, \vec{v}_\rho}{|\vec{X}^m_\rho|^2}\,, \tag{3.1}$$

where $\vec{P}^m = \vec{Id} - \vec{X}^m_s \otimes \vec{X}^m_s$. In addition, let $\vec{\omega}_d^m(q_j) := \frac{\vec{X}^m(q_{j+1}) - \vec{X}^m(q_{j-1})}{|\vec{X}^m(q_{j+1}) - \vec{X}^m(q_{j-1})|}$ be the discrete nodal tangent vector of Γ^m at the node $\vec{X}(q_j)$, which we assume to be well defined for $j = 1 \to J$; see our assumption $(\mathcal{C})$ below. Then we define the following subspace of $\underline{V}^h$:

$$\underline{V}^{h,m}_{\vec{\tau}} := \{\vec{\eta} \in \underline{V}^h : \vec{\eta}(q_j) \,.\, \vec{\omega}_d^m(q_j) = 0, \quad j = 1 \to J\}\,. \tag{3.2}$$

Note that $\underline{V}^{h,m}_{\vec{\tau}}$ is a discrete analogue of (2.7).

3.1 The isotropic case

Curve shortening flow

On employing a backward Euler discretization with respect to time, we propose the following approximation to (2.6), where we recall the weak formulation (2.8). Find $\{\vec{X}^{m+1}, \vec{\kappa}^{m+1}\} \in \underline{V}^h \times \underline{V}^{h,m}_{\vec{\tau}}$ such that

$$\langle \frac{\vec{X}^{m+1} - \vec{X}^m}{\tau_m}, \vec{\chi} \rangle^h_m - \langle \vec{\kappa}^{m+1}, \vec{\chi} \rangle^h_m = 0 \qquad \forall\ \vec{\chi} \in \underline{V}^{h,m}_{\vec{\tau}}, \tag{3.3a}$$

$$\langle \vec{\kappa}^{m+1}, \vec{\eta} \rangle^h_m + \langle \vec{X}^{m+1}_s, \vec{\eta}_s \rangle_m = 0 \qquad \forall\ \vec{\eta} \in \underline{V}^h\,, \tag{3.3b}$$

where, as noted above, the inner products $\langle \cdot, \cdot \rangle^{(h)}_m$ as well as $\cdot_s$ depend on m; and where we recall the definition of the test and trial function space $\underline{V}^{h,m}_{\vec{\tau}}$ in (3.2). We note that while the scheme (3.3a,b) for $d = 2$ does not collapse exactly to the approximation Barrett, Garcke, and Nürnberg (2007a, (2.3a,b)) with $f(r) := r$; it does collapse to that scheme's equivalent formulation Barrett, Garcke, and Nürnberg (2007a, (2.17)), on normalizing that scheme's discrete normal vectors $\vec{\omega}^m(q_j)$. In practice, the results from these two schemes are virtually indistinguishable.

Moreover, we recall that the fully discrete approximation for the curve shortening flow in Dziuk (1994) is given by (3.3a,b) with the test and trial space $\underline{V}^{h,m}_{\vec{\tau}}$ replaced by $\underline{V}^h$. We stress that this is a crucial difference, as the novel formulation in this paper allows for tangential movement, which leads to good mesh properties; see Remark 3.2 and Section 5 below. In particular, no heuristic remeshing is needed in practice.

Curve diffusion

For curve diffusion we use the formulation (2.15), and we obtain the following fully discrete version on recalling (2.16). Find $\{\vec{X}^{m+1}, \vec{\kappa}^{m+1}\} \in \underline{V}^h \times \underline{V}^{h,m}_{\vec{\tau}}$ such that

$$\langle \frac{\vec{X}^{m+1} - \vec{X}^m}{\tau_m}, \vec{\chi} \rangle^h_m - \langle \vec{\nabla}_s\, \vec{\kappa}^{m+1}, \vec{\nabla}_s\, \vec{\chi} \rangle_m = 0 \qquad \forall\ \vec{\chi} \in \underline{V}^{h,m}_{\vec{\tau}}, \tag{3.4a}$$

$$\langle \vec{\kappa}^{m+1}, \vec{\eta} \rangle^h_m + \langle \vec{X}^{m+1}_s, \vec{\eta}_s \rangle_m = 0 \qquad \forall\ \vec{\eta} \in \underline{V}^h\,, \tag{3.4b}$$

where we recall (3.1). We note that the scheme (3.4a,b) for $d = 2$ does not collapse exactly to the approximation Barrett, Garcke, and Nürnberg (2007b, (2.2a,b)). Apart from a normalization of the discrete normal vectors, the schemes differ in the way they approximate the flow (2.15). While (3.4a,b) is based on (2.16), the scheme in Barrett, Garcke, and Nürnberg (2007b) approximates a weak formulation of (2.9). As a consequence, it does not seem possible to show exact area preservation for a semi-discrete continuous in time version of (3.4a,b), something that holds for the approximation in Barrett, Garcke, and Nürnberg (2007b). However, once again in practice the results from these two schemes are virtually indistinguishable.

Willmore flow of curves

Similarly, elastic flow of curves, (2.25), can be approximated as follows, where we recall

the weak formulation (2.26a,b). Find $\{\vec{X}^{m+1}, \vec{\kappa}^{m+1}\} \in \underline{V}^h \times \underline{V}^{h,m}_{\vec{\tau}}$ such that

$$\langle \frac{\vec{X}^{m+1} - \vec{X}^m}{\tau_m}, \vec{\chi} \rangle^h_m - \langle \vec{\nabla}_s \vec{\kappa}^{m+1}, \vec{\nabla}_s \vec{\chi} \rangle_m - \tfrac{1}{2} \langle |\vec{\kappa}^m|^2 \vec{X}^m_s, \vec{\chi}_s \rangle^h_m$$
$$- [\lambda^m]_+ \langle \vec{\kappa}^{m+1}, \vec{\chi} \rangle^h_m = [\lambda^m]_- \langle \vec{\kappa}^m, \vec{\chi} \rangle^h_m \qquad \forall\ \vec{\chi} \in \underline{V}^{h,m}_{\vec{\tau}}, \quad (3.5a)$$

$$\langle \vec{\kappa}^{m+1}, \vec{\eta} \rangle^h_m + \langle \vec{X}^{m+1}_s, \vec{\eta}_s \rangle_m = 0 \qquad \forall\ \vec{\eta} \in \underline{V}^h\,, \quad (3.5b)$$

where $[r]_\pm := \pm \max\{\pm r, 0\}$, and $\vec{\kappa}^0 \in \underline{V}^{h,m}_{\vec{\tau}}$ is suitably chosen, see Section 5.

Note that for a given fixed $\lambda \in \mathbb{R}$ we set $\lambda^m = \lambda$, $m = 0 \to M-1$, whereas the time dependent choice

$$\lambda^m = - \frac{\frac{1}{2} \langle |\vec{\kappa}^m|^2 \vec{X}^m_s, \vec{\kappa}^m_s \rangle^h_m + |\vec{\nabla}_s \vec{\kappa}^m|^2_m}{|\vec{\kappa}^m|^2_{m,h}}, \quad (3.6)$$

with $|\cdot|^2_{m(,h)} := \langle \cdot, \cdot \rangle^{(h)}_m$, approximates length preserving elastic flow, recall (2.27).

A fully discrete approximation of the formulation in Deckelnick and Dziuk (2007) of (2.25), i.e. $\vec{P}\,\vec{x}_t$ replaced by $\vec{x}_t$, is given by: Find $\{\vec{X}^{m+1}, \vec{\kappa}^{m+1}\} \in \underline{V}^h \times \underline{V}^h$ such that for all $\vec{\chi}$, $\vec{\eta} \in \underline{V}^h$ it holds that

$$\langle \frac{\vec{X}^{m+1} - \vec{X}^m}{\tau_m}, \vec{\chi} \rangle^h_m - \langle \vec{\nabla}_s \vec{\kappa}^{m+1}, \vec{\nabla}_s \vec{\chi} \rangle_m - \tfrac{1}{2} \langle |\vec{\kappa}^m|^2 \vec{X}^{m+1}_s, \vec{\chi}_s \rangle_m - \lambda^m \langle \vec{\kappa}^{m+1}, \vec{\chi} \rangle^h_m = 0\,, \quad (3.7a)$$

$$\langle \vec{\kappa}^{m+1}, \vec{\eta} \rangle^h_m + \langle \vec{X}^{m+1}_s, \vec{\eta}_s \rangle_m = 0\,. \quad (3.7b)$$

Hence the main difference between (3.7a,b) and the approach corresponding to our framework, (3.5a,b), is the choice of trial space for $\vec{\kappa}^{m+1}$ and the choice of test function for the first equation, i.e. $\underline{V}^{h,m}_{\vec{\tau}}$ in place of $\underline{V}^h$. In addition, we choose to treat the third term in (3.5a) explicitly. This proves to be of no disadvantage in practice, but as the system is now symmetric, it makes proving existence and uniqueness for (3.5a,b) straightforward, and it simplifies the solution procedure for (3.5a,b).

Geodesic curvature flow

In order to approximate the geodesic curvature flow (2.19), as well as other curve evolutions on a given manifold $\mathcal{M}$, we now introduce $\vec{\omega}^m_F(q_j) := \frac{F'(\vec{X}^m(q_j))}{|F'(\vec{X}^m(q_j))|}$, recall (2.17), and set $\vec{\omega}^m_{\mathcal{M}}(q_j) := \vec{\omega}^m_d(q_j) \times \vec{\omega}^m_F(q_j)$, $j = 1 \to J$, where we assume that these are nonzero vectors. We note that $\{\vec{X}^m(q_j)\}_{j=1}^J$ may not lie exactly on $\mathcal{M}$, hence the normalization in $\vec{\omega}^m_F(q_j)$. In addition, let

$$\underline{V}^{h,m}_F := \{\vec{\eta} \in \underline{V}^h : \vec{\eta}(q_j)\,.\,\vec{\omega}^m_F(q_j) = 0, \quad j = 1 \to J\} \quad (3.8)$$

be the discrete analogue of (2.18). We then propose the following approximation to (2.19): Find $\{\delta\vec{X}^{m+1}, \kappa^{m+1}_{\mathcal{M}}\} \in \underline{V}^{h,m}_F \times W^h$, where $\vec{X}^{m+1} := \vec{X}^m + \delta\vec{X}^{m+1}$, such that

$$\langle \frac{\delta\vec{X}^{m+1}}{\tau_m}, \chi\, \vec{\omega}^m_{\mathcal{M}} \rangle^h_m - \langle \kappa^{m+1}_{\mathcal{M}}, \chi \rangle^h_m = 0 \qquad \forall\ \chi \in W^h, \quad (3.9a)$$

$$\langle \kappa^{m+1}_{\mathcal{M}}\, \vec{\omega}^m_{\mathcal{M}}, \vec{\eta} \rangle^h_m + \langle \vec{X}^{m+1}_s, \vec{\eta}_s \rangle_m = 0 \qquad \forall\ \vec{\eta} \in \underline{V}^{h,m}_F\,. \quad (3.9b)$$

Geodesic surface diffusion

Moreover, for the surface diffusion flow on manifolds, (2.20), also called geodesic surface diffusion, we introduce the approximation: Find $\{\delta\vec{X}^{m+1}, \kappa_{\mathcal{M}}^{m+1}\} \in \underline{V}_F^{h,m} \times W^h$, where $\vec{X}^{m+1} := \vec{X}^m + \delta\vec{X}^{m+1}$, such that

$$\langle \frac{\delta\vec{X}^{m+1}}{\tau_m}, \chi\, \vec{\omega}_{\mathcal{M}}^m \rangle_m^h - \langle [\kappa_{\mathcal{M}}^{m+1}]_s, \chi_s \rangle_m = 0 \qquad \forall\ \chi \in W^h \tag{3.10}$$

and (3.9b) hold.

Geodesic Willmore flow

In order to compute elastic flow of curves on a manifold we have two options. On recalling (2.32), we can either combine (3.9b) with

$$\begin{aligned}\langle \frac{\delta\vec{X}^{m+1}}{\tau_m}, \chi\, \vec{\omega}_{\mathcal{M}}^m \rangle_m^h - \langle [\kappa_{\mathcal{M}}^{m+1}]_s, \chi_s \rangle_m - \langle [\lambda^m - \mathcal{K}^m]_+\, \kappa_{\mathcal{M}}^{m+1}, \chi \rangle_m^h = \\ - \tfrac{1}{2} \langle (\kappa_{\mathcal{M}}^m)^3, \chi \rangle_m^h + \langle [\lambda^m - \mathcal{K}^m]_-\, \kappa_{\mathcal{M}}^m, \chi \rangle_m^h \qquad \forall\ \chi \in W^h\,, \end{aligned} \tag{3.11}$$

where $\mathcal{K}^m \in W^h$ with $\mathcal{K}^m(q_j) = \mathcal{K}(\vec{\Pi}_{\mathcal{M}} \vec{X}^m(q_j))$, $j = 1 \to J$, is the Gauß curvature of $\mathcal{M}$ evaluated at $\vec{\Pi}_{\mathcal{M}} \vec{X}^m$, with $\vec{\Pi}_{\mathcal{M}}$ being the orthogonal projection onto $\mathcal{M}$. In addition, $\kappa_{\mathcal{M}}^0 \in W^h$ is a suitably chosen initial value, see Section 5 for details. Similarly to (3.5a,b), for a given fixed $\lambda \in \mathbb{R}$ we set $\lambda^m = \lambda$, $m = 0 \to M-1$, whereas the time dependent choice

$$\lambda^m = \frac{\frac{1}{2} |(\kappa_{\mathcal{M}}^m)^2|_{m,h}^2 + \langle \mathcal{K}^m\, \kappa_{\mathcal{M}}^m, \kappa_{\mathcal{M}}^m \rangle_m^h - |(\kappa_{\mathcal{M}}^m)_s|_m^2}{|\kappa_{\mathcal{M}}^m|_{m,h}^2}\,, \tag{3.12}$$

similarly to (3.6), approximates length preserving geodesic elastic flow.

A second variant is based on (2.30a), and uses as an additional discrete unknown the normal curvature κ_F^{m+1}. Find $\{\delta\vec{X}^{m+1}, \{\kappa_{\mathcal{M}}^{m+1}, \kappa_F^{m+1}\}\} \in \underline{V}_F^{h,m} \times [W^h]^2$ such that

$$\begin{aligned}\langle \frac{\delta\vec{X}^{m+1}}{\tau_m}, \vec{\chi} \rangle_m^h - \langle \vec{\nabla}_s\, \vec{\pi}^h[\kappa_{\mathcal{M}}^{m+1}\, \vec{\omega}_{\mathcal{M}}^m], \vec{\nabla}_s\, \vec{\chi} \rangle_m - \langle [\lambda^m]_+\, \kappa_{\mathcal{M}}^{m+1}\, \vec{\omega}_{\mathcal{M}}^m, \vec{\chi} \rangle_m^h - \tfrac{1}{2} \langle (\kappa_{\mathcal{M}}^m)^2\, \vec{X}_s^m, \vec{\chi}_s \rangle_m^h \\ + \langle \kappa_{\mathcal{M}}^m\, \kappa_F^m, \mathrm{I\!I}(\vec{\chi}, \vec{\omega}_{\mathcal{M}}^m) \rangle_m^h = \langle [\lambda^m]_-\, \kappa_{\mathcal{M}}^m\, \vec{\omega}_{\mathcal{M}}^m, \vec{\chi} \rangle_m^h \qquad \forall\ \vec{\chi} \in \underline{V}_{F,\vec{\tau}}^{h,m}\,, \end{aligned} \tag{3.13a}$$

$$\langle \kappa_{\mathcal{M}}^{m+1}\, \vec{\omega}_{\mathcal{M}}^m, \vec{\eta} \rangle_m^h + \langle \kappa_F^{m+1}\, \vec{\omega}_F^m, \vec{\eta} \rangle_m^h + \langle \vec{X}_s^{m+1}, \vec{\eta}_s \rangle_m = 0 \qquad \forall\ \vec{\eta} \in \underline{V}^h\,, \tag{3.13b}$$

where $\vec{\chi} \in \underline{V}_{F,\vec{\tau}}^{h,m} := \underline{V}_F^{h,m} \cap \underline{V}_{\vec{\tau}}^{h,m}$ is equivalent to $\vec{\chi} = \vec{\pi}^h[\chi\, \vec{\omega}_{\mathcal{M}}^m]$ for a $\chi \in W^h$. In addition, $\kappa_{\mathcal{M}}^0$, $\kappa_F^0 \in W^h$ are again suitably chosen. We observe that in the last term on the left hand side of (3.13a) we use a slight abuse of notation, as $\vec{X}^m$ in general does not lie exactly on $\mathcal{M}$. In particular, for ease of notation we define for all $u \in C(I, \mathbb{R})$ and for an arbitrary test function $\vec{\eta} \in \underline{V}_{F,\vec{\tau}}^{h,m}$, on recalling (2.28) and on noting that in general $|F'(\vec{X}^m)| \neq 1$,

$$\langle u, \mathrm{I\!I}(\vec{\chi}, \vec{\omega}_{\mathcal{M}}^m) \rangle_m^h = -\sum_{j=1}^J \langle 1, \chi_j \rangle_m \left[u\, (\vec{\chi} \,.\, \vec{\omega}_{\mathcal{M}}^m)\, [|F'(\vec{X}^m)|]^{-1}\, F''(\vec{X}^m)\, \vec{\omega}_{\mathcal{M}}^m \,.\, \vec{\omega}_{\mathcal{M}}^m \right](q_j). \tag{3.14}$$

3.2 Properties of the discrete isotropic flows

We observe that $\delta\vec{X}^{m+1} \in \underline{V}_F^{h,m}$ weakly enforces $\vec{X}^{m+1}(q_j) \in \mathcal{M} \iff F(\vec{X}^{m+1}(q_j)) = 0$, $j = 1 \to J$, as it is a linearized approximation of these constraints. In particular, for curved manifolds the equations $F(\vec{X}^{m+1}(q_j)) = 0$, $j = 1 \to J$, are only approximately satisfied. For $k = 0 \to m$ and $j = 1 \to J$, we have that $F'(\vec{X}^k(q_j)) \,.\, (\vec{X}^{k+1}(q_j) - \vec{X}^k(q_j)) = 0$, and similarly to Deckelnick and Elliott (1998, p. 651) it formally follows, on assuming that $F(\vec{X}^0(q_j)) = 0$ and that $\frac{\vec{X}^{k+1}(q_j) - \vec{X}^k(q_j)}{\tau} = \mathcal{O}(1)$, that there exist points $\vec{\xi}_{k,j} \in \mathbb{R}^d$ such that

$$
\begin{aligned}
&|F(\vec{X}^{m+1}(q_j))| \leq \sum_{k=0}^{m} |F(\vec{X}^{k+1}(q_j)) - F(\vec{X}^k(q_j))| \\
&= \sum_{k=0}^{m} |[F''(\vec{\xi}_{k,j})\,(\vec{X}^{k+1}(q_j) - \vec{X}^k(q_j))] \,.\, (\vec{X}^{k+1}(q_j) - \vec{X}^k(q_j))| = \mathcal{O}(\tau),\ j = 1 \to J.
\end{aligned}
$$

Hence, for small time steps the vertices of the polygonal curve should stay close to $\mathcal{M}$; and this is what one generally observes in practice, see Section 5 for details. However, one could also employ a projection step that orthogonally projects $\vec{X}^{m+1}$ onto $\mathcal{M}$ at every time step, which would have the advantage of satisfying $F(\vec{X}^{m+1}(q_j)) = 0$, $j = 1 \to J$, exactly throughout the evolution. But this complicates the stability proof below, hence our preference for e.g. the approximations (3.9a,b). However, we do include numerical results using both approaches in Section 5.

Before we can proceed to prove existence and uniqueness to our approximations, we have to make the following very mild assumption.

($\mathcal{C}$) Let (*i*) $|\vec{X}_\rho^m| > 0$ for almost all $\rho \in I$, (*ii*) $\vec{X}^m(q_{j+1}) \neq \vec{X}^m(q_{j-1})$, $j = 1 \to J$, and (*iii*) $\bigcup_{j=1}^{J} \{\vec{\omega}_d^m(q_j)\}^\perp = \mathbb{R}^d$.

Remark. 3.1. *We note that* ($\mathcal{C}$) *is a very mild assumption that is only violated in very rare occasions. In fact,* (*ii*) *is not strictly necessary as it is only required for normalization of* $\vec{\omega}_d^m(q_j)$*, recall* (3.2)*. One could remove this normalization procedure, and hence this assumption, and still be able to prove the well-posedness, equidistribution and stability results below. However, for ease of exposition and as it is such a mild assumption we include it. Finally, see Barrett, Garcke, and Nürnberg (2007b, Remark 2.2) for the breakdown of* (*iii*) *in the case* $d = 2$*.*

Theorem. 3.1. *Let the assumption* ($\mathcal{C}$) *hold. Then there exists a unique solution to the systems* (3.3a,b), (3.4a,b), (3.5a,b), (3.9a,b), (3.10) *with* (3.9b), (3.11) *with* (3.9b) *and* (3.13a,b)*, respectively. In addition, the solution to* (3.3a,b) *satisfies*

$$
|\Gamma^{m+1}| + \tau_m \, |\kappa^{m+1}|_{m,h}^2 \leq |\Gamma^m| \,. \tag{3.15}
$$

Moreover, the solution to (3.4a,b) *satisfies* (3.15) *with the second term on the left hand side replaced by* $\tau_m \, |\vec{\nabla}_s \, \vec{\kappa}|_m^2$*. Furthermore, the solutions to* (3.9a,b) *and* (3.10), (3.9b), *in place of* (3.15) *satisfy*

$$
|\Gamma^{m+1}| + \tau_m \, |\kappa_{\mathcal{M}}^{m+1}|_{m,h}^2 \leq |\Gamma^m|
$$

and $|\Gamma^{m+1}| + \tau_m\,|[\kappa_{\mathcal{M}}^{m+1}]_s|_m^2 \le |\Gamma^m|$*, respectively.*

Proof. The desired results for (3.3a,b), (3.4a,b), (3.5a,b), (3.9a,b), (3.10) with (3.9b) and (3.13a,b) follow immediately from Theorems 3.2 and 3.3, below, for the choice $\phi(\vec{p}) = |\vec{p}|$. Existence and uniqueness for (3.11), (3.9b) can be shown analogously to the proof for (3.10), (3.9b). □

REMARK. 3.2. *Similarly to Barrett, Garcke, and Nürnberg (2007b, Remark 2.3), one can consider a continuous in time semidiscrete version of our schemes, e.g. of* (3.3a,b)*. In which case, we seek* $\vec{X}(t) \in \underline{V}^h$ *and* $\vec{\kappa}(t) \in \underline{V}^h_{\vec{\tau}} := \{\vec{\eta} \in \underline{V}^h : \vec{\eta}(q_j)\,.\,\vec{\omega}_d^h(q_j) = 0, \quad j = 1 \to J\}$*, where* $\vec{\omega}_d^h$ *on* $\Gamma^h(t)$*, described by* $\vec{X}(t)$*, is defined analogously to* $\vec{\omega}_d^m$ *on* Γ^m*, for all* $t \in [0,T]$ *such that*

$$\langle \vec{X}_t, \vec{\chi}\rangle^h - \langle \vec{\kappa}, \vec{\chi}\rangle^h = 0 \qquad \forall\ \vec{\chi} \in \underline{V}^h_{\vec{\tau}}, \tag{3.16a}$$

$$\langle \vec{\kappa}, \vec{\eta}\rangle^h + \langle \vec{X}_s, \vec{\eta}_s\rangle = 0 \qquad \forall\ \vec{\eta} \in \underline{V}^h; \tag{3.16b}$$

where we always integrate over the current curve Γ^h*, and* $\langle\cdot,\cdot\rangle^{(h)}$ *is the same as* $\langle\cdot,\cdot\rangle_m^{(h)}$ *with* Γ^m *and* $\vec{X}^m$ *replaced by* Γ^h *and* $\vec{X}$*, respectively. Then, on choosing* $\vec{\eta} = \vec{\omega}_d^h(q_j)\,\chi_j$ *in* (3.16b) *and on recalling that* $\vec{\omega}_d^h(q_j)\,.\,\vec{\kappa}(q_j) = 0$*, it follows with* $\vec{a}^h_{j-\frac12} := \vec{X}(q_j) - \vec{X}(q_{j-1})$*, on noting that* $\vec{\omega}_d^h(q_j) = \frac{\vec{a}^h_{j+\frac12} + \vec{a}^h_{j-\frac12}}{|\vec{a}^h_{j+\frac12} + \vec{a}^h_{j-\frac12}|}$*, that*

$$\left(\frac{\vec{a}^h_{j+\frac12}}{|\vec{a}^h_{j+\frac12}|} - \frac{\vec{a}^h_{j-\frac12}}{|\vec{a}^h_{j-\frac12}|}\right)\,.\,\left(\vec{a}^h_{j+\frac12} + \vec{a}^h_{j-\frac12}\right) = 0\,, \quad j = 1 \to J\,. \tag{3.17}$$

Clearly, (3.17) *and the Cauchy-Schwarz inequality imply that* $|\vec{a}^h_{j+\frac12}| = |\vec{a}^h_{j-\frac12}|$ *if* $\vec{a}^h_{j+\frac12}$ *is not parallel to* $\vec{a}^h_{j-\frac12}$*. Hence the scheme* (3.16a,b) *will always equidistribute the nodes along* Γ^h *if the corresponding intervals are not locally parallel; see also Barrett, Garcke, and Nürnberg (2007b) for the planar case. Although it does not appear possible to prove an analogue for e.g. the fully discrete scheme* (3.3a,b)*, in practice we see that the nodes are moved tangentially so that they will eventually be equidistributed; see Section 5 for details.*

Moreover, we note that as the above analysis is only based on the equation (3.16b) *and the fact that* $\vec{\kappa} \in \underline{V}^h_{\vec{\tau}}$*, the same equidistribution property holds for all the other (isotropic) schemes in this paper as well, and in particular for all the schemes involving* (3.3b) *or* (3.9b) *or* (3.13b)*. The anisotropic schemes discussed in Section 3.3, below, satisfy a similar criterion. Here one obtains equidistribution with respect to* ϕ*, recall* (2.39)*, in the case* $L = 1$ *and with respect to some nontrivial nonlinear function in the case* $L \ge 2$*. See Barrett, Garcke, and Nürnberg (2008a) for the details in the planar case,* $d = 2$*, which immediately carry over to the higher codimension and geodesic flows as discussed in this paper.*

3.3 The anisotropic case

The natural extension of (3.3a,b) to the anisotropic flow (2.34) for anisotropies of the form (2.39) is: Find $\{\vec{X}^{m+1}, \vec{\kappa}_\phi^{m+1}\} \in \underline{V}^h \times \underline{V}_{\vec{\tau}}^{h,m}$ such that

$$\langle \frac{\vec{X}^{m+1} - \vec{X}^m}{\tau_m}, \vec{\chi} \rangle_m^h - \langle \vec{\kappa}_\phi^{m+1}, \vec{\chi} \rangle_m^h = 0 \qquad \forall\ \vec{\chi} \in \underline{V}_{\vec{\tau}}^{h,m}\,, \tag{3.18a}$$

$$\langle \vec{\kappa}_\phi^{m+1}, \vec{\eta} \rangle_m^h + \sum_{\ell=1}^{L} \langle [\phi_\ell(\vec{X}_s^m)]^{-1}\, \vec{G}_\ell\, \vec{X}_s^{m+1}, \vec{\eta}_s \rangle_m = 0 \qquad \forall\ \vec{\eta} \in \underline{V}^h\,. \tag{3.18b}$$

Moreover, we obtain the following approximation for anisotropic curve diffusion: Find $\{\vec{X}^{m+1}, \vec{\kappa}_\phi^{m+1}\} \in \underline{V}^h \times \underline{V}_{\vec{\tau}}^{h,m}$ such that

$$\langle \frac{\vec{X}^{m+1} - \vec{X}^m}{\tau_m}, \vec{\chi} \rangle_m^h - \langle \vec{\nabla}_s\, \vec{\kappa}_\phi^{m+1}, \vec{\nabla}_s\, \vec{\chi} \rangle_m^h = 0 \qquad \forall\ \vec{\chi} \in \underline{V}_{\vec{\tau}}^{h,m}, \tag{3.19}$$

and (3.18b) hold.

Anisotropic Willmore flow for curves, (2.37), can be approximated as follows, where we recall (2.40). Find $\{\vec{X}^{m+1}, \vec{\kappa}_\phi^{m+1}\} \in \underline{V}^h \times \underline{V}_{\vec{\tau}}^{h,m}$ such that

$$\begin{aligned}\langle \frac{\vec{X}^{m+1} - \vec{X}^m}{\tau_m}, \vec{\chi} \rangle_m^h - \langle \phi''(\vec{X}_s^m)\, (\vec{\kappa}_\phi^{m+1})_s, \vec{\chi}_s \rangle_m - \tfrac{1}{2}\, \langle |\vec{\kappa}_\phi^m|^2\, \vec{X}_s^m, \vec{\chi}_s \rangle_m^h - [\lambda^m]_+\, \langle \vec{\kappa}_\phi^{m+1}, \vec{\chi} \rangle_m^h \\ = [\lambda^m]_-\, \langle \vec{\kappa}_\phi^m, \vec{\chi} \rangle_m^h \quad \forall\ \vec{\chi} \in \underline{V}_{\vec{\tau}}^{h,m},\end{aligned} \tag{3.20}$$

and (3.18b) hold, where $\vec{\kappa}_\phi^0 \in \underline{V}_{\vec{\tau}}^{h,m}$ is suitably chosen.

Similarly, we can extend the isotropic scheme to the anisotropic curvature flow on manifolds as follows. Find $\{\delta\vec{X}^{m+1}, \kappa_{\phi,\mathcal{M}}^{m+1}\} \in \underline{V}_F^{h,m} \times W^h$, where $\vec{X}^{m+1} := \vec{X}^m + \delta\vec{X}^{m+1}$, such that

$$\langle \frac{\delta\vec{X}^{m+1}}{\tau_m}, \chi\, \vec{\omega}_{\mathcal{M}}^m \rangle_m^h - \langle \kappa_{\phi,\mathcal{M}}^{m+1}, \chi \rangle_m^h = 0 \qquad \forall\ \chi \in W^h, \tag{3.21a}$$

$$\langle \kappa_{\phi,\mathcal{M}}^{m+1}\, \vec{\omega}_{\mathcal{M}}^m, \vec{\eta} \rangle_m^h + \sum_{\ell=1}^{L} \langle [\phi_\ell(\vec{X}_s^m)]^{-1}\, \vec{G}_\ell\, \vec{X}_s^{m+1}, \vec{\eta}_s \rangle_m = 0 \qquad \forall\ \vec{\eta} \in \underline{V}_F^{h,m}. \tag{3.21b}$$

In order to approximate anisotropic geodesic surface diffusion flow, (3.21a) needs to be replaced by

$$\langle \frac{\delta\vec{X}^{m+1}}{\tau_m}, \chi\, \vec{\omega}_{\mathcal{M}}^m \rangle_m^h - \langle [\kappa_{\phi,\mathcal{M}}^{m+1}]_s, \chi_s \rangle_m = 0 \qquad \forall\ \chi \in W^h. \tag{3.22}$$

Finally, on recalling (2.38) we can generalize our approximation (3.13a,b) to the anisotropic geodesic Willmore flow of curves as follows. Find $\{\delta\vec{X}^{m+1}, \{\kappa_{\phi,\mathcal{M}}^{m+1}, \kappa_{\phi,F}^{m+1}\}\} \in$

$\underline{V}_F^{h,m} \times [W^h]^2$ such that

$$\langle \frac{\delta \vec{X}^{m+1}}{\tau_m}, \vec{\chi} \rangle_m^h - \langle \phi''(\vec{X}_s^m)\,(\vec{\pi}^h[\kappa_{\phi,\mathcal{M}}^{m+1}\,\vec{\omega}_{\mathcal{M}}^m])_s, \vec{\chi}_s \rangle_m - \langle [\lambda^m]_+\,\kappa_{\phi,\mathcal{M}}^{m+1}\,\vec{\omega}_{\mathcal{M}}^m, \vec{\chi} \rangle_m^h$$
$$- \tfrac{1}{2}\,\langle (\kappa_{\phi,\mathcal{M}}^m)^2\,\vec{X}_s^m, \vec{\chi}_s \rangle_m^h + \langle \kappa_{\phi,\mathcal{M}}^m\,\kappa_{\phi,F}^m, \mathbb{I}(\vec{\chi}, \vec{\omega}_{\mathcal{M}}^m) \rangle_m^h = \langle [\lambda^m]_-\,\kappa_{\phi,\mathcal{M}}^m\,\vec{\omega}_{\mathcal{M}}^m, \vec{\chi} \rangle_m^h$$
$$\forall\ \vec{\chi} \in \underline{V}_{F,\vec{\tau}}^{h,m}\,, \tag{3.23a}$$

$$\langle \kappa_{\phi,\mathcal{M}}^{m+1}\,\vec{\omega}_{\mathcal{M}}^m, \vec{\eta} \rangle_m^h + \langle \kappa_{\phi,F}^{m+1}\,\vec{\omega}_F^m, \vec{\eta} \rangle_m^h + \sum_{\ell=1}^{L} \langle [\phi_\ell(\vec{X}_s^m)]^{-1}\,\vec{G}_\ell\,\vec{X}_s^{m+1}, \vec{\eta}_s \rangle_m = 0 \quad \forall\ \vec{\eta} \in \underline{V}^h\,, \tag{3.23b}$$

where we recall the notation in (3.14), and where $\kappa_{\phi,\mathcal{M}}^0, \kappa_{\phi,F}^0 \in W^h$ are suitably chosen.

We observe that all of the above anisotropic schemes reduce to their isotropic equivalents in §3.1 for the special case $\phi(\vec{p}) = |\vec{p}|$.

THEOREM. 3.2. *Let the assumption* ($\mathcal{C}$) *hold. Then there exists a unique solution to the systems* (3.18a,b), (3.19) *with* (3.18b), (3.20) *with* (3.18b), (3.21a,b), (3.22) *with* (3.21b) *and* (3.23a,b).

Proof. As (3.18a,b) is a linear system, existence follows from uniqueness. To investigate the latter, we consider the system: Find $\{\vec{X}, \vec{\kappa}_\phi\} \in \underline{V}^h \times \underline{V}_{\vec{\tau}}^{h,m}$ such that

$$\langle \vec{X}, \vec{\chi} \rangle_m^h - \tau_m\,\langle \vec{\kappa}_\phi, \vec{\chi} \rangle_m^h = 0 \quad \forall\ \vec{\chi} \in \underline{V}_{\vec{\tau}}^{h,m}, \tag{3.24a}$$

$$\langle \vec{\kappa}_\phi, \vec{\eta} \rangle_m^h + \sum_{\ell=1}^{L} \langle [\phi_\ell(\vec{X}_s^m)]^{-1}\,\vec{G}_\ell\,\vec{X}_s, \vec{\eta}_s \rangle_m = 0 \quad \forall\ \vec{\eta} \in \underline{V}^h. \tag{3.24b}$$

Choosing $\vec{\chi} = \vec{\kappa}_\phi \in \underline{V}_{\vec{\tau}}^{h,m}$, in (3.24a) and $\vec{\eta} = \vec{X} \in \underline{V}^h$ in (3.24b) yields on combining, that

$$\sum_{\ell=1}^{L} \langle [\phi_\ell(\vec{X}_s^m)]^{-1}\,\vec{G}_\ell\,\vec{X}_s, \vec{X}_s \rangle_m + \tau_m\,\langle \vec{\kappa}_\phi, \vec{\kappa}_\phi \rangle_m^h = 0\,. \tag{3.25}$$

It follows from (3.25), on recalling from (2.39) that $\vec{G}_\ell$, $\ell = 1 \to L$, are positive definite, that $\vec{\kappa}_\phi \equiv \vec{0}$ and that $\vec{X} \equiv \vec{X}^c \in \mathbb{R}^d$. Together with (3.24a) this yields that

$$\langle \vec{X}^c, \vec{\chi} \rangle_m^h = 0 \quad \forall\ \vec{\chi} \in \underline{V}_{\vec{\tau}}^{h,m}\,.$$

It immediately follows from assumption ($\mathcal{C}$) that $\vec{X}^c = \vec{0}$. Hence we have shown that (3.18a,b) has a unique solution $\{\vec{X}^{m+1}, \vec{\kappa}_\phi^{m+1}\} \in \underline{V}^h \times \underline{V}_{\vec{\tau}}^{h,m}$. Similarly, for (3.19), (3.18b) we find that $\sum_{\ell=1}^{L} \langle [\phi_\ell(\vec{X}_s^m)]^{-1}\,\vec{G}_\ell\,\vec{X}_s, \vec{X}_s \rangle_m + \tau_m\,\langle \vec{\nabla}_s\,\vec{\kappa}_\phi, \vec{\nabla}_s\,\vec{\kappa}_\phi \rangle_m = 0$, and so $\vec{X} \equiv \vec{X}^c$ and $\langle \vec{\kappa}_\phi, \vec{\eta} \rangle_m^h = 0$ for all $\vec{\eta} \in \underline{V}^h$. Hence $\vec{\kappa}_\phi \equiv 0$ and, as before, we find that $\vec{X}^c = \vec{0}$, and so we obtain the desired result.

In an analogous fashion, we obtain for (3.20), (3.18b) that

$$\sum_{\ell=1}^{L} \langle [\phi_\ell(\vec{X}_s^m)]^{-1}\,\vec{G}_\ell\,\vec{X}_s, \vec{X}_s \rangle_m + \tau_m\,\Big[\langle \phi''(\vec{X}_s^m)\,(\vec{\kappa}_\phi)_s, (\vec{\kappa}_\phi)_s \rangle_m + [\lambda^m]_+\,\langle \vec{\kappa}_\phi, \vec{\kappa}_\phi \rangle_m^h \Big] = 0\,.$$

As ϕ'' is positive semi-definite, recall (2.40), it follows, as above, that $\vec{X} \equiv \vec{X}^c$ and $\langle \vec{\kappa}_\phi, \vec{\eta} \rangle_m^h = 0$ for all $\vec{\eta} \in \underline{V}^h$, which implies that $\vec{\kappa}_\phi \equiv 0$ and $\vec{X}^c = \vec{0}$.

For the system (3.21a,b) we obtain analogously for $\{\delta\vec{X}, \vec{\kappa}_{\phi,\mathcal{M}}\} \in \underline{V}_F^{h,m} \times W^h$ that

$$\sum_{\ell=1}^{L} \langle [\phi_\ell(\vec{X}_s^m)]^{-1} \vec{G}_\ell \, (\delta\vec{X})_s, (\delta\vec{X})_s \rangle_m + \tau_m \, \langle \kappa_{\phi,\mathcal{M}}, \kappa_{\phi,\mathcal{M}} \rangle_m^h = 0 \,,$$

and hence the desired results follows from assumption $(\mathcal{C})$. Similarly, for (3.22), (3.21b) we find that $\sum_{\ell=1}^{L} \langle [\phi_\ell(\vec{X}_s^m)]^{-1} \vec{G}_\ell \, (\delta\vec{X})_s, (\delta\vec{X})_s \rangle_m + \tau_m \, \langle [\kappa_{\phi,\mathcal{M}}]_s, [\kappa_{\phi,\mathcal{M}}]_s \rangle_m = 0$, and so $\delta\vec{X} \equiv \vec{X}^c \in \underline{V}_F^{h,m} \cap \mathbb{R}^3$ and $\kappa_{\phi,\mathcal{M}} \equiv \kappa^c \in \mathbb{R}$. As before, assumption $(\mathcal{C})$ yields that $\vec{X}^c = \vec{0}$, and hence that $\kappa^c \, \langle \vec{\omega}_{\mathcal{M}}^m, \vec{\eta} \rangle_m^h = 0$ for all $\vec{\eta} \in \underline{V}^h$. Therefore $\kappa^c = 0$, and so we obtain the desired result.

Finally, the system (3.23a,b) can be dealt with in an analogous fashion. In particular, we obtain that

$$\begin{aligned} &\sum_{\ell=1}^{L} \langle [\phi_\ell(\vec{X}_s^m)]^{-1} \vec{G}_\ell \, (\delta\vec{X})_s, (\delta\vec{X})_s \rangle_m \\ &\qquad + \tau_m \left[\langle \phi''(\vec{X}_s^m) \, (\vec{\pi}^h[\kappa_{\phi,\mathcal{M}} \, \vec{\omega}_{\mathcal{M}}^m])_s, (\vec{\pi}^h[\kappa_{\phi,\mathcal{M}} \, \vec{\omega}_{\mathcal{M}}^m])_s \rangle_m + [\lambda^m]_+ \, \langle \kappa_{\phi,\mathcal{M}}, \kappa_{\phi,\mathcal{M}} \rangle_m^h \right] = 0 \,. \end{aligned}$$

As before, we can deduce that $\delta\vec{X} \equiv \vec{0}$, and hence that $\kappa_{\phi,\mathcal{M}} \equiv 0$ and $\kappa_{\phi,F} \equiv 0$; which proves the claim for the system (3.23a,b). □

THEOREM. 3.3. *Let the assumption $(\mathcal{C})$ hold. The solution $\{\vec{X}^{m+1}, \vec{\kappa}_\phi^{m+1}\} \in \underline{V}^h \times \underline{V}_{\vec{\tau}}^{h,m}$ to* (3.18a,b) *satisfies*

$$|\Gamma^{m+1}|_\phi + \tau_m \, |\vec{\kappa}_\phi^{m+1}|_{m,h}^2 \leq |\Gamma^m|_\phi \,. \tag{3.26}$$

Moreover, the solution to (3.19), (3.18b) *satisfies* (3.26) *with the second term on the left hand side replaced by $\tau_m \, |\vec{\nabla}_s \, \vec{\kappa}_\phi|_m^2$. In addition, the solutions to* (3.21a,b) *and* (3.22), (3.21b) *satisfy*

$$|\Gamma^{m+1}|_\phi + \tau_m \, |\kappa_{\phi,\mathcal{M}}^{m+1}|_{m,h}^2 \leq |\Gamma^m|_\phi \,. \tag{3.27}$$

and $|\Gamma^{m+1}|_\phi + \tau_m \, |[\kappa_{\phi,\mathcal{M}}^{m+1}]_s|_m^2 \leq |\Gamma^m|_\phi$, respectively.

Proof. Choosing $\vec{\chi} = \vec{\kappa}_\phi^{m+1}$ in (3.18a) and $\vec{\eta} = \frac{\vec{X}^{m+1} - \vec{X}^m}{\tau_m}$ in (3.18b) yields that

$$\sum_{\ell=1}^{L} \langle [\phi_\ell(\vec{X}_s^m)]^{-1} \vec{G}_\ell \, \vec{X}_s^{m+1}, \vec{X}_s^{m+1} - \vec{X}_s^m \rangle_m + \tau_m \, \langle \vec{\kappa}_\phi^{m+1}, \vec{\kappa}_\phi^{m+1} \rangle_m^h = 0 \,.$$

Repeating verbatim the corresponding proof in Barrett, Garcke, and Nürnberg (2008a, Theorem 2.5), which crucially depends on the chosen class (2.39) of anisotropy density functions, we can show that

$$\sum_{\ell=1}^{L} \langle [\phi_\ell(\vec{X}_s^m)]^{-1} \vec{G}_\ell \, \vec{X}_s^{m+1}, \vec{X}_s^{m+1} - \vec{X}_s^m \rangle_m \geq |\Gamma^{m+1}|_\phi - |\Gamma^m|_\phi, \tag{3.28}$$

which yields the desired result. Similarly, the result (3.27) follows from (3.28) on choosing $\chi = \kappa_{\phi,\mathcal{M}}^{m+1}$ in (3.21a) and $\vec{\eta} = \frac{\delta\vec{X}^{m+1}}{\tau_m} \in \underline{V}_F^{h,m}$ in (3.21b). The remaining results follow analogously. □

4 Solution of the discrete equations

In this section, we discuss possible solution methods for the discrete systems arising from the approximations introduced in the previous section. For ease of presentation, we only consider the isotropic case. All the methods immediately carry over to the anisotropic case, on replacing the stiffness matrix $\vec{A}$, see (4.1) below, with the obvious anisotropic version $\vec{A}_\phi$. See e.g. Barrett, Garcke, and Nürnberg (2008a) for the corresponding details in the planar case, $d = 2$. In addition, for the anisotropic Willmore flow schemes, the anisotropic matrices $\vec{\mathcal{A}}_\phi$ and $\mathcal{A}_\phi$ need to be defined, where the former is the natural anisotropic version of the matrix $\vec{\mathcal{A}}$, see below, with $\phi''(\vec{X}^m_s)$ replacing $\vec{P}^m$.

In order to solve the algebraic systems arising from our fully discrete parametric finite element approximations, we apply a Schur complement approach in each case.

For an arbitrary $n \in \mathbb{N}$, let $\vec{Id}_n \in (\mathbb{R}^{d\times d})^{n\times n}$ be the identity matrix, and similarly for $Id_n \in \mathbb{R}^{n\times n}$. We introduce also the diagonal matrices $M \in \mathbb{R}^{J\times J}$, $\vec{M} \in (\mathbb{R}^{d\times d})^{J\times J}$, and the stiffness matrices $A \in \mathbb{R}^{J\times J}$ and $\vec{A}$, $\vec{\mathcal{A}} \in (\mathbb{R}^{d\times d})^{J\times J}$ with entries

$$M_{kl} := \langle \chi_k, \chi_l \rangle^h_m, \quad \vec{M}_{kl} := M_{kl}\, \vec{Id}_1, \quad A_{kl} := \langle [\chi_k]_s, [\chi_l]_s \rangle_m, \quad \vec{A}_{kl} := A_{kl}\, \vec{Id}_1,$$
$$\text{and} \quad \vec{\mathcal{A}}_{kl} := \Big(\langle \vec{\nabla}_s\, (\chi_k\, \vec{e}_i), \vec{\nabla}_s\, (\chi_l\, \vec{e}_j) \rangle_m \Big)^d_{i,j=1}\,, \tag{4.1}$$

where, as before, $\{\vec{e}_i\}^d_{i=1}$ are the standard orthonormal vectors in $\mathbb{R}^d$.

Curve shortening flow

In addition, we define the orthogonal projection $\vec{\mathcal{P}} : (\mathbb{R}^d)^J \to \underline{\mathbb{K}} := \{\vec{z} \in (\mathbb{R}^d)^J : \vec{z}_j \,.\, \vec{\omega}^m_d(q_j) = 0,\ j = 1 \to J\}$ onto the Euclidean space associated with $\underline{V}^{h,m}_{\vec{\Gamma}}$. Then we can formulate (3.3a,b) as: Find $\{\delta\vec{X}^{m+1}, \vec{\kappa}^{m+1}\} \in (\mathbb{R}^d)^J \times \underline{\mathbb{K}}$ such that

$$\begin{pmatrix} \tau_m\, \vec{\mathcal{P}}\vec{M}\vec{\mathcal{P}} & -\vec{\mathcal{P}}\vec{M} \\ \vec{M}\vec{\mathcal{P}} & \vec{A} \end{pmatrix} \begin{pmatrix} \vec{\kappa}^{m+1} \\ \delta\vec{X}^{m+1} \end{pmatrix} = \begin{pmatrix} \vec{0} \\ -\vec{A}\,\vec{X}^m \end{pmatrix}, \tag{4.2}$$

where, with the obvious abuse of notation, $\delta\vec{X}^{m+1} = (\delta\vec{X}^{m+1}_1, \ldots, \delta\vec{X}^{m+1}_J)^T$ and $\vec{\kappa}^{m+1} = (\vec{\kappa}^{m+1}_1, \ldots, \vec{\kappa}^{m+1}_J)^T$, are the vectors of coefficients for $\vec{X}^{m+1} - \vec{X}^m$ and $\vec{\kappa}^{m+1}$, respectively. On noting that $\vec{M}\vec{\mathcal{P}} = \vec{\mathcal{P}}\vec{M}$, and on recalling that $\vec{M}$ is an invertible matrix, we can transform (4.2) to

$$\vec{\kappa}^{m+1} = \tfrac{1}{\tau_m}\, \vec{\mathcal{P}}\, \delta\vec{X}^{m+1}, \tag{4.3a}$$
$$(\vec{A} + \tfrac{1}{\tau_m}\, \vec{\mathcal{P}}\vec{M}\vec{\mathcal{P}})\, \delta\vec{X}^{m+1} = -\vec{A}\,\vec{X}^m\,. \tag{4.3b}$$

Curve diffusion

Similarly to (4.2), and on recalling (4.1), we can formulate (3.4a,b) as follows. Find $\{\delta\vec{X}^{m+1}, \vec{\kappa}^{m+1}\} \in (\mathbb{R}^d)^J \times \underline{\mathbb{K}}$ such that

$$\begin{pmatrix} \tau_m\, \vec{\mathcal{P}}\vec{\mathcal{A}}\vec{\mathcal{P}} & -\vec{\mathcal{P}}\vec{M} \\ \vec{M}\vec{\mathcal{P}} & \vec{A} \end{pmatrix} \begin{pmatrix} \vec{\kappa}^{m+1} \\ \delta\vec{X}^{m+1} \end{pmatrix} = \begin{pmatrix} \vec{0} \\ -\vec{A}\,\vec{X}^m \end{pmatrix}. \tag{4.4}$$

In order to apply a Schur complement approach to (4.4), we need to characterize the kernel of $\vec{\mathcal{P}}\vec{\mathcal{A}}\vec{\mathcal{P}}$. It clearly holds that $\vec{\mathcal{P}}\vec{\mathcal{A}}\vec{\mathcal{P}}$ is positive semidefinite, and hence

$$\vec{z} \in \ker \vec{\mathcal{P}}\vec{\mathcal{A}}\vec{\mathcal{P}} \quad \Longleftrightarrow \quad \vec{z}\,.\,\vec{\mathcal{P}}\vec{\mathcal{A}}\vec{\mathcal{P}}\,\vec{z} = 0 \quad \Longleftrightarrow \quad \vec{\mathcal{P}}\,\vec{z} \in \ker \vec{\mathcal{A}}\,.$$

It follows that $\ker \vec{\mathcal{P}}\vec{\mathcal{A}}\vec{\mathcal{P}} = \underline{\mathbb{K}}^{\perp} \oplus (\underline{\mathbb{K}} \cap \ker \vec{\mathcal{A}})$. It remains to identify $\underline{\mathbb{K}} \cap \ker \vec{\mathcal{A}}$, i.e. the discrete analogue of (2.13). We have that $\langle \vec{\nabla}_s\,\vec{\eta}, \vec{\nabla}_s\,\vec{\eta}\rangle_m = 0$ for $\vec{\eta} \in \underline{V}_{\vec{\tau}}^{h,m}$ if and only if

$$\vec{P}^m[\vec{\eta}(q_{j+1}) - \vec{\eta}(q_j)] = \vec{0} \quad \text{on } [q_j, q_{j+1}] \quad \text{and} \quad \vec{\eta}(q_j)\,.\,\vec{\omega}_d^m(q_j) = 0 \quad \text{for } j = 1 \to J, \quad (4.5)$$

where we recall (3.1). Now (4.5) can be used, under our assumption ($\mathcal{C}$), to show that $\underline{\mathbb{K}} \cap \ker \vec{\mathcal{A}} = \operatorname{span}\{\vec{k}_\ell : \ell = 1 \to K\}$, where $\{\vec{k}_\ell\}_{\ell=1}^K$ are linearly independent and $K \le d-1$. We recall (2.13), and note that also in the discrete case we observe in practice that $K = d-1$ if Γ^m lies in a two-dimensional hyperplane.

This characterization of $\ker \vec{\mathcal{P}}\,\vec{\mathcal{A}}\,\vec{\mathcal{P}}$ allows us to use a Schur complement approach as in Barrett, Garcke, and Nürnberg (2007b). In particular, on noting that $\vec{\mathcal{P}}\,\vec{k}_\ell = \vec{k}_\ell$ for $\ell = 1 \to K$, we introduce the orthogonal projection $\vec{\Pi}_M$ onto $\{\vec{X} \in (\mathbb{R}^d)^J : \vec{X}^T \vec{M}\,\vec{k}_\ell = 0, \ell = 1 \to K\}$ by $\vec{\Pi}_M := \vec{Id}_J - \vec{Q}_M\,\vec{Q}_M^T$ where the columns of $\vec{Q}_M$ form an orthonormal basis of $\operatorname{span}\{\vec{M}\,\vec{k}_\ell : \ell = 1 \to K\}$ if that space is nontrivial ($K \ge 1$), and $\vec{Q} = 0$ otherwise ($K = 0$). Then (4.4) is replaced by

$$\vec{\Pi}_M\,(\vec{A} + \tfrac{1}{\tau_m}\vec{M}\,\vec{\mathcal{P}}\,\vec{\mathcal{S}}\,\vec{\mathcal{P}}\,\vec{M})\,\vec{\Pi}_M\,\delta\vec{X}^{m+1} = -\vec{\Pi}_M\,\vec{A}\,\vec{X}^m\,, \quad (4.6)$$

where $\vec{\mathcal{S}}$ is the inverse of $\vec{\mathcal{P}}\,\vec{\mathcal{A}}\,\vec{\mathcal{P}}$ restricted on the set $(\ker \vec{\mathcal{P}}\,\vec{\mathcal{A}}\,\vec{\mathcal{P}})^{\perp}$; see Barrett, Garcke, and Nürnberg (2007b, p. 452) for the details in the case of curve networks in the plane, which is a very similar situation.

Willmore flow of curves

The system (3.5a,b) for the elastic flow of curves can be formulated as: Find $\{\delta\vec{X}^{m+1}, \vec{\kappa}^{m+1}\} \in (\mathbb{R}^d)^J \times \underline{\mathbb{K}}$ such that

$$\begin{pmatrix} \tau_m\,\vec{\mathcal{P}}(\vec{\mathcal{A}} + [\lambda^m]_+\,\vec{M})\vec{\mathcal{P}} & -\vec{\mathcal{P}}\vec{M} \\ \vec{M}\vec{\mathcal{P}} & \vec{A} \end{pmatrix} \begin{pmatrix} \vec{\kappa}^{m+1} \\ \delta\vec{X}^{m+1} \end{pmatrix} = \begin{pmatrix} \vec{\mathcal{P}}\,\vec{b} \\ -\vec{A}\,\vec{X}^m \end{pmatrix}, \quad (4.7)$$

where $\vec{b} \in (\mathbb{R}^d)^J$ with $\vec{b}_j = \left(-\frac{1}{2}\,\langle|\vec{\kappa}^m|^2\,\vec{X}_s^m, (\vec{e}_i\,\chi_j)_s\rangle_m^h - [\lambda^m]_-\,\langle\vec{\kappa}^m, \vec{e}_i\,\chi_j\rangle_m^h\right)_{i=1}^d$, $j = 1 \to J$.

The system (4.7) can once again be solved with a Schur complement approach. First, consider the simpler case when $\lambda^m > 0$ or $K = 0$, recall (4.6), so that $\vec{\mathcal{B}} := \vec{\mathcal{P}}\,(\vec{\mathcal{A}} + [\lambda^m]_+\,\vec{M})\,\vec{\mathcal{P}}$ is symmetric positive definite on $\underline{\mathbb{K}}$; and we denote its inverse on $\underline{\mathbb{K}}$ by $\vec{\mathcal{B}}^{-1}$. Then (4.7) can be transformed to

$$\vec{\kappa}^{m+1} = \tfrac{1}{\tau_m}\,\vec{\mathcal{B}}^{-1}\,\vec{\mathcal{P}}\,[\vec{M}\,\delta\vec{X}^{m+1} + \vec{b}], \quad (4.8a)$$

$$(\vec{A} + \tfrac{1}{\tau_m}\,\vec{M}\,\vec{\mathcal{P}}\,\vec{\mathcal{B}}^{-1}\,\vec{\mathcal{P}}\,\vec{M})\,\delta\vec{X}^{m+1} = -\vec{A}\,\vec{X}^m - \tfrac{1}{\tau_m}\,\vec{M}\,\vec{\mathcal{B}}^{-1}\,\vec{\mathcal{P}}\,\vec{b}. \quad (4.8b)$$

If $\lambda^m \le 0$ and $K \ge 1$, on the other hand, then the matrix $\vec{\mathcal{B}} = \vec{\mathcal{P}}\,\vec{\mathcal{A}}\,\vec{\mathcal{P}}$ is no longer invertible. Then, similarly to (4.6), we apply a Schur complement approach.

First, as $\vec{\mathcal{P}}\,\vec{k}_\ell = \vec{k}_\ell$ for $\ell = 1 \to K$, we have that

$$\vec{k}_\ell^{\,T}(\vec{M}\,\delta\vec{X}^{m+1} + \vec{b}) = 0\,, \qquad \ell = 1 \to K\,; \tag{4.9}$$

and hence it follows that

$$\vec{\kappa}^{m+1} = \tfrac{1}{\tau_m}\,\vec{\mathcal{S}}\,\vec{\mathcal{P}}\,[\vec{M}\,\delta\vec{X}^{m+1} + \vec{b}] + \sum_{\ell=1}^{K}\mu_\ell\,\vec{k}_\ell = \tfrac{1}{\tau_m}\,\vec{\mathcal{S}}\,\vec{\Pi}\,\vec{\mathcal{P}}\,[\vec{M}\,\delta\vec{X}^{m+1} + \vec{b}] + \sum_{\ell=1}^{K}\mu_\ell\,\vec{k}_\ell\,.$$

Here $\vec{S}$ is as in (4.6), and $\vec{\Pi} = \vec{Id}_J - \vec{Q}\,\vec{Q}^T$, with the columns of $\vec{Q}$ forming an orthonormal basis of $\underline{\mathbb{K}}\cap\ker\vec{\mathcal{P}}\,\vec{\mathcal{A}}\,\vec{\mathcal{P}} = \underline{\mathbb{K}}\cap\ker\vec{\mathcal{A}} = \mathrm{span}\{\vec{k}_\ell : \ell = 1 \to K\}$, so that $\vec{\Pi} : \underline{\mathbb{K}} \to (\ker\vec{\mathcal{P}}\,\vec{\mathcal{A}}\,\vec{\mathcal{P}})^\perp$ is the orthogonal projection. Hence $\delta\vec{X}^{m+1}$ satisfies

$$(\vec{A} + \tfrac{1}{\tau_m}\,\vec{M}\,\vec{\mathcal{P}}\,\vec{\Pi}\,\vec{\mathcal{S}}\,\vec{\Pi}\,\vec{\mathcal{P}}\,\vec{M})\,\delta\vec{X}^{m+1} = -\vec{A}\,\vec{X}^m - \tfrac{1}{\tau_m}\vec{M}\,\vec{\mathcal{P}}\,\vec{\Pi}\,\vec{\mathcal{S}}\,\vec{\Pi}\,\vec{\mathcal{P}}\,\vec{b} - \sum_{\ell=1}^{K}\mu_\ell\,\vec{M}\,\vec{k}_\ell\,. \tag{4.10}$$

The unique solvability of (3.5a,b) yields that the operator $\vec{\mathcal{G}}$ on the left hand side of (4.10) is symmetric positive definite. Hence $\mu_\ell \in \mathbb{R}$, $\ell = 1 \to K$, have to be chosen such that the condition (4.9) is satisfied. This can be achieved as follows. Let $\vec{X}_f := \vec{\mathcal{G}}^{-1}\,(-\vec{A}\,\vec{X}^m - \tfrac{1}{\tau_m}\vec{M}\,\vec{\mathcal{P}}\,\vec{\Pi}\,\vec{\mathcal{S}}\,\vec{\Pi}\,\vec{\mathcal{P}}\,\vec{b})$ and $\vec{X}_\ell := \vec{\mathcal{G}}^{-1}\,\vec{M}\,\vec{k}_\ell$, $\ell = 1 \to K$. Then it holds that $(\mu_j)_{j=1}^K$ is the solution of the linear system

$$\Big(\vec{k}_\ell^{\,T}\,\vec{M}\,\vec{X}_j\Big)_{\ell,j=1}^{K}(\mu_j)_{j=1}^K = \Big(\vec{k}_\ell^{\,T}\,(\vec{M}\,\vec{X}_f + \vec{b})\Big)_{\ell=1}^{K} \quad \text{and} \quad \delta\vec{X}^{m+1} = \vec{X}_f - \sum_{\ell=1}^{K}\mu_\ell\,\vec{X}_\ell\,. \tag{4.11}$$

The well-posedness of (4.11) follows as $\Big(\vec{k}_\ell^{\,T}\,\vec{M}\,\vec{X}_j\Big)_{\ell,j=1}^{K} = \Big(\vec{k}_\ell^{\,T}\,\vec{M}\,\vec{\mathcal{G}}^{-1}\,\vec{M}\,\vec{k}_j\Big)_{\ell,j=1}^{K}$ is a symmetric positive definite matrix, on recalling that $\vec{k}_\ell$, $\ell = 1 \to K$, are linearly independent, and $\vec{M}$ and $\vec{\mathcal{G}}$ are symmetric positive definite matrices.

Geodesic flows

We recall the definitions (4.1), and in addition introduce the diagonal matrix $\vec{N} \in (\mathbb{R}^3)^{J\times J}$, defined by the diagonal entries $\vec{N}_{kk} := \vec{\omega}_{\mathcal{M}}^m\,M_{kk}$, $k = 1 \to J$. Moreover, we define the orthogonal projection $\vec{\mathcal{Q}} : (\mathbb{R}^3)^J \to \underline{\mathbb{X}} := \{\vec{z} \in (\mathbb{R}^3)^J : \vec{z}_j\,.\,\vec{\omega}_F^m(q_j) = 0,\ j = 1 \to J\}$ onto the Euclidean space associated with $\underline{V}_F^{h,m}$.

The linear equations that have to be solved at each time level of the approximation (3.9a,b) can then be written as follows. Find $\{\delta\vec{X}^{m+1}, \kappa_{\mathcal{M}}^{m+1}\} \in \underline{\mathbb{X}} \times \mathbb{R}^J$ such that

$$\begin{pmatrix} \tau_m\,M & -\vec{N}^T\vec{\mathcal{Q}} \\ \vec{\mathcal{Q}}\,\vec{N} & \vec{\mathcal{Q}}\,\vec{A}\,\vec{\mathcal{Q}} \end{pmatrix}\begin{pmatrix} \kappa_{\mathcal{M}}^{m+1} \\ \delta\vec{X}^{m+1} \end{pmatrix} = \begin{pmatrix} 0 \\ -\vec{\mathcal{Q}}\,\vec{A}\,\vec{X}^m \end{pmatrix}. \tag{4.12}$$

Similarly to (4.3a,b), we can transform (4.12) to

$$\kappa_{\mathcal{M}}^{m+1} = \tfrac{1}{\tau_m}\,M^{-1}\vec{N}^T\vec{\mathcal{Q}}\,\delta\vec{X}^{m+1}, \tag{4.13a}$$

$$\vec{\mathcal{Q}}\,(\vec{A} + \tfrac{1}{\tau_m}\,\vec{N}\,M^{-1}\vec{N}^T)\,\vec{\mathcal{Q}}\,\delta\vec{X}^{m+1} = -\vec{\mathcal{Q}}\,\vec{A}\,\vec{X}^m. \tag{4.13b}$$

Analogously, we can formulate the approximation (3.10), (3.9b) for geodesic surface diffusion as: Find $\{\delta\vec{X}^{m+1}, \kappa_{\mathcal{M}}^{m+1}\} \in \underline{\mathbb{X}} \times \mathbb{R}^J$, such that

$$\begin{pmatrix} \tau_m\, A & -\vec{N}^T\vec{\mathcal{Q}} \\ \vec{\mathcal{Q}}\,\vec{N} & \vec{\mathcal{Q}}\,\vec{A}\,\vec{\mathcal{Q}} \end{pmatrix} \begin{pmatrix} \kappa_{\mathcal{M}}^{m+1} \\ \delta\vec{X}^{m+1} \end{pmatrix} = \begin{pmatrix} 0 \\ -\vec{\mathcal{Q}}\,\vec{A}\,\vec{X}^m \end{pmatrix}. \tag{4.14}$$

Following closely the Schur approach in Barrett, Garcke, and Nürnberg (2007b) and introducing the inverse S of A restricted on the set $(\ker A)^\perp \equiv (\mathrm{span}\{1\})^\perp$, where $1 := (1,\ldots,1)^T \in \mathbb{R}^J$, as well as the orthogonal projection $\vec{\Pi}$ onto $\{\vec{X} \in (\mathbb{R}^d)^J : \vec{X}^T\,\vec{\mathcal{Q}}\,\vec{N}1 = 0\}$, we can solve for δX^{m+1} in (4.14) by solving

$$\vec{\Pi}\,\vec{\mathcal{Q}}\,(\vec{A} + \tfrac{1}{\tau_m}\,\vec{N}\,S\,\vec{N}^T)\,\vec{\mathcal{Q}}\,\vec{\Pi}\,\delta\vec{X}^{m+1} = -\vec{\Pi}\,\vec{\mathcal{Q}}\,\vec{A}\,\vec{X}^m. \tag{4.15}$$

Similarly, on introducing the matrix $M_G \in \mathbb{R}^{J\times J}$ defined by $[M_G]_{kl} := \langle [\lambda^m - \mathcal{K}^m]_+\,\chi_k, \chi_l\rangle_m^h$, $k,l = 1 \to J$, the system (3.11), (3.9b) for geodesic Willmore flow can be rewritten in terms of: Find $\{\delta\vec{X}^{m+1}, \kappa_{\mathcal{M}}^{m+1}\} \in \underline{\mathbb{X}} \times \mathbb{R}^J$, such that

$$\begin{pmatrix} \tau_m\,(A + M_G) & -\vec{N}^T\vec{\mathcal{Q}} \\ \vec{\mathcal{Q}}\,\vec{N} & \vec{\mathcal{Q}}\,\vec{A}\,\vec{\mathcal{Q}} \end{pmatrix} \begin{pmatrix} \kappa_{\mathcal{M}}^{m+1} \\ \delta\vec{X}^{m+1} \end{pmatrix} = \begin{pmatrix} b \\ -\vec{\mathcal{Q}}\,\vec{A}\,\vec{X}^m \end{pmatrix}, \tag{4.16}$$

where $b \in \mathbb{R}^J$ with $b_j = \tau_m\,\langle \frac{1}{2}(\kappa_{\mathcal{M}}^m)^3 + [\lambda^m - \mathcal{K}^m]_-\,\kappa_{\mathcal{M}}^m, \chi_j\rangle_m^h$, $j = 1 \to J$.

The solution to (4.16) can be found as follows, where we closely follow the exposition in Barrett, Garcke, and Nürnberg (2007b), where the planar case "$\mathcal{M} = \mathbb{R}^2$" was treated. If $\lambda^m - \mathcal{K}_{\min}^m > 0$, where $\mathcal{K}_{\min}^m := \min_{j=1\to J} \mathcal{K}^m(q_j)$, then $\widehat{A} := A + M_G$ is a positive definite matrix, and we can solve (4.16) by solving

$$\kappa_{\mathcal{M}}^{m+1} = \tfrac{1}{\tau_m}\,\widehat{A}^{-1}[\vec{N}^T\,\vec{\mathcal{Q}}\,\delta\vec{X}^{m+1} + b], \tag{4.17a}$$

$$\vec{\mathcal{Q}}\,(\vec{A} + \tfrac{1}{\tau_m}\,\vec{N}\,\widehat{A}^{-1}\vec{N}^T)\,\vec{\mathcal{Q}}\,\delta\vec{X}^{m+1} = -\vec{\mathcal{Q}}\,\vec{A}\,\vec{X}^m - \tfrac{1}{\tau_m}\,\vec{\mathcal{Q}}\,\vec{N}\,\widehat{A}^{-1}\,b\,. \tag{4.17b}$$

If $\lambda^m - \mathcal{K}_{\min}^m \le 0$, on the other hand, we note that

$$1^T(\vec{N}^T\,\vec{\mathcal{Q}}\,\delta\vec{X}^{m+1} + b) = 0\,,$$

and hence we have that

$$\kappa_{\mathcal{M}}^{m+1} = \tfrac{1}{\tau_m}\,S\,[\vec{N}^T\vec{\mathcal{Q}}\,\delta\vec{X}^{m+1} + b] + \mu\,1 = \tfrac{1}{\tau_m}\,S\,\Pi[\vec{N}^T\vec{\mathcal{Q}}\,\delta\vec{X}^{m+1} + b] + \mu\,1\,,$$

where S is defined as above and $\Pi = Id_J - \frac{1\,1^T}{1^T 1}$ is the orthogonal projection onto $(\ker A)^\perp = (\mathrm{span}\{1\})^\perp$, and where $\mu = \frac{1^T\kappa_{\mathcal{M}}^{m+1}}{1^T 1} \in \mathbb{R}$ is unknown. Hence the solution can be found by solving

$$\vec{\mathcal{Q}}\,(\vec{A} + \tfrac{1}{\tau_m}\,\vec{N}\,\Pi S\Pi\,\vec{N}^T)\,\vec{\mathcal{Q}}\,\delta\vec{X}^{m+1} = -\vec{\mathcal{Q}}\,\left[\vec{A}\,\vec{X}^m + \tfrac{1}{\tau_m}\,\vec{N}\,\Pi S\Pi\,b + \mu\,\vec{N}\,1\right]. \tag{4.18}$$

Similarly to (4.10), we let $\vec{G}$ denote the operator on the left hand side of (4.18), which is symmetric and positive definite. Then we find the solution to (4.18) as follows. Let $\vec{X}_f := -\vec{G}^{-1}\vec{\mathcal{Q}}\,[\vec{A}\,\vec{X}^m\frac{1}{\tau_m}\,\vec{N}\,\Pi S\Pi\,b]$ and $\vec{X}_g := \vec{G}^{-1}\vec{\mathcal{Q}}\,\vec{N}\,1$. Then

$$\mu := \frac{1^T b + 1^T\,\vec{N}^T\vec{\mathcal{Q}}\,\vec{X}_f}{1^T\,\vec{N}^T\vec{\mathcal{Q}}\,\vec{X}_g} \quad \text{and} \quad \delta\vec{X}^{m+1} = \vec{X}_f - \mu\,\vec{X}_g.$$

Note that $1^T\vec{N}^T\vec{\mathcal{Q}}\,\vec{X}_g = \vec{X}_g^T\,\vec{G}\,\vec{X}_g > 0$, as $\vec{G}$ is symmetric positive definite, so μ is well defined and uniquely determined.

Finally, on introducing the matrix $\mathcal{A} \in \mathbb{R}^{J\times J}$ defined by

$$[\mathcal{A}]_{kl} := \langle\vec{\nabla}_s\,\vec{\pi}^h(\chi_k\,\vec{\omega}_{\mathcal{M}}^m), \vec{\nabla}_s\,\vec{\pi}^h(\chi_l\,\vec{\omega}_{\mathcal{M}}^m)\rangle_m,$$

and the diagonal matrix $\vec{N}_F \in (\mathbb{R}^3)^{J\times J}$, defined by the diagonal entries $[\vec{N}_F]_{kk} := \vec{\omega}_F^m\,M_{kk}$, $k = 1 \to J$, the system (3.13a,b) for geodesic Willmore flow can be rewritten in terms of: Find $\{\delta\vec{X}^{m+1}, \kappa_{\mathcal{M}}^{m+1}, \kappa_F^{m+1}\} \in \underline{\mathbb{X}} \times [\mathbb{R}^J]^2$, such that

$$\begin{pmatrix} \tau_m\,(\mathcal{A} + [\lambda^m]_+ M) & -\vec{N}^T\vec{\mathcal{Q}} \\ \vec{\mathcal{Q}}\,\vec{N} & \vec{\mathcal{Q}}\,\vec{A}\,\vec{\mathcal{Q}} \end{pmatrix} \begin{pmatrix} \kappa_{\mathcal{M}}^{m+1} \\ \delta\vec{X}^{m+1} \end{pmatrix} = \begin{pmatrix} c \\ -\vec{\mathcal{Q}}\,\vec{A}\,\vec{X}^m \end{pmatrix}, \quad \kappa_F^{m+1} = -M^{-2}\,\vec{N}_F^T\,\vec{A}\,\vec{X}^{m+1} \tag{4.19}$$

where $c \in \mathbb{R}^J$ with $c_j = \tau_m\,\big[-\frac{1}{2}\,\langle(\kappa_{\mathcal{M}}^m)^2\,\vec{X}_s^m, (\vec{\pi}^h[\chi_j\,\vec{\omega}_{\mathcal{M}}^m])_s\rangle_m^h + \langle\kappa_{\mathcal{M}}^m\,\kappa_F^m, \mathrm{I\!I}(\chi_j\,\vec{\omega}_{\mathcal{M}}^m, \vec{\omega}_{\mathcal{M}}^m)\rangle_m^h - \langle[\lambda^m]_-\,\kappa_{\mathcal{M}}^m, \chi_j\rangle_m^h\big]$, $j = 1 \to J$. As before, the system (4.19) can be solved with a Schur complement approach. To this end, in the case $\lambda^m \leq 0$, we first identify the kernel of the matrix $\mathcal{A}$. It follows from (4.5) that $\langle\vec{\nabla}_s\,\vec{\pi}^h(\eta\,\vec{\omega}_{\mathcal{M}}^m), \vec{\nabla}_s\,\vec{\pi}^h(\eta\,\vec{\omega}_{\mathcal{M}}^m)\rangle_m = 0$ for $\eta \in W^h$, if and only if

$$\eta(q_{j+1})\,\vec{P}^m\,\vec{\omega}_{\mathcal{M}}^m(q_{j+1}) = \eta(q_j)\,\vec{P}^m\,\vec{\omega}_{\mathcal{M}}^m(q_j) \quad \text{on } [q_j, q_{j+1}] \text{ for } j = 1 \to J\,. \tag{4.20}$$

Now (4.20) can be used to find at most one linearly independent null vector of $\mathcal{A}$ explicitly, recall ($\mathcal{C}$). This allows us to apply a Schur complement approach as before, and we leave the details to the reader.

5 Results

The symmetric Schur complement systems (4.3b), (4.6), (4.8b), (4.10), (4.13b), (4.15), (4.17b) and (4.18) can be easily solved with a conjugate gradient solver. But we remark that in some situations the matrices $\vec{\mathcal{Q}}\,\vec{\mathcal{A}}\,\vec{\mathcal{Q}}$ and $\mathcal{A}$ can be ill conditioned, in particular when the criteria (4.5) and (4.20) are "almost satisfied". Then it proved beneficial in practice to solve an equivalent reformulation of e.g. the nonsymmetric system (4.4) with a preconditioned BiCGSTAB solver, where the preconditioner Chen, Phoon, and Toh (2006, Eqn. (4)) proved to be particularly efficient.

The schemes (3.5a,b), (3.11) with (3.9b) and (3.13a,b) need to be supplied with suitable initial data for the discrete curvatures. To this end, we define $\vec{y}^0 \in \underline{V}^h$ such that

$$\langle\vec{y}^0, \vec{\eta}\rangle_m^h + \langle\vec{X}_s^0, \vec{\eta}_s\rangle_m = 0 \qquad \forall\ \vec{\eta} \in \underline{V}^h\,. \tag{5.1}$$

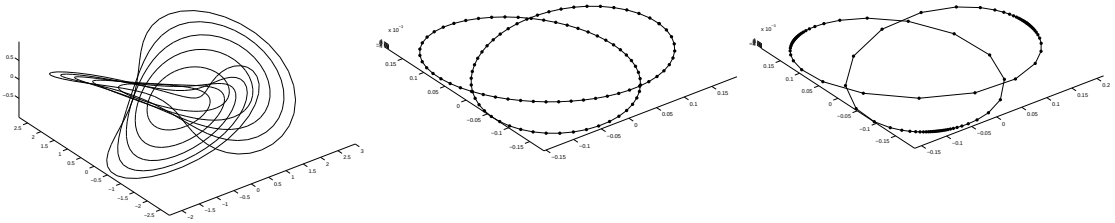

Figure 1: An example for curve shortening flow of a trefoil knot. On the left, $\vec{X}(t)$ at times $t = 0, 0.5, \ldots, 2, 2.45$. To the right, $\vec{X}(T)$ for (3.3a,b) and Dziuk's scheme (scaled).

Then $\vec{\kappa}^0 \in \underline{V}_{\vec{\tau}}^{h,m}$ and $\kappa_{\mathcal{M}}^0 \in W^h$ can be defined via

$$\langle \vec{\kappa}^0, \vec{\eta} \rangle_m^h = \langle \vec{y}^0, \vec{\eta} \rangle_m^h \qquad \forall\ \vec{\eta} \in \underline{V}_{\vec{\tau}}^{h,m}\,, \tag{5.2a}$$

$$\langle \kappa_{\mathcal{M}}^0, \eta \rangle_m^h = \langle \vec{y}^0, \eta\, \vec{\omega}_{\mathcal{M}}^0 \rangle_m^h \qquad \forall\ \eta \in W^h\,; \tag{5.2b}$$

and similarly for $\kappa_F^0 \in W^h$. The initial data $\vec{\kappa}_\phi^0$, $\kappa_{\phi,\mathcal{M}}^0$ and $\kappa_{\phi,F}^0$ for the anisotropic schemes (3.20), (3.18b) and (3.23a,b) can be defined in an analogous fashion, on introducing $\vec{y}_\phi^0$ via the obvious anisotropic variant of (5.1).

Throughout this section, unless otherwise stated, we use uniform time steps $\tau_m = \tau$, $m = 0 \to M-1$; and choose the initial approximation $\vec{X}^0$ of $\vec{x}(\cdot, 0)$ such that Γ^0 is approximatively equidistributed. In addition, we note that no remeshing was used for any of the experiments presented in this section and, unless stated otherwise, no projection to the manifold $\mathcal{M}$ was employed for the geodesic flows. For later purposes, we define

$$\vec{X}(t) := \tfrac{t-t_{m-1}}{\tau}\, \vec{X}^m + \tfrac{t_m - t}{\tau}\, \vec{X}^{m-1} \qquad t \in [t_{m-1}, t_m] \quad m \geq 1.$$

Curve shortening flow

In this section, we report on numerical simulations for our approximation (3.3a,b) of curve shortening flow, and compare our scheme to the approximation from Dziuk (1994), recall §3.1. The first experiment is for a trefoil knot in $\mathbb{R}^3$, and in particular the initial curve is given by

$$\vec{x}(\rho, 0) = ((2+\cos(6\,\pi\,\rho))\cos(4\,\pi\,\rho), (2+\cos(6\,\pi\,\rho))\sin(4\,\pi\,\rho), \sin(6\,\pi\,\rho))^T\,, \quad \rho \in I\,. \tag{5.3}$$

See Figure 1 for the results, where $J = 100$, $\tau = 10^{-3}$ and $T = 2.45$. We can clearly observe the (asymptotic) equidistribution property for our scheme (3.3a,b), as discussed in Remark 3.2. The result for the scheme from Dziuk (1994), on the other hand, shows a coalescence of mesh points, which prevents that scheme from integrating much further without their heuristic redistribution.

In addition, we performed experiments for a closed helix in $\mathbb{R}^3$. Here the open helix is defined by

$$\vec{x}_0(\varrho) = (\sin(16\,\pi\varrho), \cos(16\,\pi\,\varrho), \varrho)^T\,, \quad \varrho \in [0,1]\,, \tag{5.4}$$

and the initial curve is constructed from (5.4) by connecting $\vec{x}_0(0)$ and $\vec{x}_0(1)$ with a polygon that visits the points $\vec{0}$ and $\vec{e}_3$. We used the discretization parameters $J = 512$ and $\tau = 10^{-3}$. The results are shown in Figure 2.

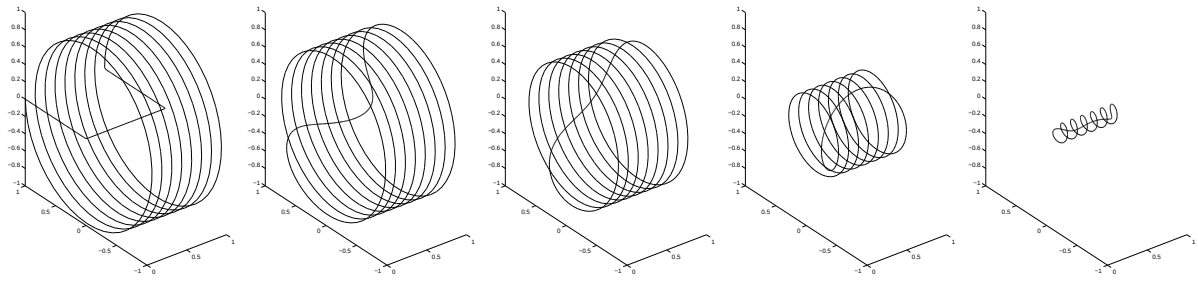

Figure 2: Isotropic curve shortening flow. Plot of $\vec{X}(t)$ at times $0, 0.1, 0.2, 0.4, 0.5$.

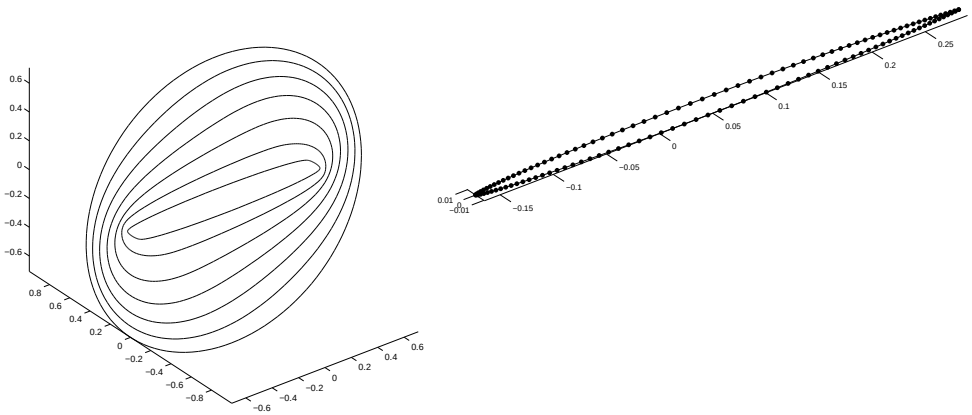

Figure 3: ($\phi(\vec{p}) = \sqrt{0.01\,p_1^2 + p_2^2 + p_3^2}$) Plot of $\vec{X}(t)$ at times $0, 0.1, \ldots, 0.6$ and at time $t = T = 0.68$ (scaled).

Anisotropic curve shortening flow

We repeated the experiment in Pozzi (2007, Fig. 3) for our scheme for anisotropic curve shortening flow in $\mathbb{R}^3$, i.e. the anisotropy is given by (2.39) with $L = 1$ and $\vec{G}_1 = \mathrm{diag}(0.01, 1, 1)$. Here the initial curve is given by the tilted unit circle

$$\vec{x}(\rho, 0) = (\tfrac{1}{\sqrt{2}}\cos(2\,\pi\,\rho), \sin(2\,\pi\,\rho), \tfrac{1}{\sqrt{2}}\cos(2\,\pi\,\rho))^T\,, \quad \rho \in I\,. \tag{5.5}$$

The discretization parameters were $J = 128$, $\tau = 10^{-3}$ and $T = 0.68$. As can be seen from the plots in Figure 3, at time $t = T$ the curve is aligned in the (x_1, x_2) plane and it has shrunk to a very elongated ellipse, as is to be expected from the chosen anisotropic energy density.

In addition, we performed experiments for a closed helix, inspired by the simulations in Pozzi (2007, Figs. 4 and 5). For the initial curve we choose the closed helix as in Figure 2, recall (5.4). For the same anisotropy as above, we performed a simulation with the discretization parameters $J = 512$ and $\tau = 10^{-3}$. The results are shown in Figures 4 and 5, where in the latter case the initial curve was rotated by 90°, in order to highlight the effect of the anisotropy.

Next we repeated the experiment in Figure 1 but now for the anisotropy (2.39) with $L = 1$ and $\vec{G}_1 = \mathrm{diag}(0.1, 1, 1)$. The results for the discretization parameters $J = 200$ and $\tau = 10^{-3}$ are shown in Figure 6. The same flow for (2.39) with $L = 3$ and $\vec{G}_1 = \mathrm{diag}(\varepsilon, 1, 1)$, $\vec{G}_2 = \mathrm{diag}(1, \varepsilon, 1)$, $\vec{G}_3 = \mathrm{diag}(1, 1, \varepsilon)$, with $\varepsilon = 10^{-3}$ is shown in Figure 7.

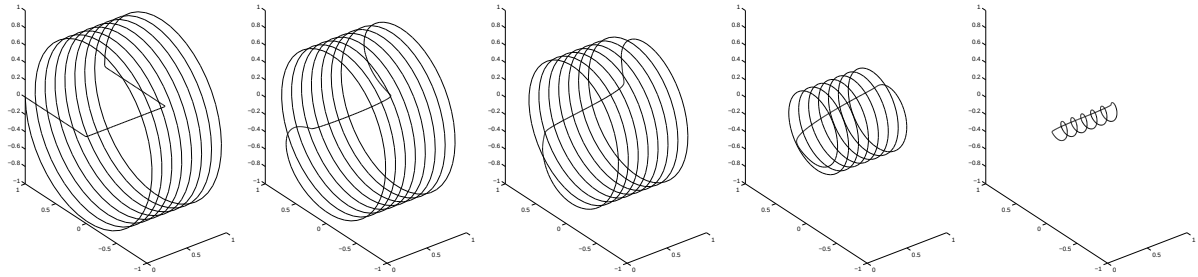

Figure 4: ($\phi(\vec{p}) = \sqrt{0.01\,p_1^2 + p_2^2 + p_3^2}$) Plot of $\vec{X}(t)$ at times $0, 0.1, 0.2, 0.4, 0.5$.

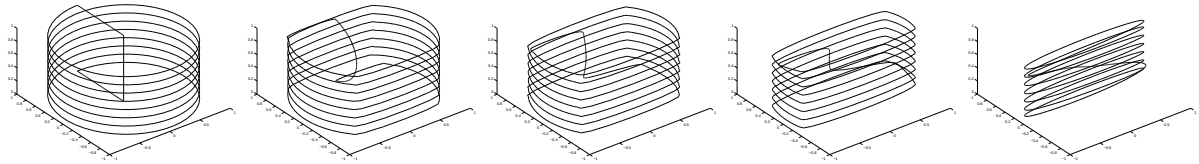

Figure 5: ($\phi(\vec{p}) = \sqrt{0.01\,p_1^2 + p_2^2 + p_3^2}$) Plot of $\vec{X}(t)$ at times $0, 0.1, 0.2, 0.4, 0.7$.

For the last two experiments we observe that in each case, as expected, the curve quickly aligns with the $x_1 - x_2$ plane (although it could have also chosen the $x_1 - x_3$ plane in the first case, or the $x_1 - x_3$ or $x_2 - x_3$ plane in the latter case), and then shrinks to a point. As it does so, the curve clearly resembles the Wulff shape of the given anisotropies, i.e. an ellipse in Figure 6 and a smooth square in Figure 7.

Curve diffusion

Here we report on results for the scheme (3.4a,b). Numerical results for $d = 2$ are very similar to the ones reported in Barrett, Garcke, and Nürnberg (2007b), and hence we only report on a single numerical simulation. We repeated the experiment in Barrett, Garcke, and Nürnberg (2007b, Fig. 8), i.e. the surface diffusion flow of a planar $8:1$ ellipse with semiminor 0.075. We let $J = 256$, $\tau = 10^{-7}$ and $T = 10^{-3}$. See Figure 8 for the results. The total relative area loss for this computation was 0.04%, which is surprisingly less than the loss of 0.09% observed for the scheme in Barrett, Garcke, and Nürnberg (2007b). Here we recall that for a continuous in time semi-discrete version of the scheme in Barrett, Garcke, and Nürnberg (2007b), exact area conservation can be shown; something that does not appear possible for (3.4a,b). We note that in practice,

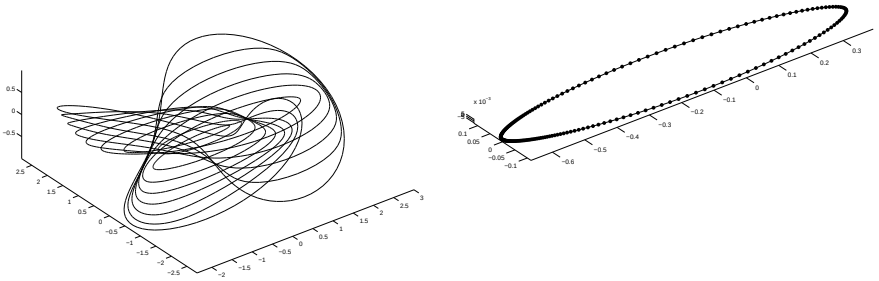

Figure 6: ($\phi(\vec{p}) = \sqrt{0.1\,p_1^2 + p_2^2 + p_3^2}$) An example for anisotropic curve shortening flow of a trefoil knot. Plots of $\vec{X}(t)$ for $t = 0, 0.5, \ldots, 3.5, 3.7$ and $\vec{X}(3.7)$ (scaled).

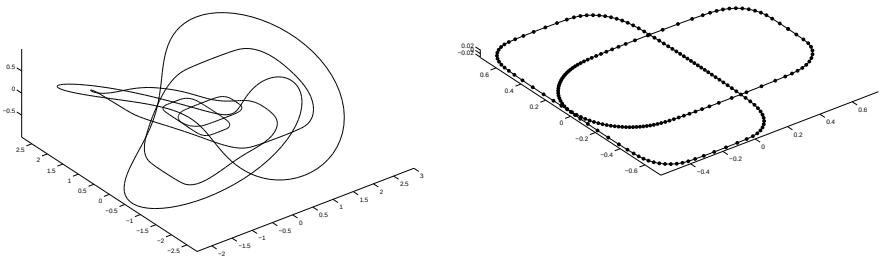

Figure 7: $(\phi(\vec{p}) = \sum_{\ell=1}^{3} \phi_\ell(\vec{p}))$ Plots of $\vec{X}(t)$ for $t = 0, 0.5, 1$ and $\vec{X}(1)$ (scaled).

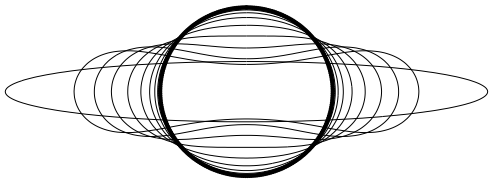

Figure 8: $(d = 2)$ Curve diffusion for an 8:1 ellipse. $\vec{X}(t)$ at times $t = 0, 10^{-4}, \ldots, 10^{-3}$.

we always observed good area conservation for (3.4a,b) and, as expected, equidistribution of mesh points for numerical steady states.

In a first computation for $d = 3$, we repeated the experiment in Figure 1, but now for the curve diffusion flow (2.10). The discretization parameters were $J = 100$, $\tau = 10^{-3}$ and $T = 4$. We compare the results of our scheme (3.4a,b) with the corresponding approximation in Dziuk, Kuwert, and Schätzle (2002), i.e. Barrett, Garcke, and Nürnberg (2007b, (2.3a,b)), which from now on will be referred to as DKS, see Figure 9. In Figure 10 we compare the ratio $r^m := h^m_{\max}/h^m_{\min}$, where $h^m_{\max} := \max_{j=1\to N} |\vec{X}^m(q_j) - \vec{X}^m(q_{j-1})|$ and $h^m_{\min} := \min_{j=1\to N} |\vec{X}^m(q_j) - \vec{X}^m(q_{j-1})|$, for the schemes (3.4a,b) and DKS. We see that while our approximation approaches an equidistributed polygonal curve, the scheme DKS leads to coalescence of vertices and it soon fails to integrate further.

For the interested reader, we continue the evolution in Figure 9 further, until the curve reaches a numerically steady state. In line with the theoretical result in Lemma 2.1, the curve evolves to a doubly covered circle; see Figure 11. However, we recall that multiply covered circles are unstable for the curve diffusion flow, see e.g. Chou (2003). The fact that the presented example leads to a doubly covered circle is due to the chosen symmetric initial data. Hence it is remarkable, that our numerical scheme is able to follow this flow

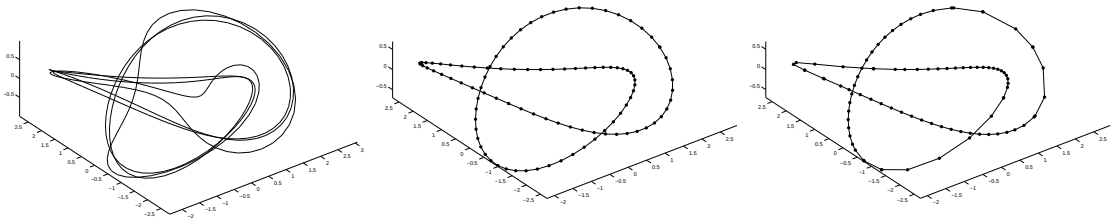

Figure 9: Curve diffusion for a trefoil knot. $\vec{X}(t)$ at times $t = 0, 2, T = 4$, and $\vec{X}(T)$ for (3.4a,b). On the right, $\vec{X}(T)$ for DKS.

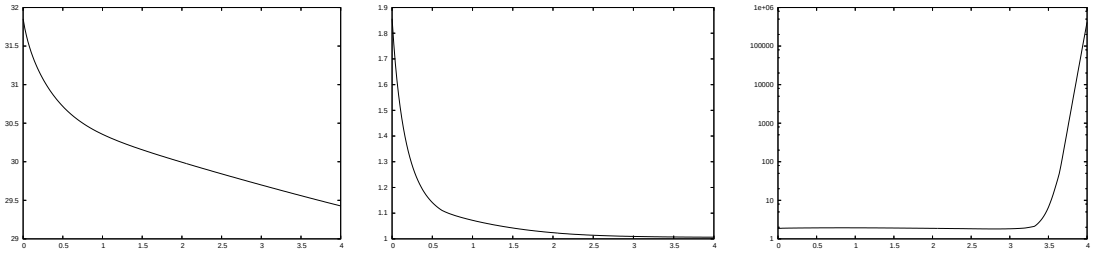

Figure 10: Plot of $|\Gamma^m|$ and r^m. On the right, a plot of $\log r^m$ for DKS.

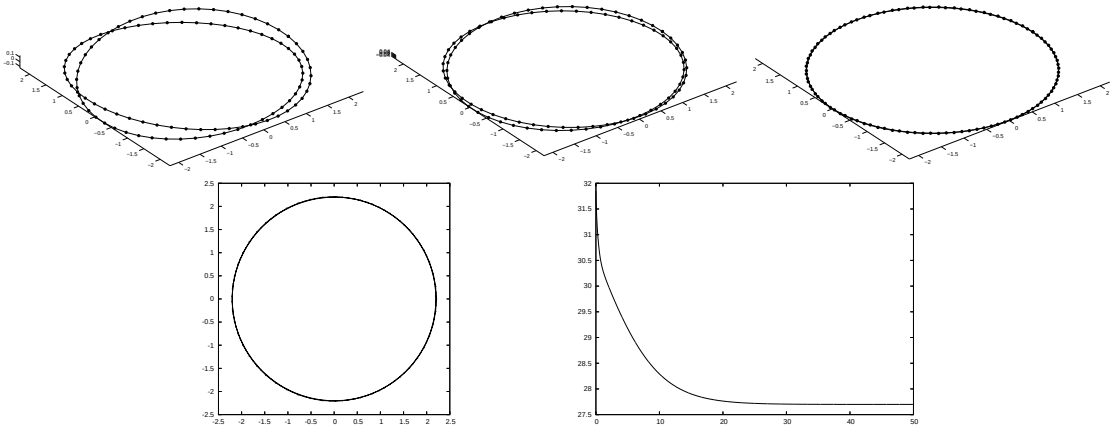

Figure 11: Plot of $\vec{X}(t)$ for $t = 20, 30, 50$. Below a $2d$ view of $\vec{X}(50)$ and a plot of $|\Gamma^m|$.

to the (unstable) steady state solution.

The instability of multiply covered circles can also be seen as follows. For curve diffusion in the plane, recall (2.9), it can be shown that the quantity $\int_\Gamma \vec{x} \,.\, \vec{\nu} \, \mathrm{d}s$ is preserved. For curves that bound a region, it holds that $\int_\Gamma \vec{x} \,.\, \vec{\nu} \, \mathrm{d}s = 2 \, \mathrm{area}(\Gamma)$, and so the above property just reflects area conservation; see also (2.21). The second variation of the length functional at a (possibly multiply covered) covered circle, under the constraint that $\int_\Gamma \vec{x} \,.\, \vec{\nu} \, \mathrm{d}s$ is fixed, gives

$$[\delta^2 \, |\Gamma|](\eta) = \int_\Gamma [(\eta_s)^2 - \varkappa^2 \, \eta^2] \, \mathrm{d}s \,,$$

where $\eta : \Gamma \to \mathbb{R}$ is a variation in the normal direction; see e.g. Garcke, Ito, and Kohsaka (2005) for a similar analysis. We hence obtain that multiply covered circles are linearly unstable under curve diffusion, as e.g. the variation $\eta(s) = \cos(\frac{\varkappa}{l} \, s)$ for an l-times covered circle yields $[\delta^2 \, |\Gamma|](\eta) < 0$ if $l \geq 2$, on noting that $\varkappa$ is constant.

In order to illustrate the instability of multiply covered circles, we include the following two experiments. The first is for $d = 2$ and uses as initial data

$$\vec{x}(\rho, 0) = (\cos(4\,\pi\,\rho) - \delta \, \cos(2\,\pi\,\rho) \, \sin(4\,\pi\,\rho), \sin(4\,\pi\,\rho) + \delta \, \cos(2\,\pi\,\rho) \, \cos(4\,\pi\,\rho))^T, \quad \rho \in I \,,$$

where we set $\delta = 0.2$. Note that this corresponds to the above mentioned perturbation for a unit circle in the case $l = 2$. The evolution can be seen in Figure 12, where we observe that the double covering unravels and the curve flows towards a singularity. Note that

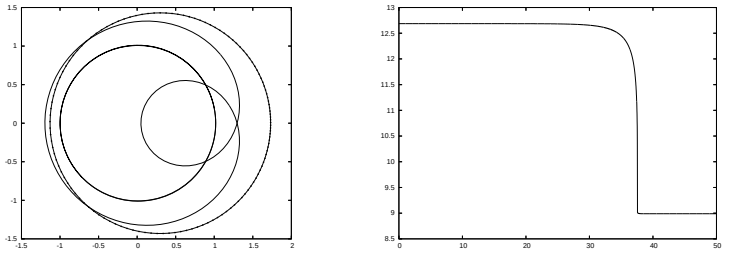

Figure 12: $(d = 2)$ $\vec{X}(t)$ at times $t = 0$, 37, 50. A plot of $|\Gamma^m|$ on the right.

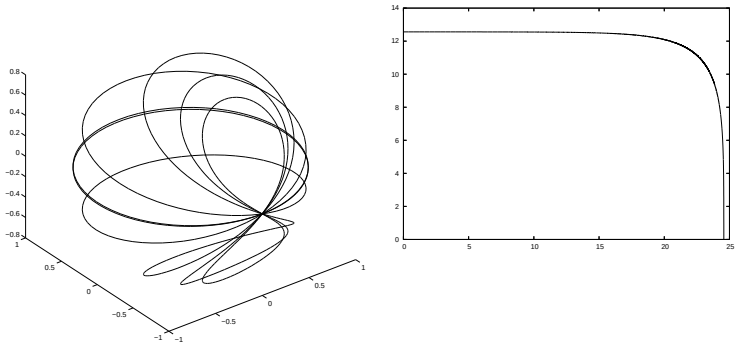

Figure 13: $\vec{X}(t)$ at times $t = 0$, 20, 24, 24.4, 24.5. A plot of $|\Gamma^m|$ on the right.

our numerical scheme simply integrates over the singularity (a cusp), so that the eventual steady state is a single covered circle. This is a well-known phenomenon of parametric approximations, see e.g. Deckelnick, Dziuk, and Elliott (2005, Fig. 4.2.) for an example for the curve shortening flow. The discretization parameters for this experiment were $J = 128$, $\tau = 10^{-4}$ and $T = 50$.

The second experiment is for $d = 3$ and uses as initial data

$$\vec{x}(\rho, 0) = (\sin(4\,\pi\,\rho), \cos(4\,\pi\,\rho), \delta\,\cos(2\,\pi\,\rho))^T, \quad \rho \in I\,,$$

where here we set $\delta = 0.01$. We show the evolution in Figure 13, where this time the doubly covered circle first opens up, and then shrinks to a point. The discretization parameters are $J = 128$, $\tau = 10^{-3}$ and $T = 24.568$, which was the approximate extinction time.

The curve diffusion flow for the closed helix as shown in Figure 2 can be seen in Figure 14, where we used the discretization parameters $J = 512$ and $\tau = 10^{-3}$.

Anisotropic curve diffusion

In an experiment for our scheme (3.19), (3.18b), with the anisotropy ϕ as in Figure 6, we start with the initial data (5.5) and choose as discretization parameters $J = 128$, $\tau = 10^{-3}$ and $T = 5$. The results can be seen in Figure 15, where we observe that the curve attains a Wulff shape in the $x_1 - x_2$ plane.

Willmore flow of curves

In this section, we present numerical simulations for our approximation (3.5a,b) of the Willmore flow of curves, and compare some of the results to the schemes (3.7a,b) from Deckelnick and Dziuk (2007), and to the corresponding scheme from Dziuk, Kuwert,

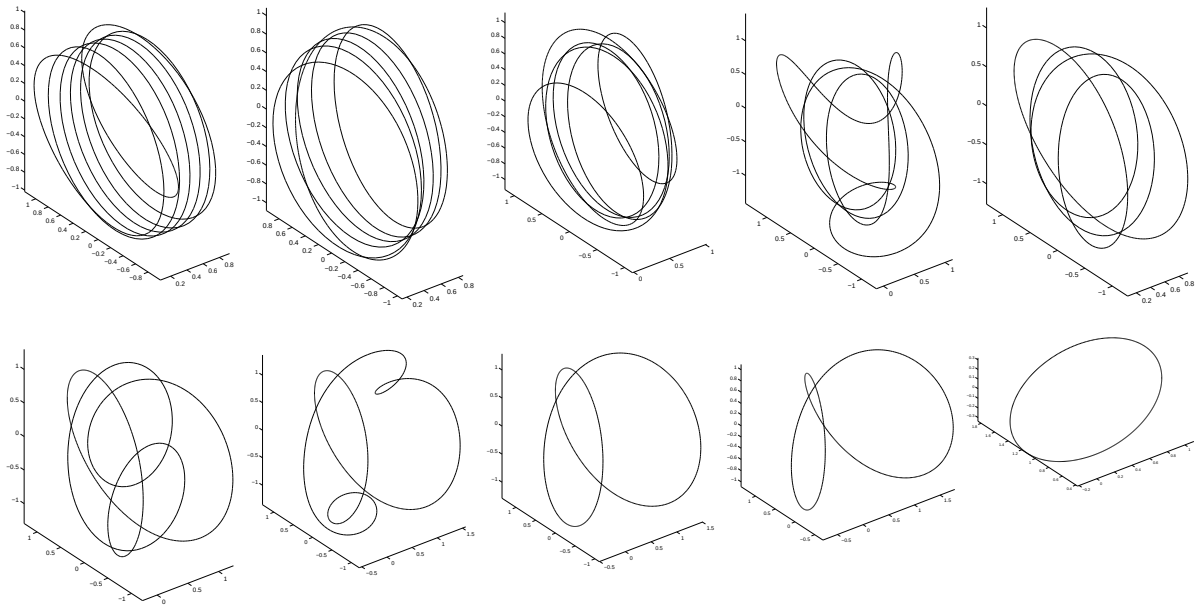

Figure 14: Plot of $\vec{X}(t)$ at times $t = 5$, 10, 15, 19, 20, 23, 24, 25, 30, 50.

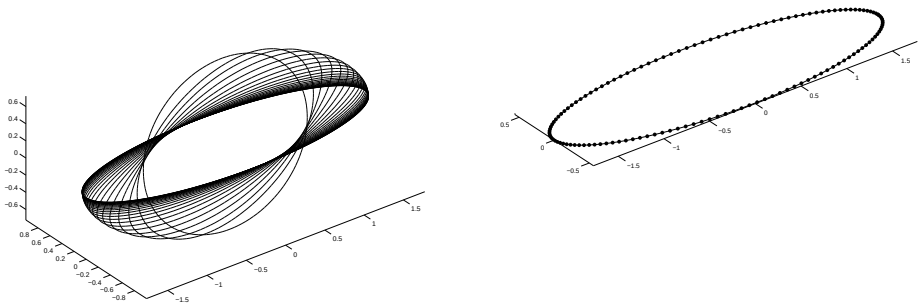

Figure 15: $\phi(\vec{p}) = \sqrt{0.1\,p_1^2 + p_2^2 + p_3^2}$. Plots of $\vec{X}(t)$ at times $t = 0, 0.2, \ldots, T = 5$ and at $t = T$.

and Schätzle (2002). The latter two schemes will be referred to as DD and DKS in this section.

The first experiment is for (2.25) with $\lambda = 0$. The initial curve is given by a $2:1$ lemniscate. As discretization parameters we choose $J = 100$, $\tau = 5 \times 10^{-4}$ and $T = 0.2$. In Figure 16 we show the evolutions for the three schemes as well as a plot of the discrete Willmore energy

$$\mathcal{W}^m := \begin{cases} \frac{1}{2}\,|\vec{\kappa}^{m+1}|_{m,h} & m = 0 \to M-1, \\ \frac{1}{2}\,|\vec{\kappa}^{M}|_{M,h} & m = M. \end{cases}$$

As can be seen from the plots, the lack of sufficient tangential movement of vertices leads to very long segments in the evolution of the schemes DKS and DD. We note that the scheme DKS fails soon after the shown time $T = 0.2$. For the other two schemes we continue the evolution until time $T = 6$, see Figure 17 for the results.

The remaining experiments in this subsection are for $d = 3$. First, we repeated the experiment in Figure 1, but now for the elastic flow of curves, (2.25) with the length

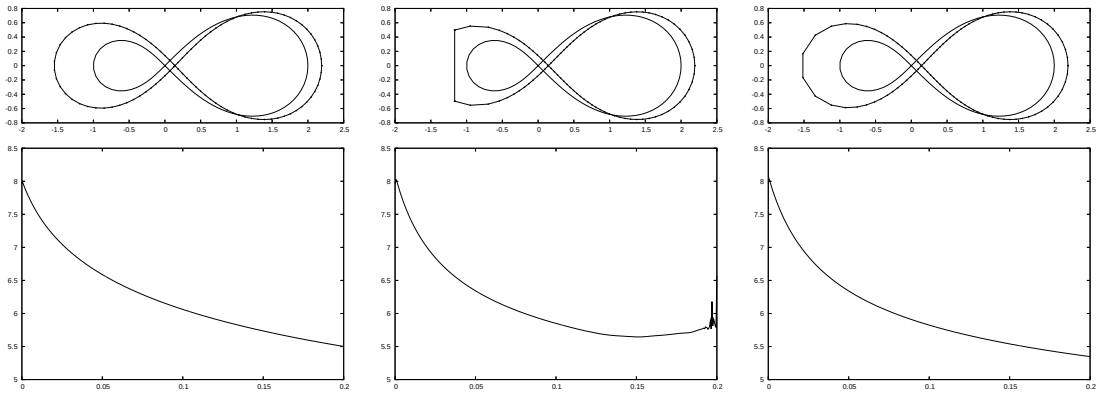

Figure 16: ($d = 2$) Evolution for (3.5a,b), DKS and DD. Plots of $\vec{X}(t)$, $t = 0, T = 0.2$. The discrete energy $\mathcal{W}^m$ below.

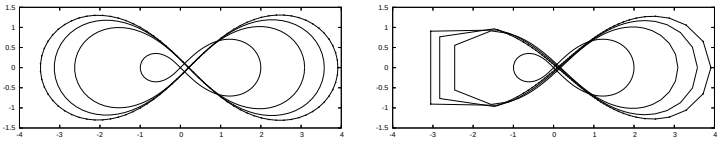

Figure 17: ($d = 2$) Evolution for (3.5a,b) and DD. Plots of $\vec{X}(t)$, $t = 0, 2, 4, 6$.

preserving choice (2.27). The discretization parameters were $J = 100$, $\tau = 10^{-3}$ and $T = 200$. We show the evolution in Figure 18, where the numerical steady state solution is a doubly covered circle. Here we recall that multiply covered circles are only stable for $d = 2$, see e.g. Langer and Singer (1985). Hence it is once again remarkable, that our numerical method manages to follow this flow to the (unstable) steady state solution.

The length preserving Willmore flow for the closed helix as shown in Figure 2 can be seen in Figure 19. The discretization parameters for (3.5a,b) with (3.6) were $J = 512$ and $\tau = 10^{-3}$.

Anisotropic Willmore flow of curves

In a first experiment for our approximation (3.20), (3.18b) for the flow (2.37) with $\lambda = 0$, we repeated the experiment in Figure 17, but now for the anisotropic energy densities $\phi(\vec{p}) = \sqrt{0.25\,p_1^2 + p_2^2}$ and $\phi(\vec{p}) = \sqrt{p_1^2 + 0.25\,p_2^2}$, see Figure 20. We observe that in each case, the lemniscate clearly aligns itself with the chosen anisotropy. Here we note for the reader that in a simpler experiment for the same anisotropies for a starting unit circle, say, the curve would first change towards a Wulff shape, i.e. a shape so that $\vec{\varkappa}_\phi$ is constant on Γ, see e.g. Giga (2006), and then expand almost self-similarly, with the asymptotic limit being an expanding Wulff shape, i.e. an ellipse.

The next experiment is for $d = 3$, and we start with the trefoil knot (5.3) and

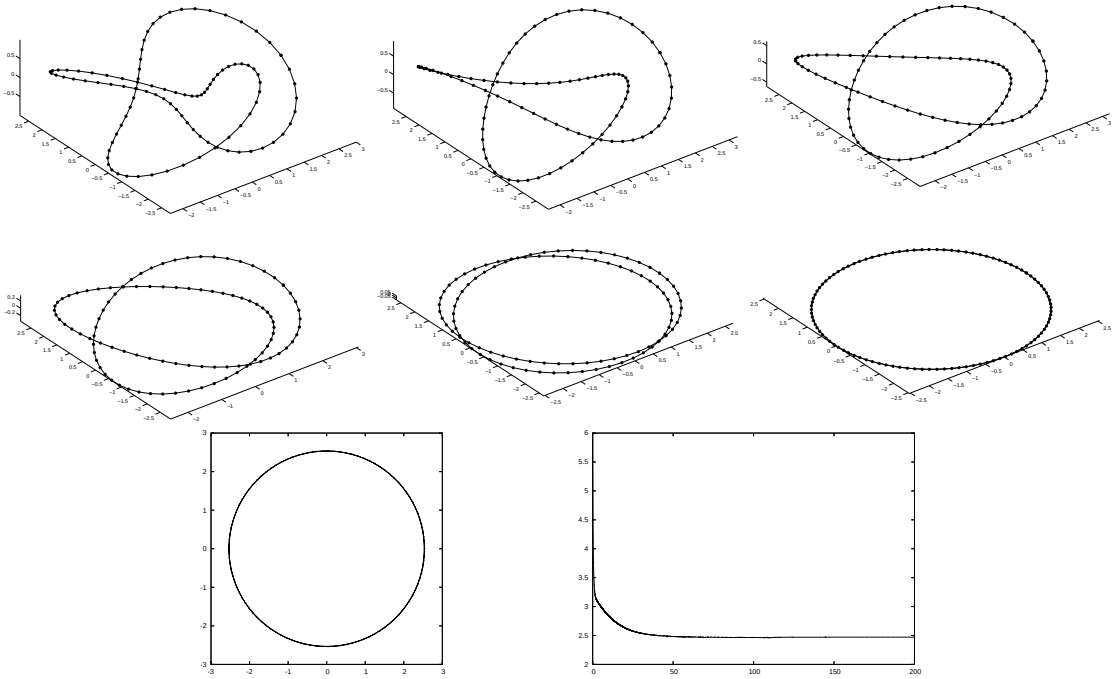

Figure 18: Plot of $\vec{X}(t)$ at times $t = 0, 2, 10, 20, 50, 200$. Below a $2d$ view of $\vec{X}(200)$ and a plot of $\mathcal{W}^m$.

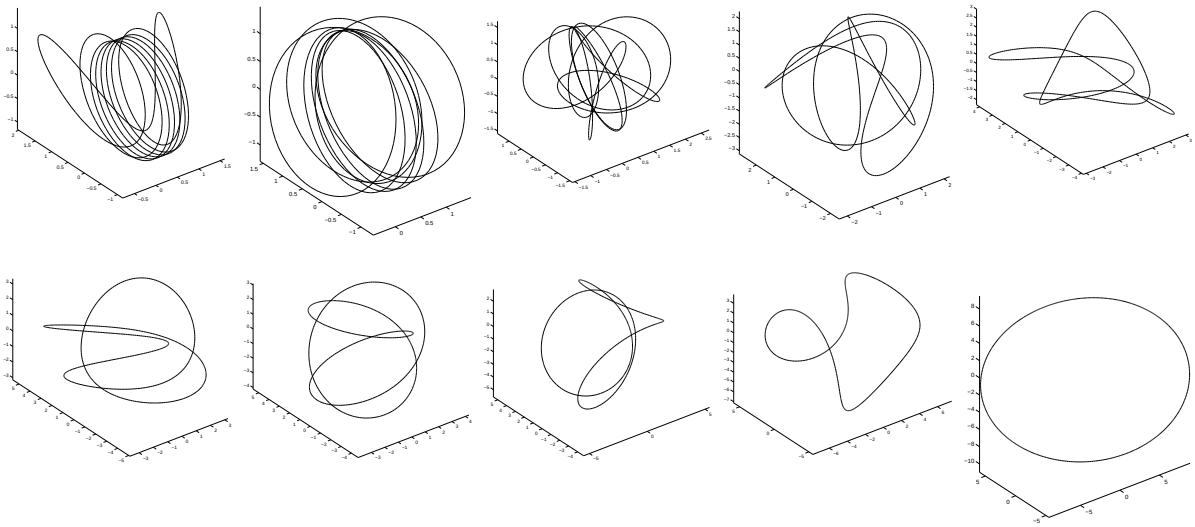

Figure 19: Plot of $\vec{X}(t)$ at times $t = 5$, 25, 50, 100, 200, 300, 500, 1000, 2000, 10000.

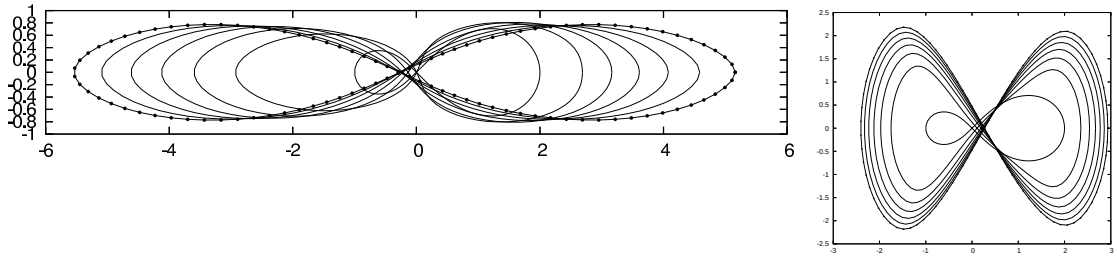

Figure 20: ($d = 2$, $\phi(\vec{p}) = \sqrt{0.25\,p_1^2 + p_2^2}$ (left) and $\phi(\vec{p}) = \sqrt{p_1^2 + 0.25\,p_2^2}$ (right)) Anisotropic Willmore flow of a lemniscate. Plots of $\vec{X}(t)$, $t = 0, 1, \ldots, 6$.

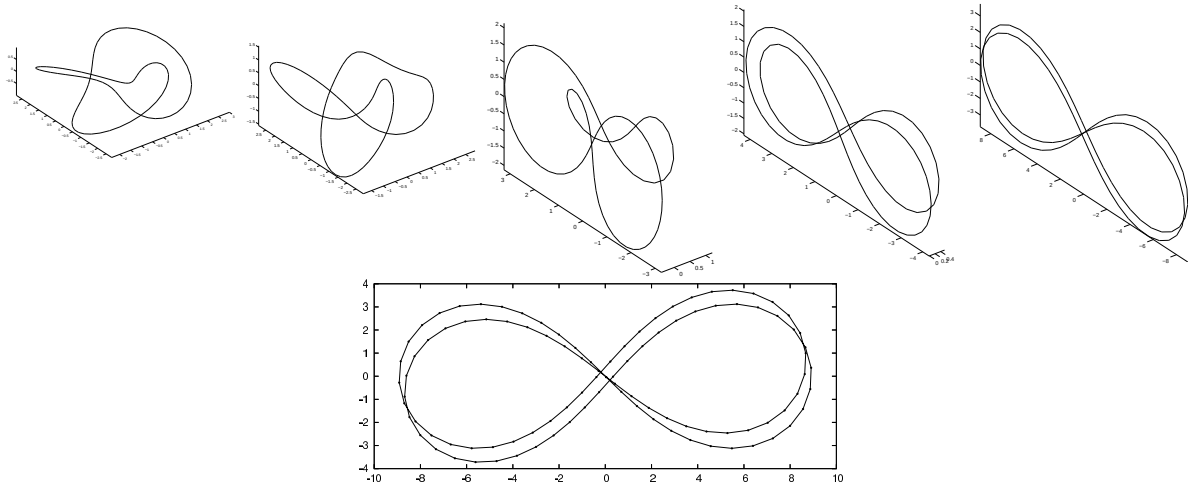

Figure 21: ($\phi(\vec{p}) = \sqrt{0.75\,p_1^2 + p_2^2 + p_3^2}$) Plots of $\vec{X}(t)$ at times $t = 0$, 0.5, 2, 10, 200. A $2d$ plot of $\vec{X}(T)$ in the $x_2 - x_3$ plane below.

used the same discretization parameters as in Figure 18. We used the anisotropic energy density $\phi(\vec{p}) = \sqrt{0.75\,p_1^2 + p_2^2 + p_3^2}$ and set $\lambda = 0$. The numerical results for our scheme (3.20), (3.18b) are shown in Figure 21. The same computation for the density $\phi(\vec{p}) = \sqrt{p_1^2 + 0.75\,p_2^2 + p_3^2}$ can be seen in Figure 22. Here the observed behaviour is quite interesting. In contrast to the corresponding results for anisotropic curve shortening and anisotropic curve diffusion flow, the results shown here do not always settle in the plane "favoured" by the chosen anisotropy. Of course, this is due to the energy (2) considered here. On recalling that $\vec{\varkappa}_\phi = \phi''(\vec{x}_s)\,\vec{x}_{ss}$, it is easy to see that for the anisotropies in Figures 21 and 22 it is beneficial, with regards to the energy, for the curve to remain in one of the three coordinate planes. In which of the three planes the curve ends up, depends (highly nontrivially) on the initial data.

Geodesic curvature flow

Here we test our approximation (3.9a,b) for the geodesic curvature flow (2.19) with the following true solution. Let $\Gamma(t)$ be a circle with radius $r(t)$ on the unit sphere in $\mathbb{R}^3$. Then

$$\vec{x}(\rho, t) = (r(t)\,\cos g(\rho), r(t)\,\sin g(\rho), [1 - r^2(t)]^{\frac{1}{2}})^T\,, \quad r(t) := [1 - (1 - r^2(0))\,\exp(2\,t)]^{\frac{1}{2}}\,, \tag{5.6}$$

with $r(0) \in (0, 1]$, is an exact solution of (2.19), where $g(\rho) = 2\,\pi\,\rho + 0.1\,\sin(2\,\pi\,\rho)$ in order

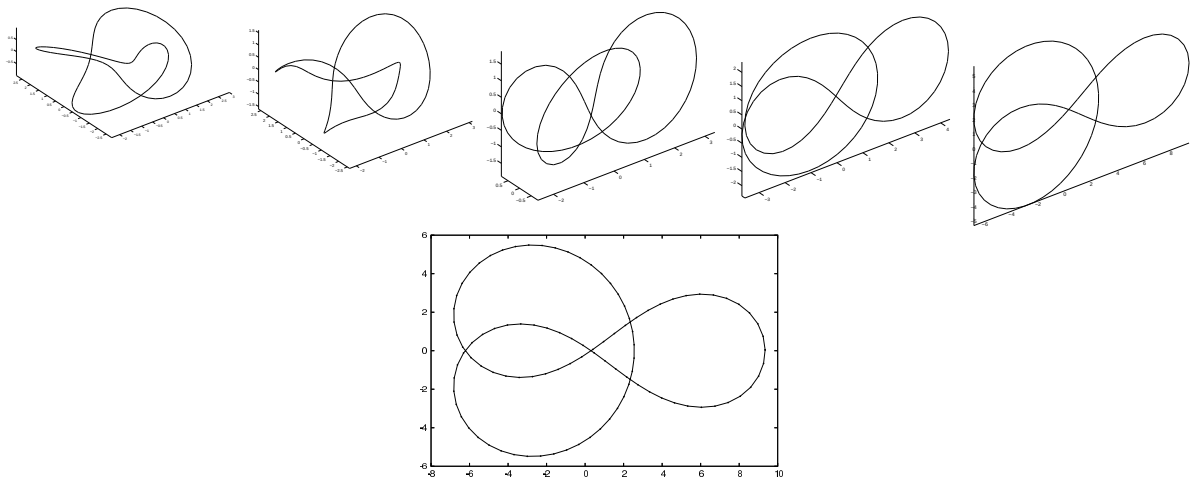

Figure 22: ($\phi(\vec{p}) = \sqrt{p_1^2 + 0.75\,p_2^2 + p_3^2}$) Plots of $\vec{X}(t)$ at times $t = 0,\ 0.5,\ 2,\ 10,\ 200$. A $2d$ plot of $\vec{X}(T)$ in the $x_1 - x_3$ plane below.

J	$\|\vec{X} - \vec{x}\|_{L^\infty}$	eoc
64	9.0903e-03	–
128	2.3143e-03	1.973752
256	5.8128e-04	1.993271
512	1.4550e-04	1.998214
1024	3.6386e-05	1.999564

Table 1: Absolute errors for the geodesic curvature flow.

to make the initial distribution of nodes in our approximation of (5.6) non-uniform. We use (5.6) in order to perform a convergence test for our approximation (3.9a,b), see Table 1. We used $\tau = 0.5\,h^2$ and $T = 2$, with the initial circle starting at an altitude of $x_3 = 0.1$, so that $r(0) = \sqrt{0.99}$ and the extinction time is given by $\overline{T} = \frac{1}{2}\,\ln\frac{1}{1-r^2(0)} \approx 2.303$. Here, and in what follows, we always compute the error $\|\vec{X} - \vec{x}\|_{L^\infty} := \max_{m=1\to M} \|\vec{X}(t_m) - \vec{x}(\cdot, t_m)\|_{L^\infty}$, where $\|\vec{X}(t_m) - \vec{x}(\cdot, t_m)\|_{L^\infty} := \max_{j=1\to J} \min_{\rho\in J} |\vec{X}^m(q_j) - \vec{x}(\rho, t_m)|$, between $\vec{X}$ and the true solution on the interval $[0, T]$. The results in Table 1 indicate a convergence rate for the error of $O(h^2)$.

As an example computation we present the above evolution for a circle on the unit sphere for the discretization parameters $J = 100$, $\tau = 10^{-3}$ and $T = 2.3$. See Figure 23 for the results. The corresponding evolution on a $2:1:1$ ellipsoid is on the right hand side in the same figure, where now $T = 2.5$.

In what follows, we look at geodesic curvature flows towards several different geodesics on a torus. To this end, we chose as the manifold $\mathcal{M}$ a torus with radii R and r, implicitly defined by the equation $0 = (R - \sqrt{z_1^2 + z_2^2})^2 + z_3^2 - r^2$. Throughout we set $R = 4$ and $r = 1$, unless otherwise stated. The discretization parameters for our scheme (3.9a,b) were $J = 200$ and $\tau = 10^{-2}$. Some results can be seen in Figure 24, where in each case we plot the initial and final curves, as well as the evolution of $|\Gamma^m|$. In each case, the maximum distance of a vertex of Γ^M to $\mathcal{M}$ was less than 10^{-4}. In addition, a more complicated flow

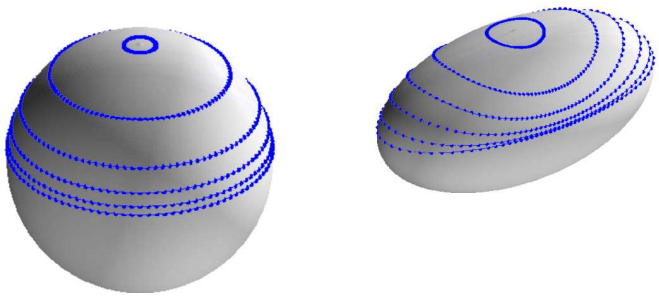

Figure 23: An example for geodesic curvature flow on the unit sphere and on a $2:1:1$ ellipsoid. In each case, we show $\vec{X}(t)$ at times $t = 0,\ 0.5,\ 1,\ 1.5,\ 2,\ T$.

can be seen in more detail in Figure 25. The evolution starts with a curve given by

$$\vec{x}(\rho, 0) = ((R + r\,\cos v(\rho))\,\cos u(\rho), (R + r\,\cos v(\rho))\,\sin u(\rho), r\,\sin v(\rho))^T, \quad \rho \in I\,,$$

where $u(\rho) = 2\pi\,(\rho + \frac{3}{4}\,\sin(2\pi\,\rho))$ and $v(\rho) = 10\,\pi\,\rho$. We used the same discretization parameters as before, except $\tau = 2 \times 10^{-3}$.

Now we give some example evolutions for curves on a sickle torus, where the smaller radius r varies between 0.5 and 2, and $R = 4$ as before. In particular, the sickle torus is given by the equation $0 = (R - \sqrt{z_1^2 + z_2^2})^2 + z_3^2 - [r(z_1, z_2)]^2$, where $r(z_1, z_2) := r_1 + \frac{r_2 - r_1}{2}\,(1 - \cos(\arctan(\frac{z_2}{z_1}))$ with $r_1 = 2$ and $r_2 = 0.5$.

The first experiment is for a vertical circular curve. Of course, on the standard torus, any such circle would be a steady state solution for the geodesic curvature flow. However, on the sickle torus, there exist only two such steady states: one where the tube is thinnest ($\theta = \pi$, say) and one where it is largest ($\theta = 0$). So if we start with the circle just left of the latter position, and in particular choose $\theta = -0.1\,\pi$, then the curve should move towards the energy minimizing geodesic at the thinnest point. This is what we observe in Figure 26. The discretization parameters were the same as before. Note that at time $t = T$, the maximum distance of the curve to the manifold was 4.6×10^{-3}. Next we repeated the experiments in Figures 24 and 25 now for the sickle torus. The results for the same parameters as before can be seen in Figures 27 and 28.

Anisotropic geodesic curvature flow

We considered also anisotropic geodesic curve evolutions. We begin with the geodesic curvature flow, (3.21a,b). In the first experiment, the initial curve is given by a circle on the unit sphere, either at the equator, or 0.1 above the equator, and in each case turned by 45° degrees. The anisotropy was chosen as in Figure 6, and the discretization parameters were $J = 128$, $\tau = 10^{-2}$ and $T = 2.8$. The results can be seen in Figure 29. We note that the curve which started on the tilted equator aligns itself with the chosen anisotropy and becomes stationary on the equator. As this stationary solution is unstable, it is once again remarkable that our numerical method can integrate this evolution correctly. The second evolution, however, yields a curve that moves towards the north pole. As it does so it attains an elliptic shape aligned with the anisotropy and eventually shrinks a point.

Geodesic surface diffusion

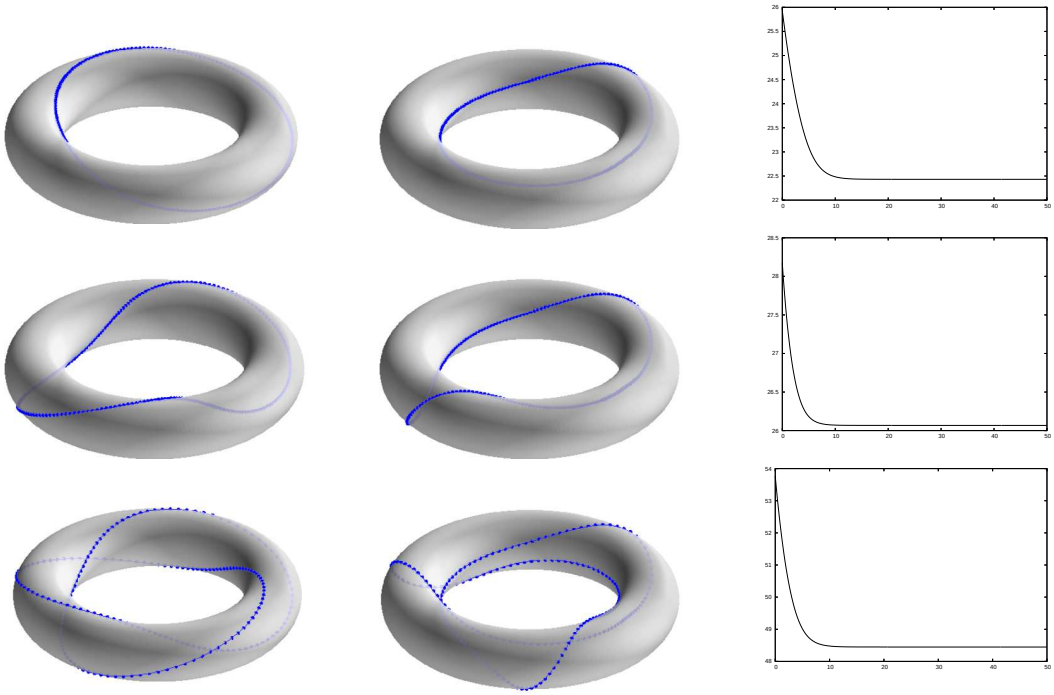

Figure 24: Flows towards geodesics on a torus. $\vec{X}(t)$, $t = 0,\ 50$. A plot of $|\Gamma^m|$ on the right.

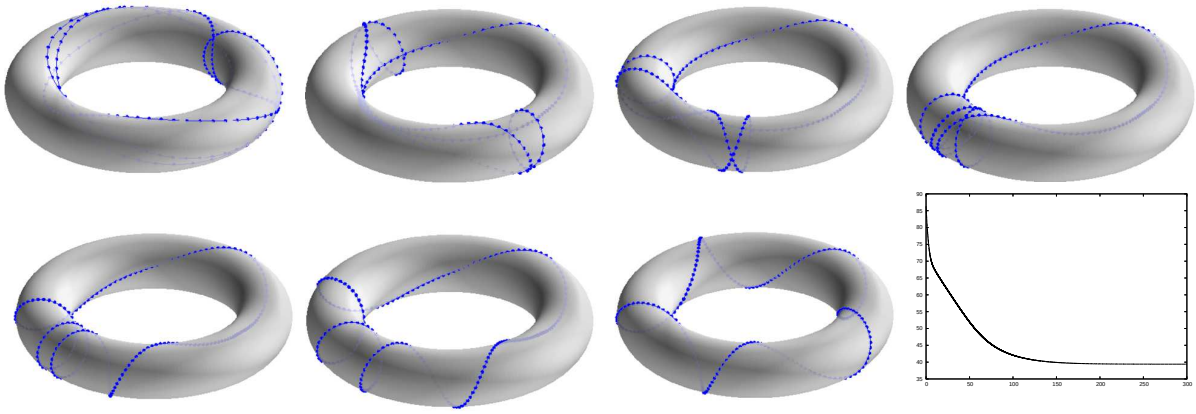

Figure 25: Flow towards a geodesic on a torus. $\vec{X}(t)$, $t = 0,\ 25, \ldots, 125,\ T = 300$. A plot of $|\Gamma^m|$ on the right.

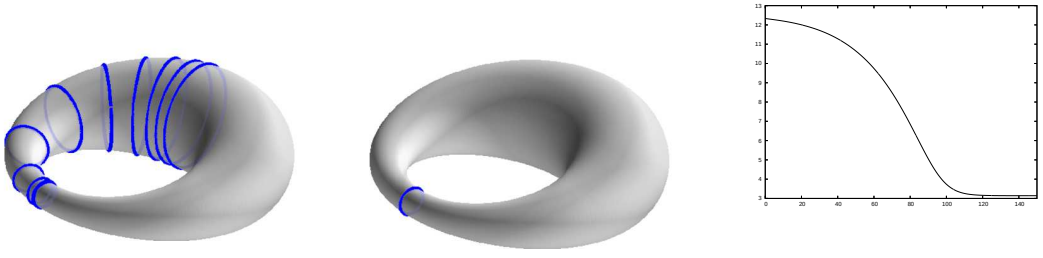

Figure 26: Flow towards a simple geodesic on a sickle torus. $\vec{X}(t)$, $t = 0, 15, \ldots, 150$. A plot of $|\Gamma^m|$ on the right.

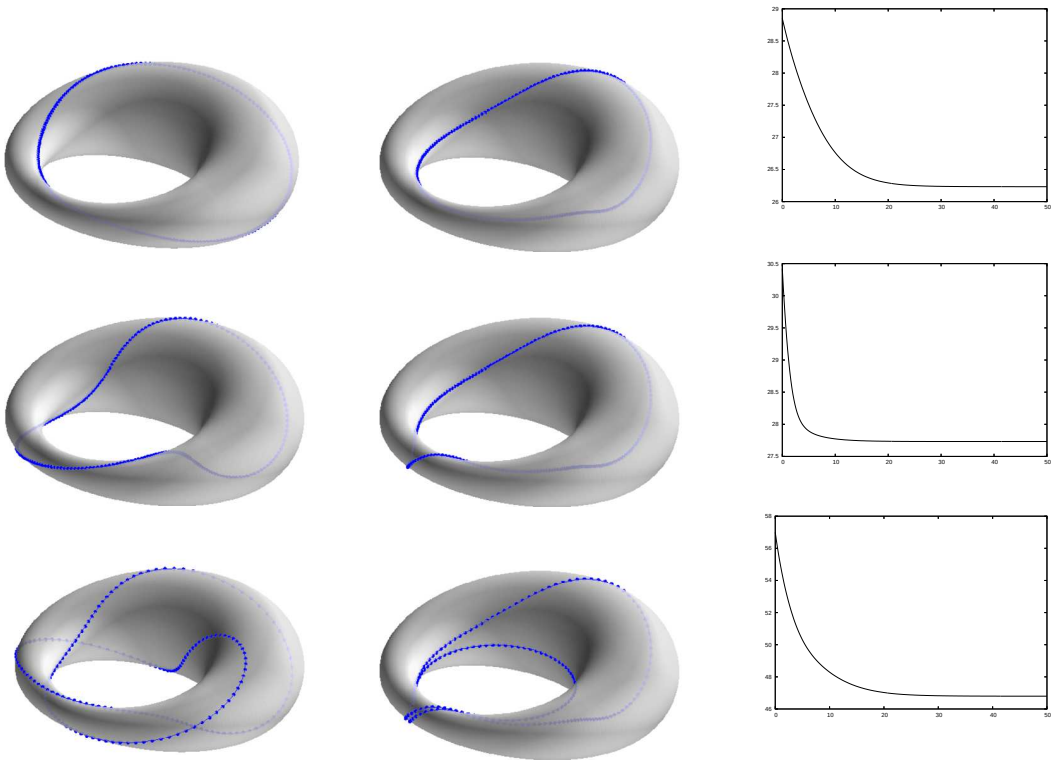

Figure 27: Flows towards geodesics on a sickle torus. $\vec{X}(t)$, $t = 0,\ 50$. A plot of $|\Gamma^m|$ on the right.

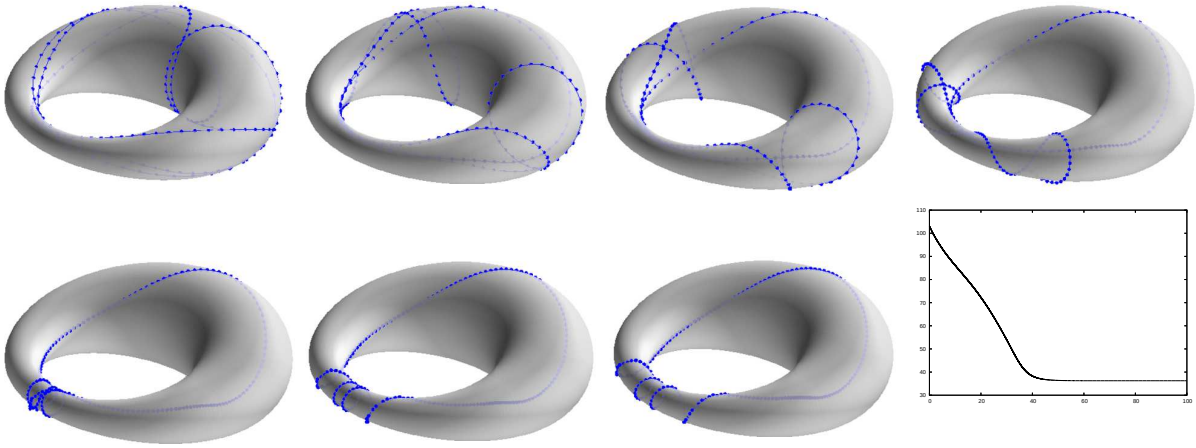

Figure 28: Flow towards a geodesic on a sickle torus. $\vec{X}(t)$, $t = 0, 10, \ldots, 50, T = 100$. A plot of $|\Gamma^m|$ on the right.

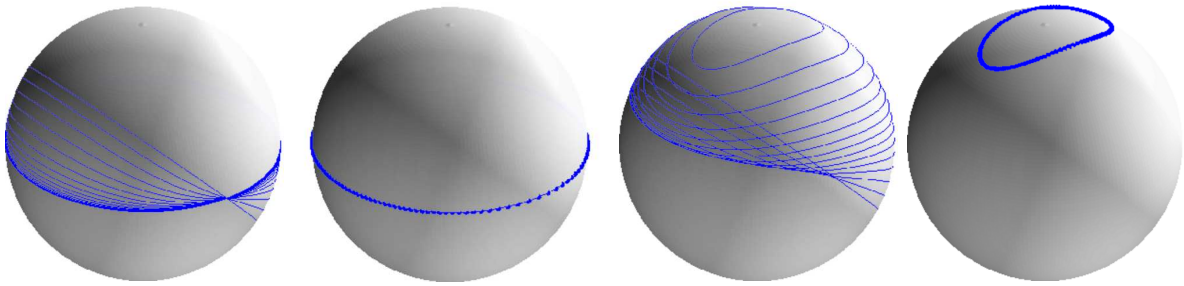

Figure 29: $\phi(\vec{p}) = \sqrt{0.1\,p_1^2 + p_2^2 + p_3^2}$. Anisotropic geodesic curve shortening flow on the unit sphere. Left starting on an equator, right starting 0.1 above equator. We plot $\vec{X}(t)$ for $t = 0, 0.2, \ldots, T = 2.8$ and $\vec{X}(T)$.

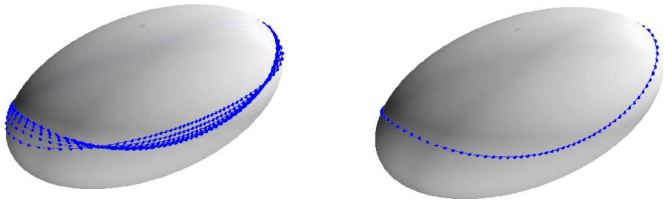

Figure 30: An example for surface diffusion flow on a $2:1:1$ ellipsoid. $\vec{X}(t)$ at times $t = 0, 0.2, \ldots, T = 3$ and $t = T$.

We repeated the experiment for the ellipsoid in Figure 23 now for geodesic surface diffusion, employing our scheme (3.10), (3.9b). The results are shown in Figure 30. We note that the final plot is a numerical steady state. We recall from (2.21) that this curve is a numerical approximation to the shortest curve on the manifold that encloses the same area as $\Gamma(0)$.

The evolution for a letter "C" that is projected onto a unit sphere can be seen in Figure 31. Here we chose $J = 100$ and $\tau = 10^{-4}$. We note that the approximately polygonal circle that was attained at time $T = 0.5$ has maximum distance 4.4×10^{-3} from the manifold $\mathcal{M}$. If we use the larger time step size $\tau = 10^{-3}$, however, this distance increases to 2.2×10^{-2} and the curve develops some oscillations. However, this problem can be prevented when using the orthogonal projection $\vec{\Pi}_{\mathcal{M}}$ back onto $\mathcal{M}$ after every time step, see Figure 32 for the corresponding results. It is interesting to note, that the observed oscillations for the larger time step size appear despite the stability result in Theorem 3.1 for our scheme (3.10), (3.9b). To underline this fact, we also present a plot of $|\Gamma^m|$ over time in Figure 32, both for the case $\tau = 10^{-3}$ and $\tau = 10^{-4}$.

Anisotropic geodesic surface diffusion

The next experiments are for the approximation (3.22), (3.21b) for geodesic surface diffusion. Here we start with an initial "circle" on a $2:1:1$ ellipsoid, which is tilted by 45°. In Figure 33 we show the evolution for the anisotropic density $\phi(\vec{p}) = \sqrt{0.01\,p_1^2 + p_2^2 + p_3^2}$ and the isotropic case $\phi(\vec{p}) = |\vec{p}|$. The discretization parameters were $J = 100$, $\tau = 10^{-3}$

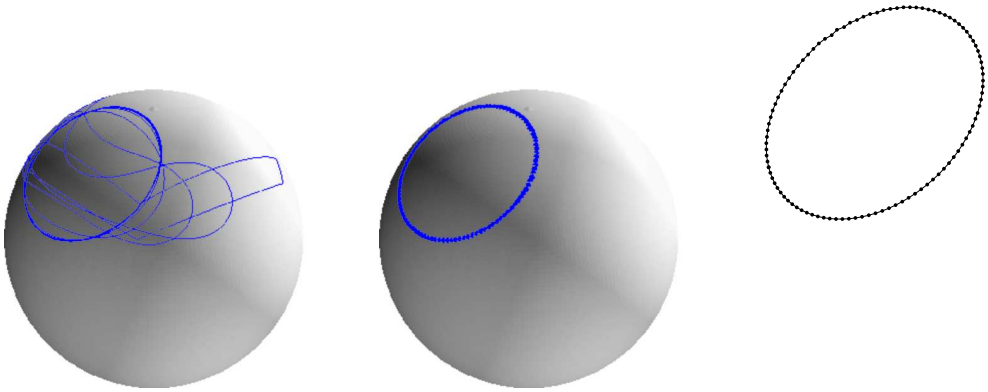

Figure 31: An example for surface diffusion flow on a unit sphere. Here $\tau = 10^{-4}$. $\vec{X}(t)$ at times $t = 0, 0.01, \ldots, T = 0.5$ and $\vec{X}(T)$.

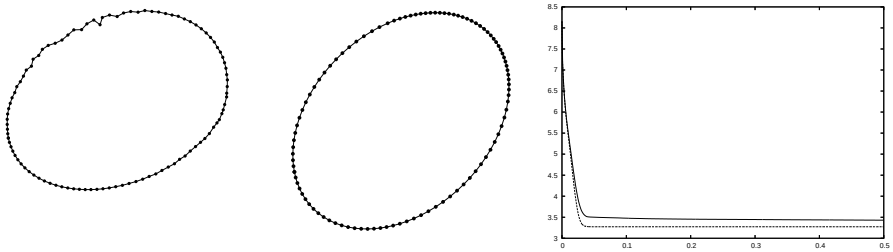

Figure 32: $\vec{X}(T)$ for the time step size $\tau = 10^{-3}$ without (left) and with a projection $\vec{\Pi}_{\mathcal{M}}$ being used after each time step (middle). On the right, a plot of $|\Gamma^m|$ for $\tau = 10^{-3}$ (solid) and $\tau = 10^{-4}$ (dashed) without the projection.

and $T = 9$. We observe that in the isotropic case the curve evolves to a vertically aligned circle on the manifold, while the anisotropic flow leads to a horizontally aligned ellipse on the manifold. In both cases, as discussed before, the obtained numerical results are approximations to the minimizer of the given weighted length among all curves that enclose the same area as $\Gamma(0)$.

Geodesic Willmore flow of curves

First we perform a convergence test for our approximations (3.11), (3.9b) and (3.13a,b) of geodesic Willmore flow (2.32). To this end, similarly to (5.6), we define a true solution for the geodesic Willmore flow on the unit sphere. In particular, let

$$\vec{x}(\rho, t) = (r(t)\,\cos g(\rho), r(t)\,\sin g(\rho), [1 - r^2(t)]^{\frac{1}{2}})^T\,, \quad r(t) = [1 - (1 - r^4(0))\,e^{-2\,t}]^{\frac{1}{4}}, \tag{5.7}$$

with $r(0) \in (0, 1]$ and $g(\rho)$ as in (5.6). Starting with an initial circle at an altitude of $x_3 = 0.75$, so that $r(0) = \frac{1}{4}\sqrt{7}$, we compare our discrete solutions from the two schemes (3.11), (3.9b) and (3.13a,b), respectively, with the true solution (5.7). We set $\tau = 0.5\,h^2$ and $T = 1$ and report on the observed errors in Table 2, where we note that the experiments indicate that the convergence rate for the error is $O(h^2)$.

It can be easily shown that a geodesic circle with radius r on the unit sphere is a stationary solution of (2.32), if and only if

$$r = 1 \qquad \text{or} \qquad r = [2\,\lambda - 1]^{-\frac{1}{2}} \quad \text{if} \quad \lambda > 1\,, \tag{5.8}$$

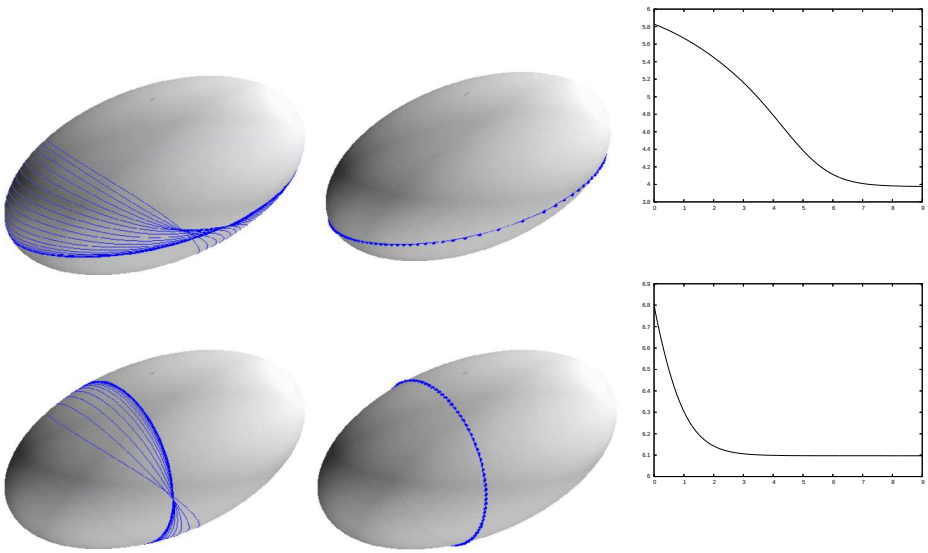

Figure 33: An example for anisotropic surface diffusion on an ellopsoid. We plot $\vec{X}(t)$ for $t = 0, 0.5, \ldots, T = 9$, $\vec{X}(T)$ and the energy $|\Gamma|_\phi$. The case $\phi(\vec{p}) = \sqrt{0.01\,p_1^2 + p_2^2 + p_3^2}$ is above, with $\phi(\vec{p}) = |\vec{p}|$ below.

J	(3.11), (3.9b)		(3.13a,b)	
	$\|\vec{X} - \vec{x}\|_{L^\infty}$	eoc	$\|\vec{X} - \vec{x}\|_{L^\infty}$	eoc
64	6.2955e-03	–	5.9935e-03	–
128	1.5464e-03	2.025407	1.4766e-03	2.021120
256	3.8497e-04	2.006096	3.6785e-04	2.005090
512	9.6142e-05	2.001507	9.1890e-05	2.001138
1024	2.4029e-05	2.000390	2.2963e-05	2.000597

Table 2: Absolute errors for the geodesic Willmore flow.

which in the latter case means that its "altitude" with respect to the chosen equator is given by $[1 - r^2(t)]^{\frac{1}{2}} = [1 - (2\,\lambda - 1)^{-1}]^{\frac{1}{2}}$. In a numerical example for $\lambda = 2.5$, we show the evolution of a circle on the unit sphere. The circle starts off at height 0.1 above the "equator" and moves towards the steady state solution of radius $r = \frac{1}{2}$ at an altitude of $x_3 = \frac{1}{2}\sqrt{3}$. The parameters were $J = 100$, $\tau = 10^{-3}$ and $T = 2.0$, where here and in what follows we used the approximation (3.11), (3.9b). See Figure 34 for the results, where we also show a plot of the discrete energy $\mathcal{W}^m_{\mathcal{M},\lambda}$, defined by

$$\mathcal{W}^m_{\mathcal{M},\lambda} := \begin{cases} \frac{1}{2}\,|\kappa^{m+1}_{\mathcal{M}}|_{m,h} + \lambda\,|\Gamma^m| & m = 0 \to M-1, \\ \frac{1}{2}\,|\kappa^{M}_{\mathcal{M}}|_{M,h} + \lambda\,|\Gamma^M| & m = M. \end{cases} \tag{5.9}$$

Next we show an example for geodesic Willmore flow on a torus, where the torus is given as in Figure 25. The evolution for a circle that is homotopic to a point can be seen in Figure 35. The discretization parameters were $J = 100$, $\tau = 10^{-3}$ and $T = 50$. We note that as there are no geodesics on the torus that are homotopic to a point, see e.g. Bliss (1902), this flow cannot reach a geodesic as a steady state. This is confirmed by the

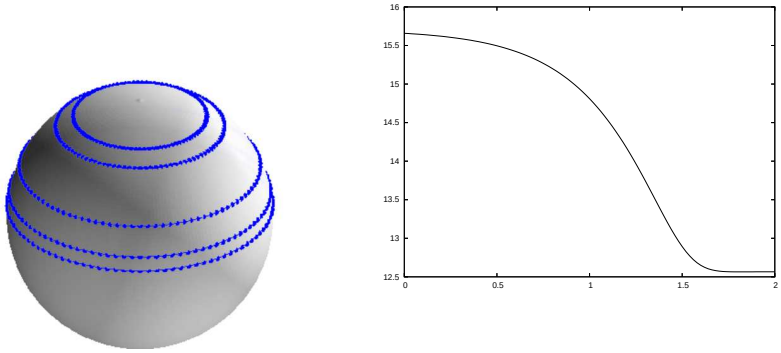

Figure 34: ($\lambda = 2.5$) An example for geodesic Willmore flow on the unit sphere. $\vec{X}(t)$ at times $t = 0,\ 0.5,\ 1,\ 1.5,\ 2$. A plot of $\mathcal{W}^m_{\mathcal{M},\lambda}$ on the right.

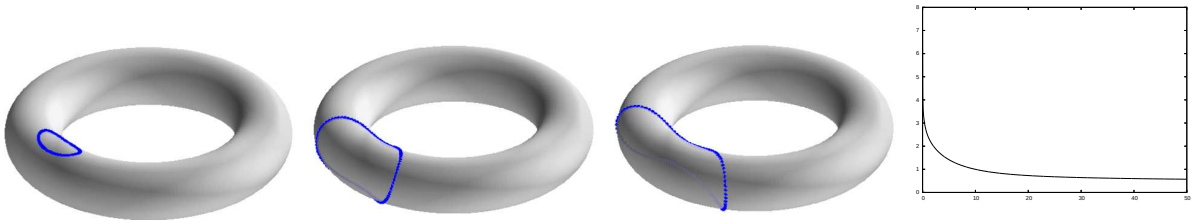

Figure 35: Flow for a circle on a torus. $\vec{X}(t)$, $t = 0, 10, T = 50$; and a plot of $\mathcal{W}^m_{\mathcal{M}}$ (right).

numerical results, where the discrete energy $\mathcal{W}^M_{\mathcal{M}}$ is bounded well away from zero.

We now compare the evolution of an initially smoothed polygonal curve on the unit sphere, which is slightly raised above the equator, for the flow (2.32) with different values of λ. Some results for the discretization parameters $J = 200$ and $\tau = 10^{-3}$ can be seen in Figure 36. As expected, the flow for $\lambda = 0$ yields a curve on the equator, while for $\lambda > 0$ we obtain a numerical steady state as predicted in (5.8). The most interesting evolution is for $\lambda < 0$, where growth in the length of the curve is encouraged. For the value $\lambda = -0.5$ shown here, this eventually leads to a triple covering of a circle at the equator.

Next we present some computations for the length preserving geodesic Willmore flow on the unit sphere. The results for our scheme (3.11), (3.9b) with the choice (3.12) different initial curves can be seen in Figure 37. Here we chose $J = 100$, $T = 1$ and $\tau = 5 \times 10^{-6}$. After 200 time steps we increased the time step size to $\tau = 5 \times 10^{-4}$.

Anisotropic geodesic Willmore flow of curves

Finally, we present some computations for our scheme (3.23a,b) for anisotropic geodesic Willmore flow, recall (2.38). As the initial curve we chose the tilted circle above the equator as in Figure 29. Some experiments for different choices of λ and ϕ can be seen in Figures 38 and 39. The discretization parameters were $J = 128$ and $\tau = 10^{-3}$. We observe that as in the isotropic case, recall (5.8), for large values of $\lambda > 0$ the curve attains a steady state away from the equator, with the steady state being aligned with the Wulff shape of the chosen anisotropy. For small values of $\lambda > 0$, however, the flow does not always yield the energy minimizing equator in the $x_1 - x_2$ plane. In particular, for $\lambda = 0.1$ the presented simulation finds as steady state the equator inside the $x_2 - x_3$ plane, which

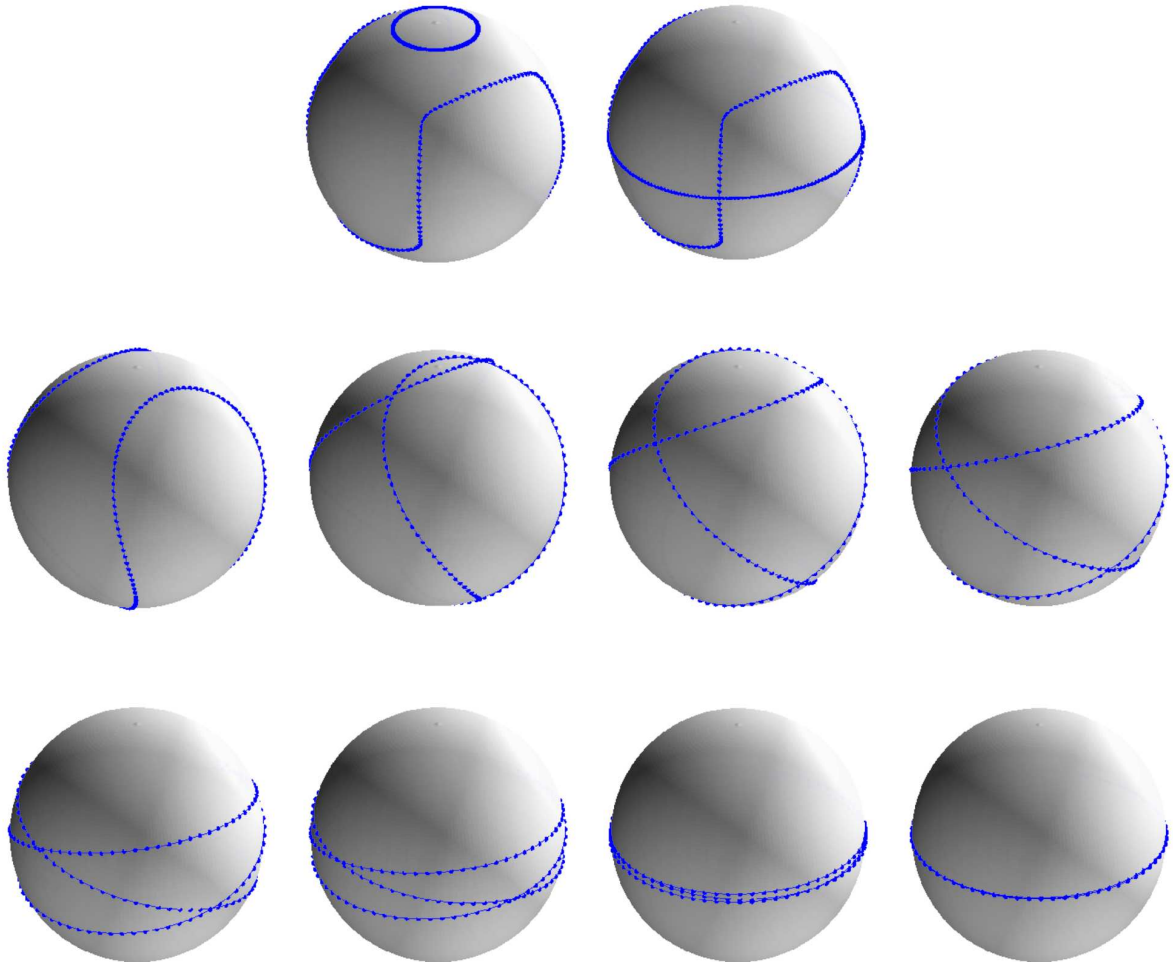

Figure 36: Willmore flow on the unit sphere. $\vec{X}(t)$ at times $t = 0, 1$ for $\lambda = 5, 0$. Below, the evolution $\vec{X}(t)$, $t = 0.5$, 1, 1.5, 2, 3, 4, 7, 10, for $\lambda = -0.5$.

here is not the global minimizer.

6 Conclusions

We present novel variational approximations of geometric gradient flows for closed curves in $\mathbb{R}^d$, $d \geq 2$, and on two-dimensional manifolds in $\mathbb{R}^3$, including anisotropic variants. We are able to prove well-posedness for the introduced discretizations, and prove stability for the approximations of the gradient flows for (anisotropic) length.

While there exist corresponding parametric finite element approximations of the higher codimension flows, see Dziuk (1994), Dziuk, Kuwert, and Schätzle (2002), Pozzi (2007), Deckelnick and Dziuk (2007), our schemes have excellent properties with respect to distribution of mesh points. In particular, no remeshing is needed in practice, something that is generally needed for existing approaches in the literature. In addition, our approximation

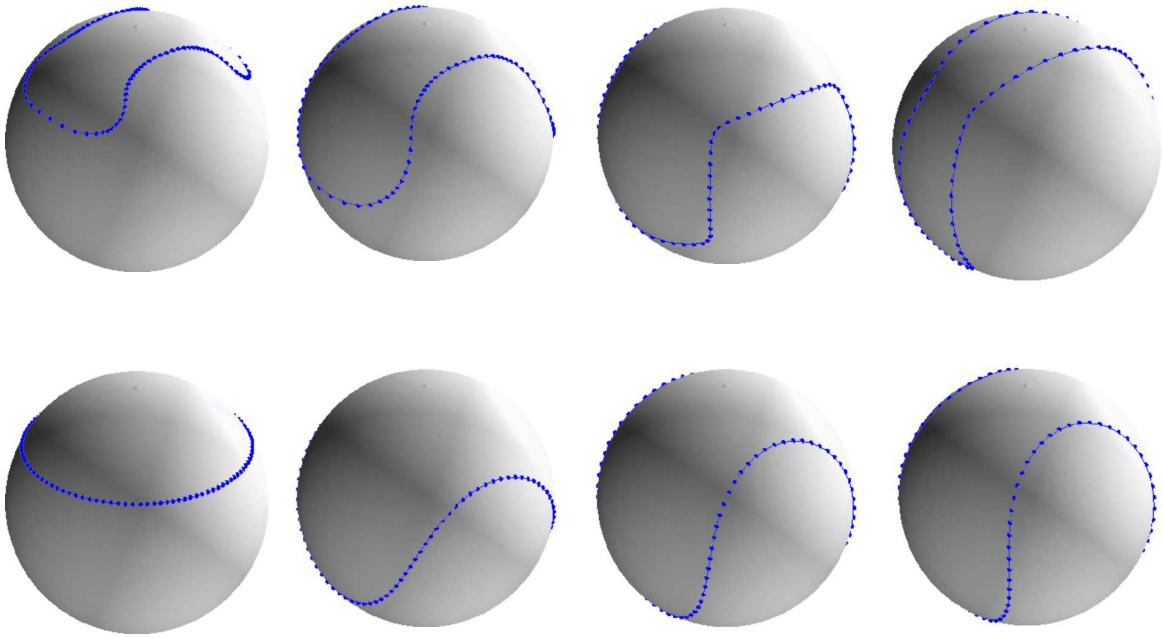

Figure 37: Length preserving geodesic Willmore flow on a unit sphere. Above $\vec{X}^0$ and below $\vec{X}^M$ with $|\Gamma^M| = 5.48, 7.8, 9.27, 10.1$.

of (2.37) is the first parametric scheme for the numerical approximation of anisotropic Willmore flow for curves in the literature.

Moreover, we present fully practical approximations for geodesic geometric evolution equations, something that is new in the literature. Again, these schemes lead to asymptotically equidistributed curves in practice. Natural applications of these novel approximations are the computation of closed geodesics on given manifolds, as well as simple isoperimetric problems on manifolds. Extending these schemes to include the case of geodesics with fixed endpoints, as well as more complicated partitioning problems, will be the subject of our future research.

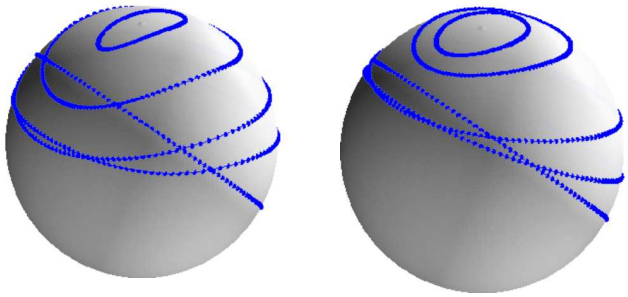

Figure 38: $\phi(\vec{p}) = \sqrt{0.1\,p_1^2 + p_2^2 + p_3^2}$, $\lambda = 5$ (left), $\phi(\vec{p}) = \sqrt{0.5\,p_1^2 + p_2^2 + p_3^2}$, $\lambda = 5$ (right). In each case we plot $\vec{X}(t)$, $t = 0,\ 0.2,\ 0.4,\ 0.6$, $T = 2$.

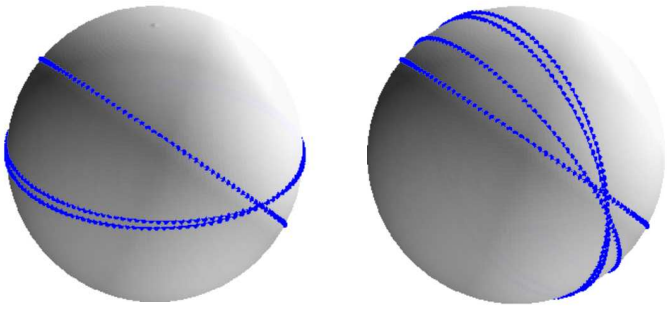

Figure 39: ($\phi(\vec{p}) = \sqrt{0.5\,p_1^2 + p_2^2 + p_3^2}$) $\lambda = 0.5$ (left) and $\lambda = 0.1$ (right). We plot $\vec{X}(t)$, $t = 0,\ 5,\ 10,\ T = 20$.

References

Barbosa, J. L., M. do Carmo, and J. Eschenburg (1988). Stability of hypersurfaces of constant mean curvature in Riemannian manifolds. *Math. Z. 197*(1), 123–138.

Barrett, J. W., H. Garcke, and R. Nürnberg (2007a). On the variational approximation of combined second and fourth order geometric evolution equations. *SIAM J. Sci. Comput. 29*(3), 1006–1041.

Barrett, J. W., H. Garcke, and R. Nürnberg (2007b). A parametric finite element method for fourth order geometric evolution equations. *J. Comput. Phys. 222*(1), 441–467.

Barrett, J. W., H. Garcke, and R. Nürnberg (2008a). Numerical approximation of anisotropic geometric evolution equations in the plane. *IMA J. Numer. Anal. 28*(2), 292–330.

Barrett, J. W., H. Garcke, and R. Nürnberg (2008b). On the parametric finite element approximation of evolving hypersurfaces in $\mathbb{R}^3$. *J. Comput. Phys. 227*(9), 4281–4307.

Barrett, J. W., H. Garcke, and R. Nürnberg (2008c). A variational formulation of anisotropic geometric evolution equations in higher dimensions. *Numer. Math. 109*(1), 1–44.

Bliss, G. A. (1902). The geodesic lines on the anchor ring. *Ann. of Math. (2) 4*(1), 1–21.

Brunnett, G. and P. E. Crouch (1994). Elastic curves on the sphere. *Adv. Comput. Math. 2*(1), 23–40.

Chen, X., K.-K. Phoon, and K.-C. Toh (2006). A modified SSOR preconditioner for sparse symmetric indefinite linear systems of equations. *Internat. J. Numer. Methods Engrg. 65*, 785–807.

Cheng, L.-T., P. Burchard, B. Merriman, and S. Osher (2002). Motion of curves constrained on surfaces using a level-set approach. *J. Comput. Phys. 175*(2), 604–644.

Chopp, D. L. and J. A. Sethian (1993). Flow under curvature: singularity formation, minimal surfaces, and geodesics. *Experiment. Math. 2*(4), 235–255.

Chou, K.-S. (2003). A blow-up criterion for the curve shortening flow by surface diffu-

sion. *Hokkaido Math. J. 32*(1), 1–19.

Clarenz, U. (2004). The Wulff shape minimizes an anisotropic Willmore functional. *Interfaces Free Bound. 6*(3), 351–359.

Deckelnick, K. and G. Dziuk (2007). Error analysis for the elastic flow of parameterized curves. Preprint, University Magdeburg.

Deckelnick, K., G. Dziuk, and C. M. Elliott (2005). Computation of geometric partial differential equations and mean curvature flow. *Acta Numer. 14*, 139–232.

Deckelnick, K. and C. M. Elliott (1998). Finite element error bounds for a curve shrinking with prescribed normal contact to a fixed boundary. *IMA J. Numer. Anal. 18*(4), 635–654.

Diewald, U. (2005). *Anisotrope Krümmungsflüsse parametrischer Flächen sowie deren Anwendung in der Flächenverarbeitung*. Ph. D. thesis, University Duisburg-Essen, Duisburg.

Dziuk, G. (1991). An algorithm for evolutionary surfaces. *Numer. Math. 58*(6), 603–611.

Dziuk, G. (1994). Convergence of a semi-discrete scheme for the curve shortening flow. *Math. Models Methods Appl. Sci. 4*, 589–606.

Dziuk, G. (1999). Discrete anisotropic curve shortening flow. *SIAM J. Numer. Anal. 36*, 1808–1830.

Dziuk, G. (2007). Computational parametric Willmore flow. Preprint No. 13-07, University Freiburg, Germany.

Dziuk, G., E. Kuwert, and R. Schätzle (2002). Evolution of elastic curves in $\mathbb{R}^n$: existence and computation. *SIAM J. Math. Anal. 33*, 1228–1245.

Elliott, C. M. and H. Garcke (1997). Existence results for diffusive surface motion laws. *Adv. Math. Sci. Appl. 7*(1), 465–488.

Garcke, H., K. Ito, and Y. Kohsaka (2005). Linearized stability analysis of stationary solutions for surface diffusion with boundary conditions. *SIAM J. Math. Anal. 36*(4), 1031–1056.

Garcke, H. and S. Wieland (2006). Surfactant spreading on thin viscous films: nonnegative solutions of a coupled degenerate system. *SIAM J. Math. Anal. 37*, 2025–2048.

Giga, Y. (2006). *Surface Evolution Equations*. Basel, Boston, Berlin: Birkhäuser.

Langer, J. and D. A. Singer (1984). The total squared curvature of closed curves. *J. Differential Geom. 20*(1), 1–22.

Langer, J. and D. A. Singer (1985). Curve straightening and a minimax argument for closed elastic curves. *Topology 24*(1), 75–88.

Linnér, A. and R. Renka (2005). Discrete periodic geodesics in a surface. *Experiment. Math. 14*(2), 145–152.

Luckhaus, S. and T. Sturzenhecker (1995). Implicit time discretization for the mean curvature flow equation. *Calc. Var. Partial Differential Equations 3*(2), 253–271.

Pozzi, P. (2007). Anisotropic curve shortening flow in higher codimension. *Math. Methods Appl. Sci. 30*(11), 1243–1281.

Spira, A. and R. Kimmel (2007). Geometric curve flows on parametric manifolds. *J. Comput. Phys. 223*(1), 235–249.

Taylor, J. E. and J. W. Cahn (1994). Linking anisotropic sharp and diffuse surface motion laws via gradient flows. *J. Statist. Phys. 77*(1-2), 183–197.